COLD ELASTIC COLLISIONS OF SODIUM AND RUBIDIUM

A Thesis
Presented to
The Academic Faculty

By

John Breuer

In Partial Fulfillment
Of the Requirements for the Degree
Master of Science in Physics

Georgia Institute of Technology

August, 2009

COLD ELASTIC COLLISIONS OF SODIUM AND RUBIDIUM

Dr. T. A. Brian Kennedy
School of Physics
Georgia Institute of Technology

Dr. Andrew Zangwill
School of Physics
Georgia Institute of Technology

Dr. Michael S. Chapman
School of Physics
Georgia Institute of Technology

Date Approved
June, 18th 2009

This work is dedicated to my fiancée Julia Petersen

ACKNOWLEDGEMENTS

This work would not have been possible without the help and support of several people. I truly appreciate to have had the chance to meet those people, who were an enrichment for both my scientific career and my personal life.

First of all I want to thank Dr. Chandra Raman, who gave me the idea for this thesis. I started working in his lab last summer, where I have learnt a lot about ultracold atomic physics in a relatively short period of time. In this context I also want to thank for great discussions with Dr. Gustavo Telles, Matthew Gibbs and Tetsuya Ishikawa. They always were there for me when questions and technical issues in the lab occured.

I am very thankful for all the valuable discussions with Dr. Brian Kennedy. He is definitely one of the greatest teachers I have ever met. His course about quantum mechanics changed my opinion about theoretical physics completely. I always enjoyed solving the very instructive homework assignments. Brian supported me in many ways with this work. He always found time for answering my questions, although he was not currently working on this topic. Because of his thorough explanations and his great class I now have a much better understanding about quantum mechanics and I know that I want to proceed my career at least somewhat into the theoretical direction.

Likewise I want to thank Dr. Andrew Zangwill. His class on electromagnetism was very helpful and instructive. Andrew also helped me with administrative barriers which occured along the completion of my Master's degree here in Atlanta.

Without my scholarship from the Studienstiftung des deutschen Volkes I would not have been able to study abroad. I appreciate this financial support throughout the last 4 years of my studies. This stipend made a lot of things so much easier for me and I cannot be thankful enough for that.

Furthermore I want to mention the World Student Fund, which allowed me to get a tuition waiver and so I did not have to pay the expensive out-of-state fees.

I also want to thank my fiancée Julia and my family for their support and encouragement to study abroad. Julia and I had to be apart for the last year and I appreciate her faithfulness and motivating words. The anticipation of our upcoming wedding in July and the start of our life together carried me through the setbacks which occured from time to time during this work. Having Julia in my life, is the greatest blessing which ever happened to me!

TABLE OF CONTENTS

LIST OF TABLES

LIST OF FIGURES

SUMMARY

In this thesis we numerically compute the scattering lengths and bound states for sodium-rubidium collisions at low energy. This work was motivated by experiments which aim to produce Bose-Einstein condensates (BEC) mixtures of sodium-rubidium. Elastic collision properties are important for the rethermalization of the atoms during the evaporative cooling process. Inelastic processes, which we also discuss to some extent, cause trap losses in those experiments. In order to reach the required temperature and density the elastic collision rates should be sufficiently large compared to the inelastic rates. The scattering lengths, which completely specify the elastic collision parameters at low energy, determine the miscibility and phase diagram of the sodium-rubidium condensate mixture. We calculate the scattering lengths approximately and find agreement with previous calculations indicating that miscible phases of sodium and rubidium condensates do not appear to be feasible in the absence of external fields.

CHAPTER 1

INTRODUCTION

Recent theoretical work on cold and ultracold collisions is closely related to the experimental efforts made in achieving Bose-Einstein condensation (BEC). Therefore we would like to give a short review of the history of BEC, the related technical difficulties and the path to its final realization in 1995 (see e.g. [1]).

In 1924 Satyendra Nath Bose wrote a paper on the quantum statistics of photons [2]. Albert Einstein reviewed his work and extended Bose's considerations to massive bosons. That was the hour of birth of Bose-Einstein statistics. Nowadays we know that all particles with integer spin (i.e. bosons) follow this statistics. When confined in an external potential, the peculiar feature of Bose gases at low temperature is that (below a critical temperature) a macroscopic number can occupy the ground state of the potential. That implies a coherent state of massive particles similar to the coherent state of massless photons in a laser beam. Simple quantum statistical considerations allow us to calculate the critical temperature T_C for an ideal Bose gas below which BEC occurs,

$$T_C = \frac{h^2}{2\pi m k_B} \left(\frac{n}{\zeta(3/2)} \right)^{2/3} \tag{1.1}$$

with the mass m of each boson and the Riemann zeta function $\zeta(3/2) \approx 2.612$. The reason for the occurance of BEC is that the chemical potential μ, which indicates how much energy is needed to add or remove a particle to a particular state, tends to zero at low temperatures for bosons. It is important to note that the critical temperature for

BEC (below mK) is orders of magnitude below the critical temperature for comparable states of matter like superfluidity or superconductivity. That's why very sophisticated experimental methods had to be developed before BEC could be firstly realized. Interactions play a crucial role in those experiments as we will see in the following.

The first efforts to create BEC in a dilute gas have been made with spin-polarized hydrogen. Theoretical work by Hecht [3] and Stwalley and Nosanow [4] suggested that spin-polarized hydrogen remains an atomic gas down to zero temperature at sufficiently low pressures, because there are no bound states in its triplet potential and spin-flip collisions, in which molecules could be formed, are suppressed in those experiments [1]. Experiments have been done in the 1980s and 90s in dilution refrigerators whose walls were coated with superfluid helium. The advantage of using hydrogen was that one completely understood its collisional properties. Nevertheless it turned out that BEC cannot be realized with hydrogen in this setup because of recombination at the walls and three-body recombination (if the density of the gas gets too large).

At the same time, but independently, the technology laser-cooling was developing. The idea of using laser light for cooling atoms came from papers by Hänsch and Schawlow [5] and Wineland and Dehmelt [6]. Raab et al. managed to realize the first magneto-optical trap (MOT) with sodium atoms in 1987 [7]. Furthermore it was observed that one succeeded to cool atoms below the theoretical Doppler limit. That was a big mystery at this time, but after a couple of years theoreticians explained the sub-Doppler temperatures with the effect of polarization gradients and the influence of differential light shifts (Sisyphus cooling) (see [8],[9],[10],[11] and [12]). All those experiments were done with alkali atoms. At the beginning of the 1990s there were two groups of physicists, those, who proposed to achieve BEC in hydrogen, and those, who proposed to do the same with alkalis using laser cooling methods.

At this point the lowest reachable temperatures (with laser-cooling) were still too high for BEC [13]. A promising concept came once again from the hydrogen groups: evaporative cooling. Early work was done by Harold Hess from the MIT [14]. The principle is very easy and well-known from everyday routines like the cooling of a cup of coffee. In ultracold atomic physics atoms are confined in a magnetic trap and by lowering the boundaries of this potential the hot atoms leave the trap and after rethermalization the remaining cloud has an overall lower temperature. The lowest temperatures obtained with hydrogen were around 100 μK, which was still too high for BEC. Nevertheless, inspired by this work, the JILA group at the University of Colorado at Boulder (and also Ketterle's group at the MIT) adapted the concept of evaporative cooling for their alkali experiments. In combination with laser-cooling it seemed to be a very promising opportunity which finally led to the successful realization of BEC of ^{87}Rb in 1995 [15], for which Eric A. Cornell, Carl E. Wieman and Wolfgang Ketterle were awarded the Nobel prize in 2001.

Atomic collisions are crucial in all those experiments. On the one hand collisions with the walls of the chamber or with background atoms lead to heating and trap losses. On the other hand elastic collisions ("good" collisions) are important for the rethermalization of the remaining atoms in evaporative cooling. Three-body collisions and dipolar relaxation ("bad" collisions) also cause trap losses, because atoms change their spin state and are therefore expelled from the trap zone. The principle concern for cooling is therefore to increase the ratio of good to bad collisions in order to obtain sufficiently high densities of the trapped atoms at sufficiently low temperatures. Hydrogenic collision properties were well-known in the 1980s, which was mainly the reason why most groups were using it for their experiments. On the other hand there was little information about the cold collision properties of alkalis at the beginning of the 1990s. The promising of achieving BEC with alkalis due to the new cooling techniques initiated the study of this field. Eventually photoassociation methods were developed and these led to accurate data about the alkali interaction potentials [16].

The research reported in this thesis was motivated by experiments with ultracold sodium-rubidium vapors. Scattering lengths for Na-Rb, which completely determine the low-energy elastic collision parameters, have been stated in [17] and [18]. Whereas experimental and numerical methods to obtain the interaction potentials have been described in detail (e.g. in [18],[19]), the actual calculation of the scattering lengths was not discussed. In most cases very sophisticated programs, similar to the one described in [20], are used to analyze the potential. In this work we therefore want to present a simple numerical procedure for computing the scattering lengths and bound state energies for a non-analytical potential in order to confirm the results of previous calculations.

We start with basic ideas of quantum mechanical scattering theory in the second chapter, which we support with illustrative examples. In the third chapter we talk specifically about collisions between alkali atoms. We concentrate on elastic scattering, but briefly discuss inelastic collisions. We present our calculations which determine the scattering lengths for Na-Rb numerically and find agreement with the literature [18]. In the last chapter we present the connection between cold collision theory and BEC experiments and apply some of those ideas to Na-Rb mixtures.

CHAPTER 2

FUNDAMENTALS OF SCATTERING THEORY

Scattering theory is a very important topic in quantum mechanics. One of the first major results in scattering theory was achieved by Ernest Rutherford in 1911 [21]. He described classically the scattering of alpha particles at a gold foil caused by the Coulomb interaction. Due to an amazing coincidence, it turns out that his classically derived result for the differential cross section agrees with the quantum mechanical calculation. Among many others Mott and Massey have worked on quantum scattering theory and they have published a comprehensive work on the theory of atomic collisions [22].

In this chapter we would like to present the basic ideas of scattering theory. We concentrate mainly on elastic processes, but also introduce some ideas about inelastic collisions. We will in particular work in the low energy limit, as that is the regime in which cold atomic experiments take place. We complete the theoretical derivations with illustrative examples.

2.1 Elastic collisions

It is very important to understand the treatment of elastic collisions before describing more complex interactions. In the first part of this section we present the most general results. Afterwards we restrict our discussion to interactions at low energy and give the analytically solvable example of the rectangular well.

2.1.1 Two-body elastic scattering

The theory of two-body elastic collisions is very well covered in [23]. We want to give a short review of this topic in order to derive the most important results.

We start with two bodies with masses m_1 and m_2 which are interacting in a central potential $V(r)$. Hence, the motion can be separated into the center of mass and relative motion. The latter is the interesting part and can be described as the motion of a single particle with relative coordinate $\vec{r} = \vec{r_1} - \vec{r_2}$ and reduced mass $\mu = m_1 m_2/(m_1 + m_2)$. The energy of the relative motion is given by $\hbar^2 k^2/(2\mu)$ and the momentum is $\vec{p} = \hbar\vec{k}$.

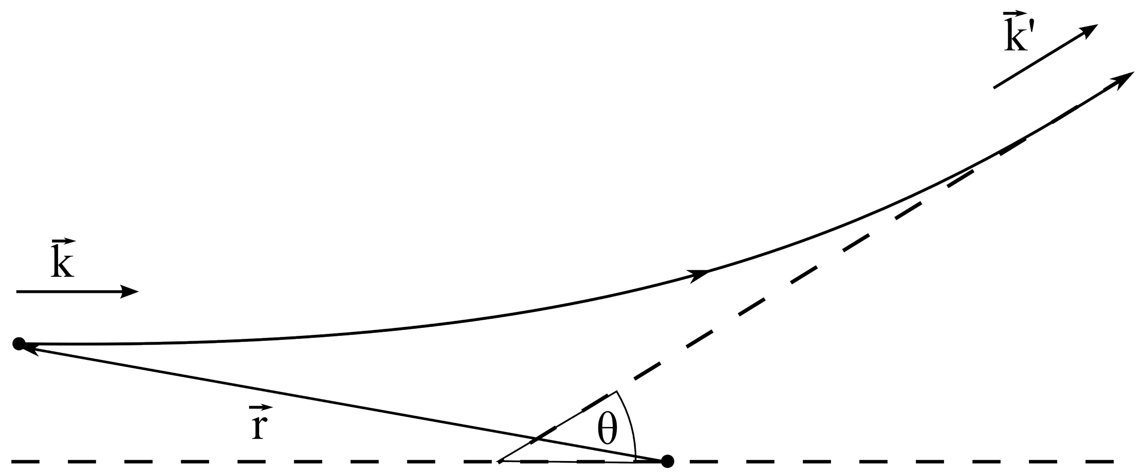

Figure 2.1: Scattering process in a central potential with scattering angle θ. The relative coordinate is $\vec{r}$ and the incoming (outgoing) wave vectors are $\vec{k}$ ($\vec{k}'$).

If we make use of the fact that the potential goes to zero for large distances, we can write the asymptotic wave function far outside the scattering region as a superposition of the incoming plane wave and the scattered (outgoing) spherical wave

$$\psi^+(\vec{r}) \simeq \frac{1}{(2\pi)^{3/2}} \left[e^{i\vec{k}\cdot\vec{r}} + f(\vec{k}, \vec{k}') \cdot \frac{e^{ikr}}{r} \right] \tag{2.1}$$

with the scattering amplitude $f(\vec{k},\vec{k}')$, which can be generally written as

$$f(\vec{k},\vec{k}') = -\frac{1}{4\pi}\frac{2\mu}{\hbar^2}(2\pi)^3 \int d^3r \frac{1}{(2\pi)^{3/2}} e^{-i\vec{k}'\cdot\vec{r}} V(\vec{r})\psi^+(\vec{r}) \ . \tag{2.2}$$

Note that eq. (2.1) and (2.2) together define an integral equation for the asymptotic wave function.

Using the fact that $\psi(\vec{r}) = \langle\vec{r}|\psi\rangle$ and $V(\vec{r})\delta(\vec{r}-\vec{r}\,') = \langle\vec{r}|\,\hat{V}(\hat{\vec{r}})\,|\vec{r}\,'\rangle$ and the definition for the transition operator $\hat{T}\,|\vec{k}\rangle = \hat{V}\,|\psi\rangle$, where $|\vec{k}\rangle$ is a plane wave state, we can rewrite $f(\vec{k},\vec{k}')$:

$$\begin{aligned} f(\vec{k},\vec{k}') &= -\frac{1}{4\pi}\frac{2\mu}{\hbar^2}(2\pi)^3 \langle\vec{k}'|\,\hat{V}\,|\psi^+\rangle \\ &= -\frac{1}{4\pi}\frac{2\mu}{\hbar^2}(2\pi)^3 \langle\vec{k}'|\,\hat{T}\,|\vec{k}\rangle \ . \end{aligned} \tag{2.3}$$

In case of a weak interaction the problem can be treated perturbatively and in the first Born approximation $\hat{T} \approx \hat{V}$.

With the partial wave expansion, which means expanding the state in a complete set of spherical wave states $|E,l,m\rangle$, we can rewrite the scattering amplitude. The transition operator $\hat{T}$ is a scalar operator, as it commutes with $\hat{L}^2$ and $\hat{\vec{L}}$ for a **spherically symmetric potential**. Therefore its matrix elements are diagonal in terms of the spherical wave states (diagonal in energy because of elastic scattering and diagonal in l,m as it is a rotational scalar operator)

$$\langle E',l',m'|\,\hat{T}\,|E,l,m\rangle = T_l(E)\delta_{ll'}\delta_{mm'}\delta(E-E') \ . \tag{2.4}$$

We get after a little calculation (shown in [23]):

$$f(\vec{k},\vec{k}') = -\frac{4\pi^2}{k}\sum_{l,m} T_l\left(E = \frac{\hbar^2k^2}{2\mu}\right) Y_l^m(\hat{k}')Y_l^{m*}(\hat{k}) \ . \tag{2.5}$$

Choosing our coordinate system so that the **z-axis points into the k-direction**, it follows that

$$f(\vec{k},\vec{k}') = f(k,\theta) = \sum_{l=0}^{\infty}(2l+1)f_l(k)P_l(\cos\theta) \tag{2.6}$$

with the partial-wave amplitude

$$f_l(k) \equiv -\frac{\pi T_l(E=\frac{\hbar^2 k^2}{2\mu})}{k} \ . \tag{2.7}$$

Each partial wave contribution $s, p, d, ...$ has a different angular momentum $l = 0, 1, 2, ...$

Now we go back to eq. (2.1) and use the partial wave expansion for a plane wave:

$$e^{ikz} = \sum_l (2l+1)P_l(\cos\theta)\left(\frac{e^{ikr} - e^{-i(kr-l\pi)}}{2ikr}\right) \ . \tag{2.8}$$

Therefore we can write the wave function at large distances as

$$\begin{aligned} \psi^+(\vec{r}) &\simeq \frac{1}{(2\pi)^{3/2}}\left[e^{ikz} + f(k,\theta)\cdot\frac{e^{ikr}}{r}\right] \\ &= \frac{1}{(2\pi)^{3/2}}\sum_l (2l+1)\frac{P_l(\cos\theta)}{2ik}\left[(1+2ikf_l(k))\frac{e^{ikr}}{r} - \frac{e^{-i(kr-l\pi)}}{r}\right] \ . \end{aligned} \tag{2.9}$$

It is now helpful to look at the plane wave function in eq. (2.8) as a superposition of an outgoing and incoming spherical wave. The presence of scattering just changes the coefficient of the outgoing part in eq. (2.9)

$$1 \to 1 + 2ikf_l(k) \ . \tag{2.10}$$

Due to probability conservation and the continuity equation this coefficient must have an absolute value of 1 and can therefore be written as

$$1 + 2ikf_l(k) = e^{2i\delta_l(k)} \ . \tag{2.11}$$

Thus, we see that the scattering process can just change the phase of the outgoing wave. This phase shift $\delta_l(k)$ is a real number (it can be complex in the case of inelastic scattering - see section 2.2.2). If we write the scattering amplitude in terms of $\delta_l(k)$, we get

$$f(k,\theta) = \frac{1}{2ik}\sum_{l=0}^{\infty}(2l+1)\left(e^{2i\delta_l(k)}-1\right)P_l(\cos\theta)\ . \tag{2.12}$$

Now we want to describe how the phase shifts δ_l can be determined for a given radially symmetric potential $V(r)$. We can factorize the wave function at any point in space

$$\psi(\vec{r}) = R_l(r)Y_l^m(\theta,\phi)\ , \tag{2.13}$$

where $Y_l^m(\theta,\phi)$ are the spherical harmonics and the function $R_l(r)$ solves the radial Schrödinger equation

$$-\frac{\hbar^2}{2\mu}\left(\frac{d^2R_l(r)}{dr^2}+\frac{2}{r}\frac{dR_l(r)}{dr}\right)+\left(V(r)+\frac{\hbar^2 l(l+1)}{2\mu r^2}-E\right)R_l(r)=0\ . \tag{2.14}$$

It is essential to (numerically) solve this equation in order to obtain the phase shifts δ_l in the following way. Assuming that the range of the potential is limited, i.e. $V(r)=0$ for $r>r_0$ and using the fact that $E=\hbar^2k^2/(2\mu)$, we can rewrite this equation as the spherical Bessel differential equation (multiply by r^2, divide by $-\hbar^2/(2\mu)$ and define the new variable $\rho\equiv kr$)

$$\rho^2\frac{d^2}{d\rho^2}R_l(\rho)+2\rho\frac{d}{d\rho}R_l(\rho)+\left(\rho^2-l(l+1)\right)R_l(\rho)=0\ . \tag{2.15}$$

This equation can be solved by spherical Bessel and Neumann functions or their linear combinations [24]

$$h_l^{(1)}=j_l+in_l \quad \text{and} \quad h_l^{(2)}=j_l-in_l\ . \tag{2.16}$$

Those functions are called spherical Hankel functions. The whole system has a rotational symmetry around the z-axis (=$\vec{k}$-direction) and therefore cannot depend on ϕ. That's why we just have to use the spherical harmonics $Y_l^0(\theta)$, which are proportional to the Legendre polynomials $P_l(\cos\theta)$, i.e. the whole solution for $r > r_0$ has the form

$$\psi^+(\vec{r}) = \frac{1}{(2\pi)^{3/2}} \sum_l i^l (2l+1) \left(c_l^{(1)} h_l^{(1)}(kr) + c_l^{(2)} h_l^{(2)}(kr) \right) P_l(\cos\theta) \ . \tag{2.17}$$

Considering now the asymptotic behavior of the spherical Hankel functions

$$h_l^{(1)} \xrightarrow{r\to\infty} \frac{e^{i(kr - l\pi/2)}}{ikr} \quad \text{and} \quad h_l^{(2)} \xrightarrow{r\to\infty} -\frac{e^{-i(kr-l\pi/2)}}{ikr} \ , \tag{2.18}$$

and using the fact the $i^l = \exp(il\pi/2)$ yields

$$\psi^+(\vec{r}) \to \frac{1}{(2\pi)^{3/2}} \sum_l (2l+1) \frac{P_l(\cos\theta)}{ikr} \left(c_l^{(1)} e^{ikr} - c_l^{(2)} e^{-i(kr - l\pi)} \right) \ . \tag{2.19}$$

Comparing this result to eq. (2.9) using the definition of the phase shift (eq. (2.11)) leads to the coefficients $c_l^{(1,2)}$

$$c_l^{(1)} = \frac{1}{2} e^{2i\delta_l(k)} \quad \text{and} \quad c_l^{(2)} = \frac{1}{2} \ . \tag{2.20}$$

It follows that

$$\begin{aligned} \psi^+(\vec{r}) &\simeq \frac{1}{(2\pi)^{3/2}} \sum_l (2l+1) \frac{P_l(\cos\theta)}{2ikr} \left(e^{2i\delta_l(k) + ikr} - e^{-i(kr-l\pi)} \right) \\ &= \frac{1}{(2\pi)^{3/2}} \sum_l (2l+1) \frac{P_l(\cos\theta)}{kr} e^{i(\delta_l(k) + \frac{l\pi}{2})} \sin\left(kr - \frac{l\pi}{2} + \delta_l(k) \right) \ . \end{aligned} \tag{2.21}$$

Now we need to find the solution of the radial Schrödinger equation for $r < r_0$. If it is necessary, this calculation has to be done numerically. Claiming continuity of each partial wave at $r = r_0$, i.e. matching $R_l(r < r_0)$ and $R_l(r > r_0)$ together, eventually yields the phase shifts δ_l.

After this derivation we can write down the differential and total scattering cross sections:

$$\frac{d\sigma}{d\Omega} = |f(k,\theta)|^2 = \frac{1}{4k^2}\left|\sum_{l=0}^{\infty}(2l+1)\left(e^{2i\delta_l(k)}-1\right)P_l(\cos\theta)\right|^2 \tag{2.22}$$

$$\sigma_{tot} = \int |f(k,\theta)|^2\, d\Omega = \frac{4\pi}{k^2}\sum_{l=0}^{\infty}(2l+1)\sin^2\delta_l(k)\ . \tag{2.23}$$

The total cross section can be easily calculated using the optical theorem:

$$\sigma_{tot} = \frac{4\pi}{k}\mathrm{Im}f(k,\theta=0)\ . \tag{2.24}$$

It is worth mentioning, that we talked so far about distinguishable particles. For indistinguishable bosons or fermions the wave function has to be symmetrized or antisymmetrized (due to the spin-statistics theorem of Pauli [25]).

At the beginning of this chapter we started off by separating the center of mass and relative motion. While the former is invariant under particle exchange, the latter changes sign because $\vec{r} = \vec{r_1} - \vec{r_2}$. That's why the symmetrized (antisymmetrized) spatial scattering wave function has to be (eq. (2.9) and eq. (2.12))

$$\begin{aligned}
\psi^+_{\substack{s\\a}}(\vec{r}) &= \frac{1}{\sqrt{2}}\cdot\left(\psi^+(\vec{r})\pm\psi^+(-\vec{r})\right) = \frac{1}{\sqrt{2}}\cdot\left(\psi^+(r,\theta,\phi)\pm\psi^+(r,\pi-\theta,\pi+\phi)\right)\\
&\simeq \frac{1}{\sqrt{2}}\cdot\frac{1}{(2\pi)^{3/2}}\left[\left(e^{ikz}\pm e^{-ikz}\right)+\frac{e^{ikr}}{r}\cdot\left(f(k,\theta)\pm f(k,\pi-\theta)\right)\right]\\
&= \frac{1}{\sqrt{2}}\cdot\frac{1}{(2\pi)^{3/2}}\left(e^{ikz}\pm e^{-ikz}\right)\\
&\quad+\frac{1}{\sqrt{2}}\cdot\frac{1}{(2\pi)^{3/2}}\frac{e^{ikr}}{r}\cdot\frac{1}{ik}\sum_{l=0}^{\infty}\left(1\pm(-1)^l\right)(2l+1)\left(e^{2i\delta_l(k)}-1\right)P_l(\cos\theta)\ ,
\end{aligned} \tag{2.25}$$

where we used the fact that $P_l(-x) = (-1)^l P_l(x)$. Note that the second term of the scattering wave function contains r, which is the magnitude of the relative coordinate and hence does not change sign.

Thus for identical bosons the contribution of even partial waves (s,d,...) is twice as large as for distinguishable particles whereas odd partial waves vanish. For identical fermions the opposite is true. Furthermore the total cross section for the allowed partial waves in case of indistinguishable particles is twice as large as for distinguishable particles.

Because for sufficiently low energy partial waves higher than s-waves are supressed (see next section), identical ultracold fermions are basically noninteracting and cannot be cooled. Nevertheless one can cool such gases by mixing fermions with different spin-states which act as distinguishable particles [26].

2.1.2 *Low energy limit*

In this work we concentrate on collisions in cold and ultracold gases which implies that the colliding atoms will have very low energy (below mK). The mean kinetic energy for an ideal gas at a temperature of 1 mK is, for example,

$$E = \frac{3}{2} k_B \cdot T = 1.3 \times 10^{-7} \mathrm{eV} \ , \tag{2.26}$$

and corresponds to an average velocity of (with $\mu \approx 18$ a.u. for $^{23}\mathrm{Na}^{85}\mathrm{Rb}$)

$$v = \sqrt{\frac{2E}{\mu}} \simeq 1.2 \ \mathrm{m/s} \ . \tag{2.27}$$

The effective potential is the sum of the radial potential and the centrifugal barrier $\frac{\hbar^2 l(l+1)}{2\mu r^2}$. Therefore it is easy to see that for lower incident energies fewer partial waves contribute to the scattering, because this barrier prevents large l partial waves from entering the scattering region. In the limit $k \rightarrow 0$ the atoms cannot come close enough except in the $l = 0$ case. Hence, for sufficiently low temperatures one just has to consider s-wave collisions. Figure 2.2 shows the long-range part of the Na-Rb potential (we present the properties of alkali potentials in section 3.1), which is to leading order the van der Waals term and the centrifugal barrier:

$$V(r) = -\frac{C_6}{r^6} + \frac{\hbar^2 l(l+1)}{2\mu r^2} \tag{2.28}$$

with $C_6 = 1.3237 \cdot 10^7\ \mathrm{cm}^{-1} \cdot \mathring{\mathrm{A}}^6 = 1.9067\ \mathrm{K} \cdot \mathring{\mathrm{A}}^6$ [18] and $\mu \approx 18$ a.u. The centrifugal barrier for the p-wave has a height of 0.4 mK and for the d-wave 2.0 mK.

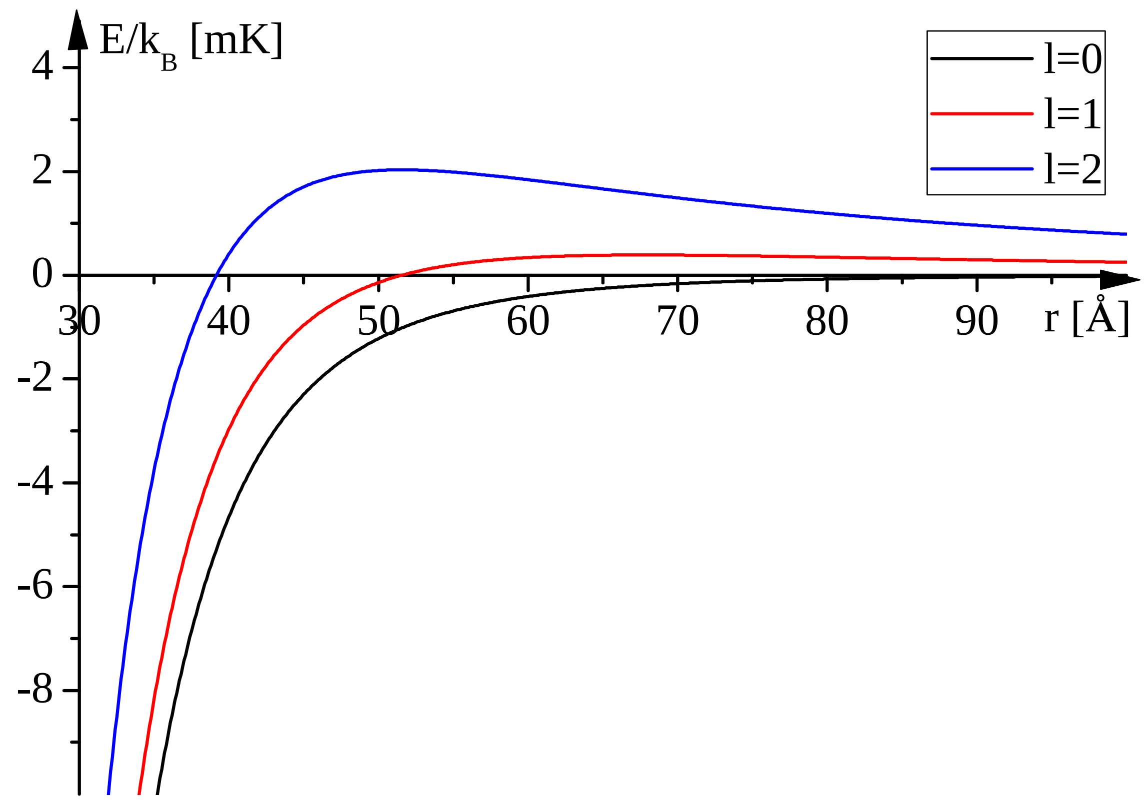

Figure 2.2: Centrifugal barrier in long-range part of Na-Rb potential for s-, p- and d-wave (see eq. (2.28))

We will therefore just look at s-wave scattering in the following, which is always valid for sufficiently low energies. That simplifies enormously all the relations from the last section. The wave function at large distances becomes, for example,

$$\psi^+(\vec{r}) \simeq \frac{1}{(2\pi)^{3/2}} \frac{1}{kr} e^{i\delta_0(k)} \sin\left(kr + \delta_0(k)\right) \ . \tag{2.29}$$

On the other hand, the wave function has to satisfy the radial Schrödinger equation (eq. (2.14)). Defining $u_l(r) = r \cdot R_l(r)$ in the usual way, substituting and rearranging yields the well-known one dimensional Schrödinger equation

$$\left\{ \frac{d^2}{dr^2} + \frac{2\mu}{\hbar^2}\left(E - V(r)\right) - \frac{l(l+1)}{r^2} \right\} u_l(r) = 0 \ . \tag{2.30}$$

As we look for the asymptotic solution ($V(r) = 0$) in the low energy limit ($E = 0$) for s-wave scattering ($l = 0$), the problem simplifies to

$$\frac{d^2}{dr^2} u_0(r) = 0 \tag{2.31}$$

with the simple solution

$$u_0(r) = C(r - a) \ , \tag{2.32}$$

where C and a are constants. On the other hand, we can extract $u_l(r)$ from eq. (2.29), which we derived from the partial wave expansion,

$$u_0(r) = \sin\left(kr + \delta_0(k)\right) \ . \tag{2.33}$$

Those two asymptotic solutions have to agree for $k \to 0$. Taking the logarithmic derivative yields

$$\frac{u_0'(r)}{u_0(r)} = k \cot\left(kr + \delta_0(k)\right) \overset{k\to 0}{\to} \frac{1}{r - a} \ . \tag{2.34}$$

That leads us to the definition of the scattering length (if we set $r = 0$):

$$\lim_{k\to 0} k \cot \delta_0(k) = -\frac{1}{a} \tag{2.35}$$

or,

$$a = -\lim_{k\to 0} \frac{\tan \delta_0(k)}{k} \ . \tag{2.36}$$

For small k we can expand the phase shift:

$$a = -\lim_{k\to 0} \frac{\tan\left\{\delta_0(k=0) + k\cdot\delta_0'(k=0)\right\}}{k} = -\delta_0'(k=0)\ , \tag{2.37}$$

where we used the fact that $\delta_0(k=0)$ is an integer multiple of π, as can be seen from eq. (2.11). That is also stated in Levinson's theorem [27]

$$\delta_0(k=0) = n_b\pi\ , \tag{2.38}$$

where n_b is the number of bound states of the potential. Therefore we find

$$\delta_0(k \ll 1) \simeq n_b\pi - ak\ . \tag{2.39}$$

The physical meaning of the scattering length can be seen from the long range wave function

$$\psi^+(r) \sim \sin k(r-a)\ . \tag{2.40}$$

In the finite region where the potential is nonzero the wave function is oscillating rapidly, but outside of this range it is proportional to $k(r-a)$. That's why the scattering length gives a shift of the origin of the long-range sinusoidal wave function. It is either positive, zero or negative (see Figure 2.3). It can be shown that a negative (positive) scattering length causes effectively an attraction (repulsion). Figuratively, the free wave is sucked in towards (pushed away from) the origin. Furthermore we note the total cross section in the low energy limit (by substituting eq. (2.37) into eq. (2.23)):

$$\sigma_{tot} = 4\pi a^2\ . \tag{2.41}$$

Note that $\sigma_{tot} = 8\pi a^2$ for identical bosons, which follows from the preceding discussion (eq. (2.25)).

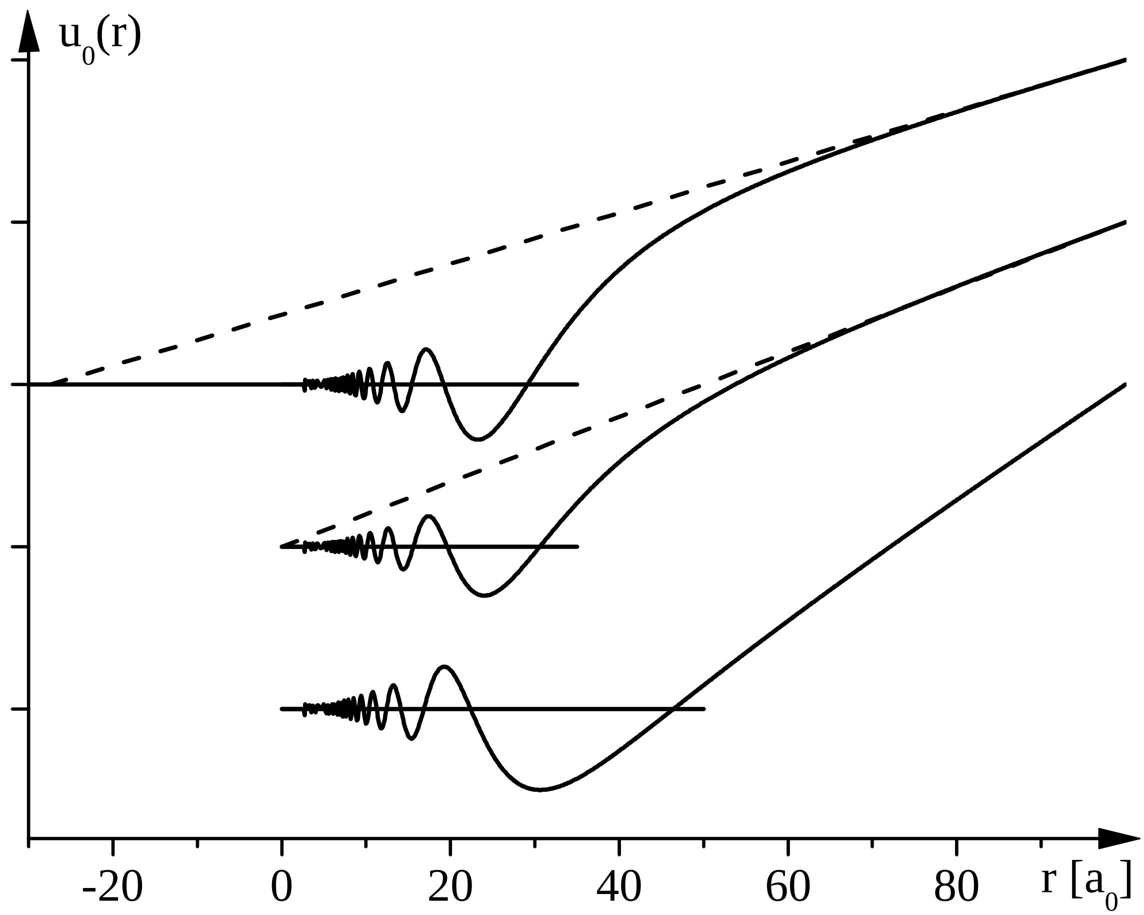

Figure 2.3: Illustration of the meaning of the scattering length. It can be positive, zero or negative (or even diverge as discussed e.g. in 2.1.3). In this figure we can read off a scattering length of -27, 0 and 46 a_0, respectively.

2.1.3 Example: Rectangular Well

In order to illustrate the solution of an elastic scattering problem, we would like to present the analytically solvable example of the rectangular well. It is rather simple but nevertheless very instructive. The potential is given by

$$V(r) = \begin{cases} -V_0 & \text{for } r < R \\ 0 & \text{for } r > R \end{cases} \tag{2.42}$$

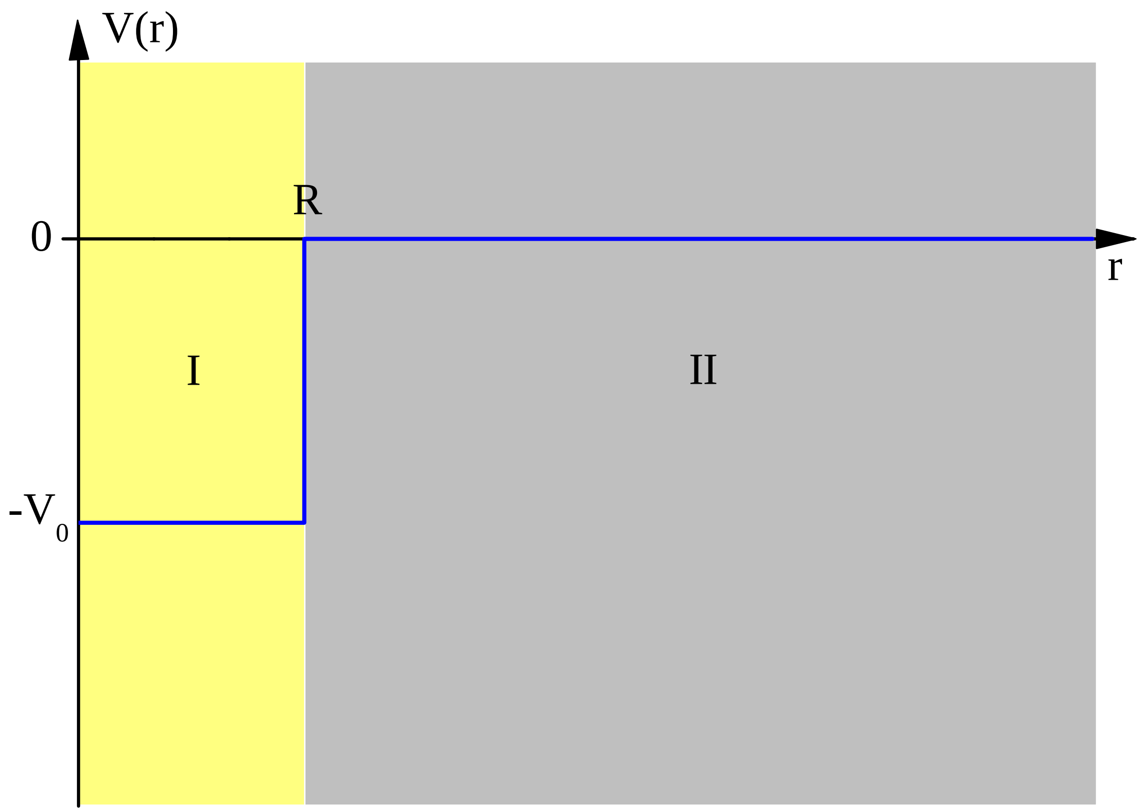

Figure 2.4: Rectangular well potential

The Schrödinger equation (eq. (2.30)) has the simple oscillating solutions (for l=0)

$$u_0(r) = \begin{cases} A \sin \kappa r & \text{for } r < R \\ B \sin(kr + \delta_0) & \text{for } r > R \end{cases} \tag{2.43}$$

with $\kappa = \sqrt{\frac{2m}{\hbar^2}(E+V_0)}$ and $k = \sqrt{\frac{2m}{\hbar^2}\,|E|}$. The solution for the three different energies $E = \pm\frac{V_0}{2}, 0$ is shown in Figure 2.6(a). The phase for the wave inside the barrier must be zero, because $u(r=0) \stackrel{!}{=} 0$. Furthermore we claim u and u' to be continuous at $r = R$. That yields

$$\left.\frac{u}{u'}\right|_{r=R} = \frac{1}{\kappa}\tan\kappa R = \frac{1}{k}\tan(kR+\delta_0)\ . \tag{2.44}$$

Therefore the phase shift is given by

$$\delta_0(k) = \arctan\left(\frac{k}{\kappa}\tan\kappa R\right) - kR\ . \tag{2.45}$$

If $\kappa R \neq (2n+1)\frac{\pi}{2}$ (n integer), we can approximate the arc tangent by its argument as $k \to 0$. Therefore we get

$$\begin{aligned}\delta_0(k) &= \frac{k}{\kappa}\tan\kappa R - kR \\ &= -k\left(R\left(1-\frac{\tan\kappa R}{\kappa R}\right)\right) \\ &= -ka\ ,\end{aligned} \tag{2.46}$$

where we used eq. (2.37) in order to write the scattering length as

$$a = R\left(1-\frac{\tan\kappa R}{\kappa R}\right)\ . \tag{2.47}$$

On the other hand, if $\kappa R = (2n+1)\frac{\pi}{2}$, the scattering length diverges in this limit. But the approximation in eq. (2.46) still holds, if we calculate the scattering length with the definition in eq. (2.35) and the exact phase shift eq. (2.45). A plot for the scattering length is given in Figure 2.5. More complicated potentials behave similarly, and we will discuss the example of alkali atoms in chapter 3. (One should therefore compare Figure 2.5 to Figure 3.2, respectively eq. (2.47) to eq. (3.13).)

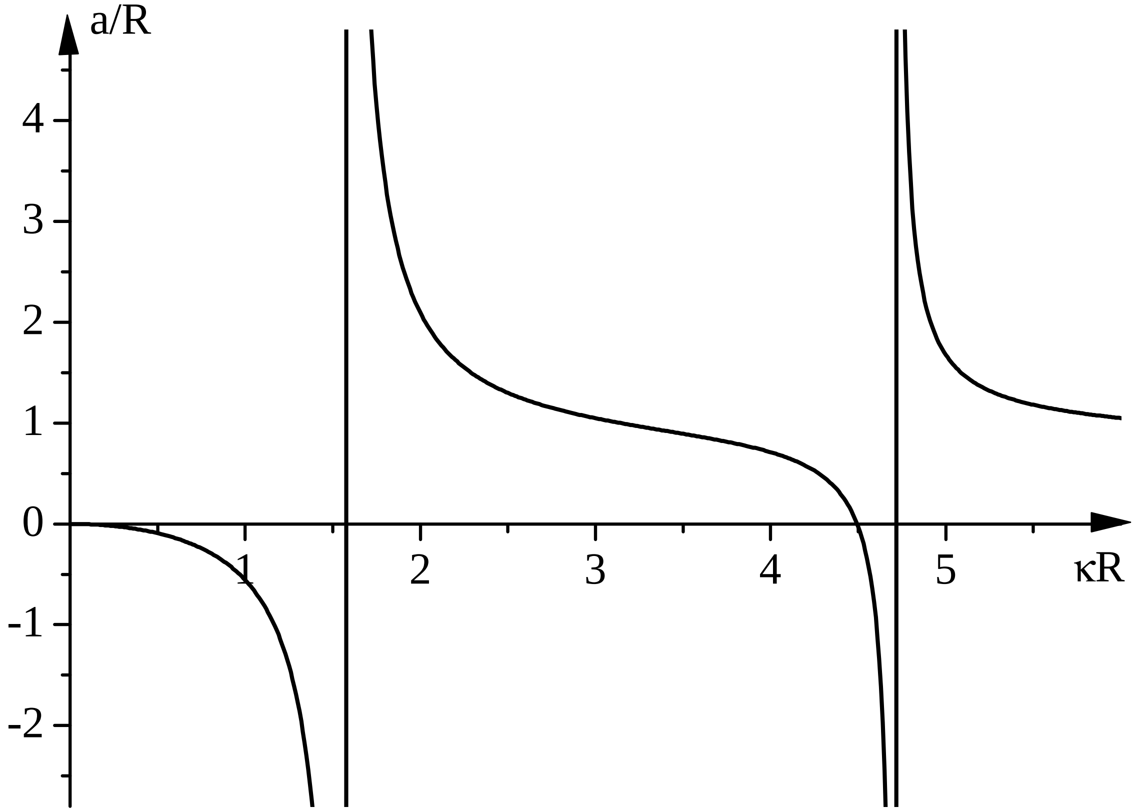

Figure 2.5: Scattering length for the rectangular well calculated according to eq. (2.47).

Now we want to take a closer look at the meaning of the scattering length in this example. We can find appropriate combinations of V_0 and R, so that the potential has a positive, negative and infinite scattering length (Figure 2.6(b), 2.6(c), 2.6(d)).

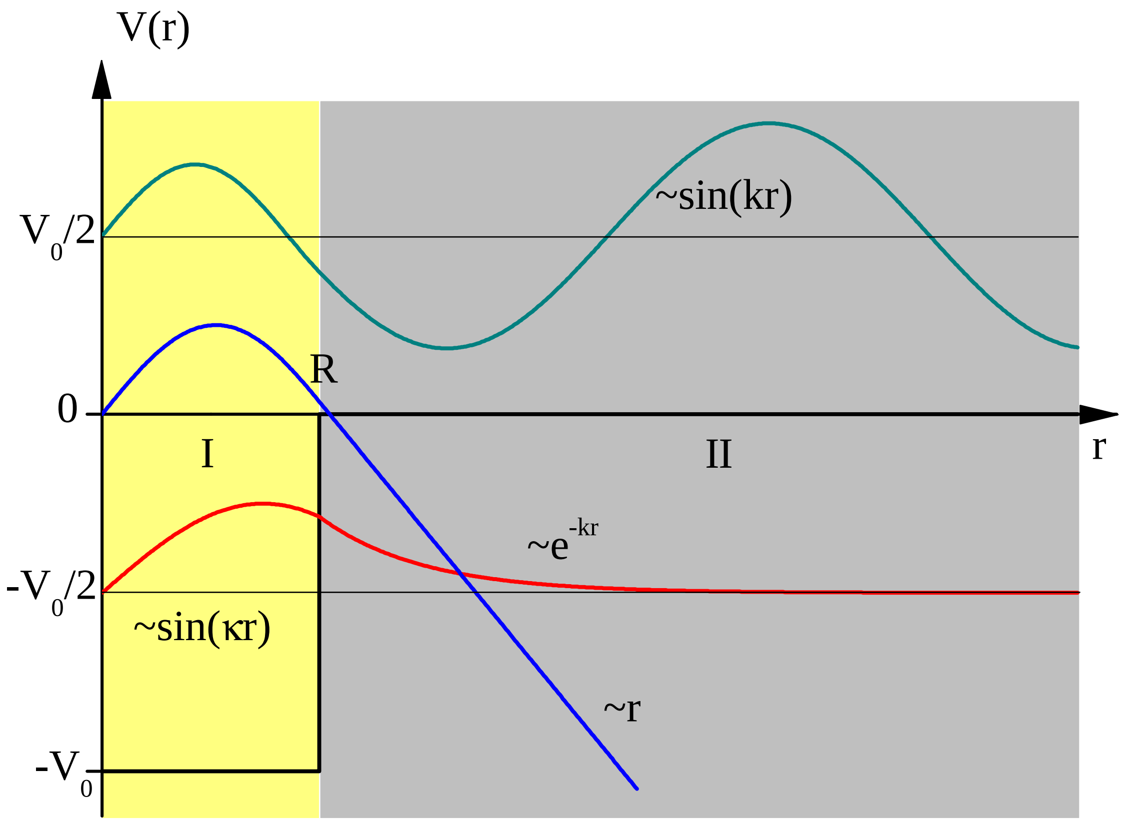

(a) Analytical solution for various energies

Figure 2.6: Solution for the rectangular well

The change in sign and the resonance-like behavior of the scattering length can be explained by the development of a new bound state. We see that the bound state solution outside the well is proportional to $\exp(-kr)$. When $k \to 0$, this is a constant function, which agrees with the solution in Figure 2.6(d). The pole in the plot of the scattering length in Figure 2.5 is therefore equivalent to a quasi-bound state at zero energy. To emphasize this fact, we calculate the energy of the bound state. We know now that the solution for infinitesimal negative energies is proportional to $\exp(-kr)$. From the previous discussion we can also see that the solution for infinitesimal positive

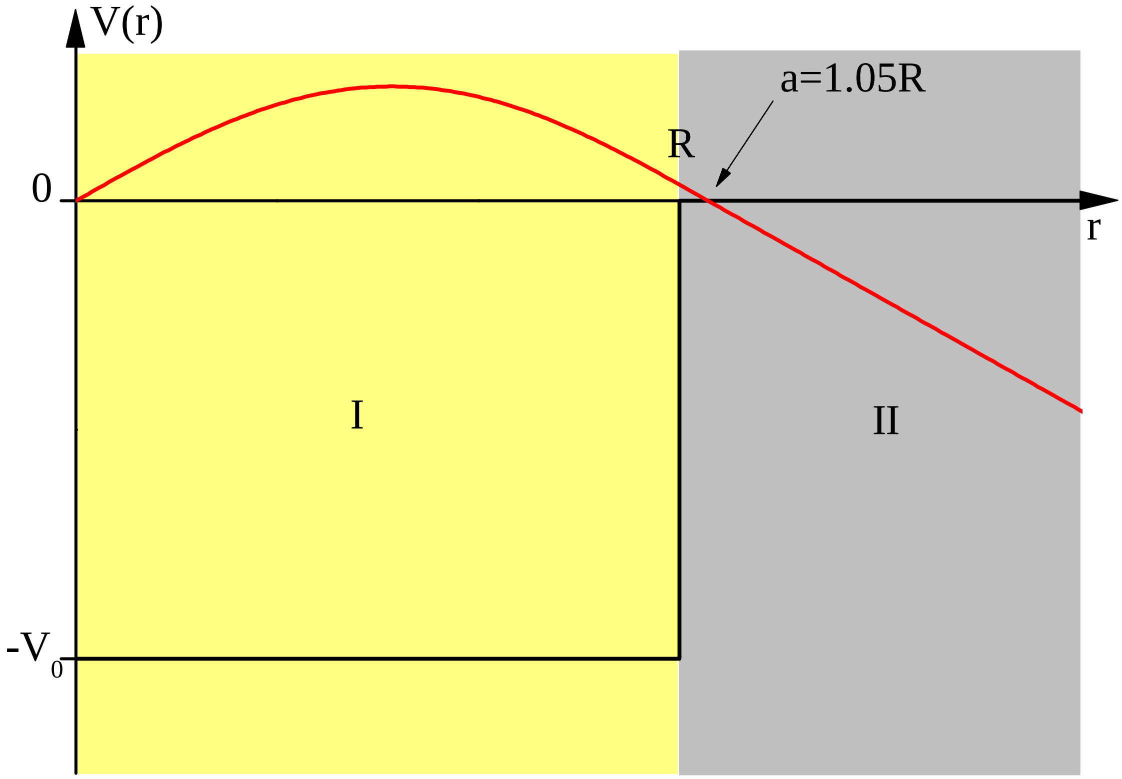

(b) Positive scattering length

Figure 2.6: Continued

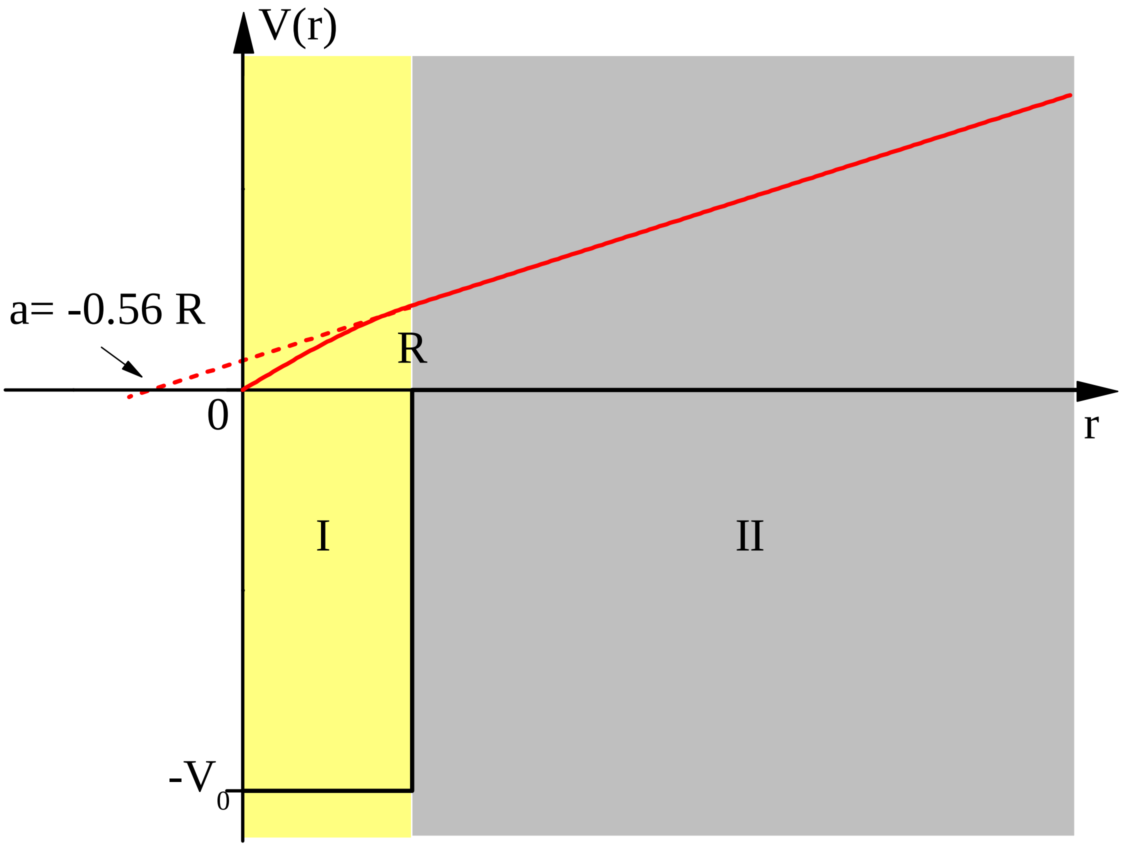

(c) Negative scattering length

Figure 2.6: Continued

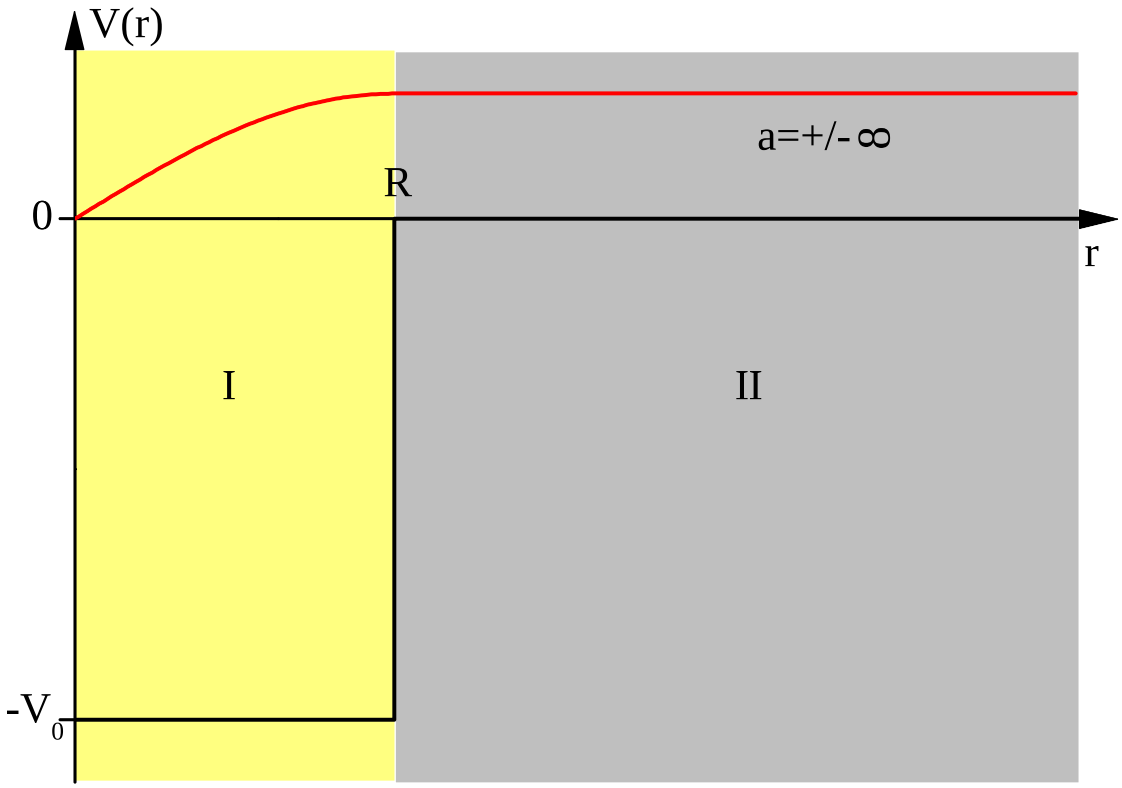

(d) Resonant bound state at zero energy

Figure 2.6: Continued

energies is proportional to $(r-a)$ (eq. (2.40)). Now we take the logarithmic derivative at $r = R$

$$-\frac{ke^{-kR}}{e^{-kR}} = \frac{1}{R-a} \overset{R \ll |a|}{\simeq} -\frac{1}{a} \tag{2.48}$$

$$\Rightarrow k \simeq \frac{1}{a} \ . \tag{2.49}$$

The energy of the bound state is therefore given by

$$E_{bs} = \frac{\hbar^2 k^2}{2\mu} = \frac{\hbar^2}{2\mu a^2} \ . \tag{2.50}$$

Furthermore the cross section shows a Lorentzian behavior near the resonances for small k. That can be seen from the following derivation. Firstly we rewrite the phase shift (eq.(2.45) and (2.47))

$$\delta_0(k) = \arctan\left(-ka + kR\right) - kR \ . \tag{2.51}$$

For $k \ll 1$ and $a \gg R$ (i.e. near resonance with a quasi-bound state) we can approximate this as

$$\delta_0(k) \simeq \arctan\left(-ka\right) \ . \tag{2.52}$$

Now it follows for the total cross section (eq.(2.23))

$$\sigma_0 = \frac{4\pi}{k^2}\sin^2\delta_0(k) = \frac{4\pi}{k^2}\frac{\tan^2\delta_0(k)}{1+\tan^2\delta_0(k)} \simeq \frac{4\pi a^2}{1+k^2a^2} \ . \tag{2.53}$$

We compare this behavior to the exact solution in Figure 2.7. Note that this approximation is just valid for $a \gg R$, which means near the resonances. One can see that the limit of $k \to 0$ holds and we get the expected cross section of $4\pi a^2$.

It is also very interesting that there are cases where the total cross section is zero. Especially at very low temperatures where higher partial waves are unimportant, one finds energies where the incident wave gets almost perfectly transmitted. This

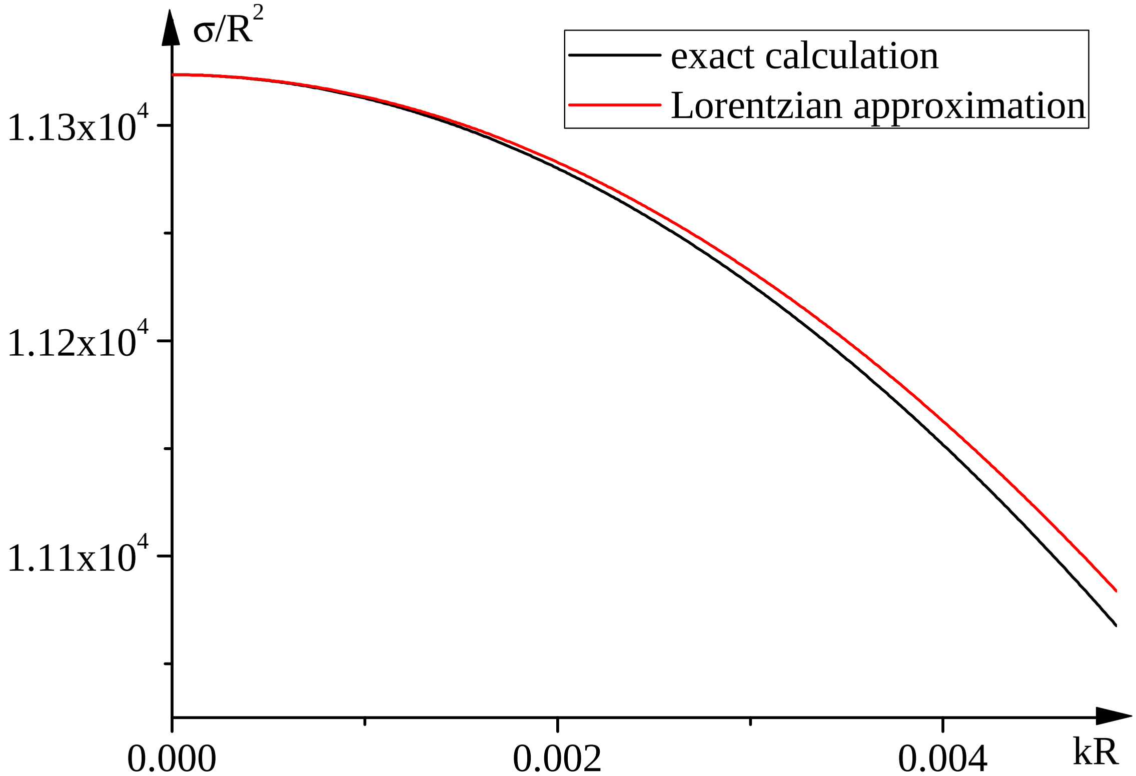

Figure 2.7: Lorentzian behavior of the total cross section for rectangular well for low energies (with $\kappa R = 1.55 \;\Rightarrow\; a \simeq -30R$)

effect is called Ramsauer-Townsend effect. It was first discovered by Carl Ramsauer in 1920 when he measured the transmission of slow electrons through gases [28]. It was the first sign of the wave properties of electrons and led to the definition of the cross section. In classical electromagnetism one would expect a lower cross section for faster electrons, because they should interact less with the gas molecules when they have a higher velocity. The quantum mechanical derivation above gives a qualitative explanation for this effect.

2.2 Inelastic collisions

So far we have dealt with single channel elastic scattering, i.e. the system has just one possible kinetic energy for the relative motion at each internuclear distance. That is true, for example, for the scattering of a single electron in a central potential. As soon as one is considering composite systems, such as atoms, with several internal degrees of freedom (and therefore different energy levels), exchange collisions (i.e. inelastic collisions) become important. In general there are different values for the kinetic energy, because the system can be in the ground state or different possible excited states for a given total energy. Therefore the initial and final internal state of a scattering process do not have to be the same. The criteria for a possible transition during the process are the conservation laws (conservation of energy, angular momentum), which are consequences of symmetries. When we refer to atoms, the total rotational invariance in the absence of external fields leads to the conservation of the overall angular momentum, which corresponds to a set of good quantum numbers (often denoted by F, M_F).

Inelastic processes are generally more difficult to compute, because accurate information about possible coupled states is required. Inelastic collisions at low energy can be described by a complex scattering length with its real (imaginary) part corresponding to the elastic (inelastic) scattering.

We begin this section by dealing with the special case of a potential with two channels at short-range and one channel at long-range, which can be treated elastically to a first approximation. Afterwards we investigate the simplest case of two coupled channels which leads to the close-coupling equation. For illustrative purposes, we present an example for the numerical solution of the close-coupling equation in Appendix B.

2.2.1 Two-channel elastic scattering length and elastic spin-flip cross section

Here we want to present a simple approach to compute the low energy scattering parameters of alkali collisions which we will use later on in section 3.5. Alkali interaction potentials in the absence of external fields are dominated by the hyperfine interaction at long-range and the central potential at short-range (see section 3.1). As the atoms approach each other, the electronic clouds overlap and the spin wave functions form a singlet and triplet state. To a first approximation the interaction is therefore diagonal in the singlet/triplet representation at small interatomic distances. However, at long-range the interaction is diagonal in the hyperfine representation. Between those two regimes, in the so-called recoupling region, a diagonal representation of the interaction does not exist. An exact treatment of the scattering problem would therefore require a close-coupling calculation (see next section). However, if one ignores the recoupling region, i.e. assumes that the transition between the long-range hyperfine states and short-range singlet and triplet states occurs suddenly, the recoupling can be done by projection of the corresponding angular momentum eigenstates (see [29], [30]). Hence, the scattering problem simplifies to a single channel calculation at short-range and the projection of the singlet/triplet state on the initial and final states, respectively.

The following derivation is similar to the discussion in [31]. As we will treat the singlet and triplet channel separately, we get two different scattering amplitudes (corresponding to eq. (2.12))

$$f^{(S)}(k,\theta) = \frac{1}{2ik}\sum_{l=0}^{\infty}\left[e^{2i\delta_l^{(S)}(k)} - 1\right](2l+1)P_l(\cos\theta) \ . \tag{2.54}$$

As we look particularly at s-wave scattering ($l = 0$) in the low energy limit ($k \to 0$), we find (after using L'Hospital's rule once):

$$f^{(S)} = \lim_{k\to 0}\left[\frac{d}{dk}\delta_0^{(S)}(k)\right] \cdot e^{2i\delta_0^{(S)}(k)} \ . \tag{2.55}$$

Using eq. (2.37) and (2.38), which is Levinson's theorem, implies

$$f^{(S)} = -a^{(S)} \ . \tag{2.56}$$

In the general case where we allow exchange collisions (i.e. the initial and final spin-states of the atoms are different), we can write the asymptotic wave function as (compare to eq. (2.1))

$$\begin{aligned} &\Psi(\vec{r}; f_1, m_{f_1}, f_2, m_{f_2}) \xrightarrow{R\to\infty} \chi(f_1, m_{f_1})\chi(f_2, m_{f_2})e^{i\vec{k}\cdot\vec{r}} \\ &+ \sum_{\substack{f_1', m_{f_1}' \\ f_2', m_{f_2}'}} \chi(f_1', m_{f_1}')\chi(f_2', m_{f_2}') \cdot f^{(f_1, m_{f_1}, f_2, m_{f_2}; f_1', m_{f_1}', f_2', m_{f_2}')}(k,\theta) \cdot \frac{e^{ikr}}{r} \ , \end{aligned} \tag{2.57}$$

where we sum over all possible final hyperfine states for the scattered wave. The primed and unprimed quantum numbers indicate the final and initial states respectively. $\vec{r}$ is the relative coordinate and χ denotes the spin wave functions.

Now we want to write the scattering amplitude $f^{(f_1,\ldots)}$ in terms of the known scattering amplitude $f^{(S)}$. Recoupling yields

$$f^{(f_1, m_{f_1}, f_2, m_{f_2}; f_1', m_{f_1}', f_2', m_{f_2}')}(k,\theta) = \sum_{S}\sum_{m_S, I, m_I} A_{S, m_s, I, m_I}^{f_1, m_{f_1}, f_2, m_{f_2}} A_{S, m_s, I, m_I}^{f_1', m_{f_1}', f_2', m_{f_2}'} f(S; k, \theta) \ . \tag{2.58}$$

The coefficients A are derived in the Appendix A.

Restricting ourselves to **elastic scattering**, which means **no exchange collisions**, i.e. $f_1 = f_1', m_{f_1} = m_{f_1}', \ldots$, yields the simple form (using eq. (2.56) and (A.4)):

$$f^{(f_1, m_{f_1}, f_2, m_{f_2})} = -\sum_S P^{(S)} \cdot a^{(S)} \;, \tag{2.59}$$

where the $P^{(S)}$ are also derived in the Appendix A. If we now define analogical to eq. (2.56) a "combined" scattering length a, we get

$$a = a^{(0)} P^{(0)} + a^{(1)} P^{(1)} \tag{2.60}$$

as a weighted average of the singlet and triplet scattering lengths.

Now we would like to compute the spin-flip cross section in this approximation. We just consider the case when one atom changes its hyperfine state, but the other one remains unchanged, i.e. $f_1 \neq f_1', m_{f_1} = m_{f_1}', f_2 = f_2', m_{f_2} = m_{f_2}'$ ($m_{f_1} = m_{f_1}'$ follows from angular momentum conservation). In this case eq. (2.38) can be simplified to (see Appendix A)

$$f^{(f_1 \to f_1')} = \frac{\sqrt{M_{SF}}}{2} \left(a^{(1)} - a^{(0)} \right) \;. \tag{2.61}$$

M_{SF} depends on the participating hyperfine channels. Therefore the spin-flip cross section can be written as

$$\sigma_{SF} = 4\pi \left| f^{(f_1 \to f_1')} \right|^2 = M_{SF} \pi \left(a^{(1)} - a^{(0)} \right)^2 \;. \tag{2.62}$$

Note that this cross section is still an approximation, because in reality there are other interactions besides spin-coupling which are responsible for spin-flips and inelastic processes. On the other hand we restrict ourselves to a partially elastic process, because the second atom does not change its state. Nevertheless, this approximation is often used in order to estimate inelastic transition rates ([32],[17]).

2.2.2 *Two-channel scattering and close-coupling equation*

In this section we would like to investigate the simplest case of inelastic scattering for two coupled channels, which leads to the close-coupling equation. For the interested reader we present a numerical solution for this equation with a simple example in Appendix B.

As we have seen in section 2.1.1, solving the elastic scattering problem reduces to solving the Schrödinger equation and claiming a particular long-range behavior for its solution (see eq. (2.1)). That is in principle also true for the description of inelastic scattering, but the scalar potential and scattering amplitudes are replaced by corresponding matrices.

The following derivation is for example given in [22]. We denote the relative coordinate with $\vec{r}$, the relative momentum with $\vec{p}$ and the two asymptotic states with $|0\rangle$ and $|1\rangle$. Note that those states could already be product states, e.g. $|0\rangle \equiv |f_1, m_{f_1}; f_2, m_{f_2}\rangle$ in the case of the hyperfine interaction. The Hamiltonian of the relative motion is given by

$$\hat{H} = \frac{\hat{p}^2}{2\mu} + \hat{V}(\hat{\vec{r}}) \ . \tag{2.63}$$

And we can write our overall state in coordinate representation

$$|\Psi\rangle = \left\{ \int d^3r \, |\vec{r}\rangle \langle\vec{r}| \otimes \sum_{i=0,1} |i\rangle \langle i| \right\} |\Psi\rangle \ , \tag{2.64}$$

or

$$|\Psi\rangle = \sum_{i=0,1} \int d^3r F_i(\vec{r}) \cdot |\vec{r}, i\rangle \tag{2.65}$$

with $F_i(\vec{r}) = \langle\vec{r}, i|\Psi\rangle$. The Schrödinger equation

$$\hat{H} \, |\Psi\rangle = \left(\frac{\hat{p}^2}{2\mu} + \hat{V}(\hat{\vec{r}}) \right) |\Psi\rangle \tag{2.66}$$

can be written as a coupled differential equation. Therefore we multiply it from the left side with $\langle i|$ and get (using $\hat{H}\,|i\rangle = E_i\,|i\rangle = \frac{\hbar^2}{2\mu}k_i^2\,|i\rangle$)

$$\langle i|\,\hat{H}\,|\Psi\rangle = E_i\langle i|\Psi\rangle = \langle i|\left(\frac{\hat{p}^2}{2\mu} + \hat{V}(\hat{\vec{r}})\right)|\Psi\rangle \ . \tag{2.67}$$

Slight rearranging and inserting some butterfly operators leads to

$$\begin{aligned} E_i\langle i|\Psi\rangle &= \int d^3r E_i F_i(\vec{r}) = \langle i|\left(\frac{\hat{p}^2}{2\mu} + \hat{V}(\hat{\vec{r}})\right)|\Psi\rangle \\ &= \int d^3r \int d^3r' \langle i|\vec{r}\rangle\, \langle\vec{r}|\,\frac{\hat{p}^2}{2\mu}\,|\vec{r'}\rangle\,\langle\vec{r'}|\Psi\rangle + \int d^3r\,\langle i|\,\hat{V}(\hat{\vec{r}})\,|\Psi\rangle \\ &= \int d^3r\left(-\frac{\hbar^2}{2\mu}\nabla^2 F_i(\vec{r}) + \sum_{j=0,1}\langle i|\,\hat{V}(\hat{\vec{r}})\,|j\rangle\,F_j(\vec{r})\right) . \end{aligned} \tag{2.68}$$

That yields the close-coupling equations

$$\left(\frac{\hbar^2}{2\mu}\nabla^2 + E_i\right)F_i(\vec{r}) = \sum_j V_{ij}(\vec{r})F_j(\vec{r}) \qquad (i=0,1)\ , \tag{2.69}$$

where we used that $\langle\vec{r}|\,\frac{\hat{p}^2}{2\mu}\,|\vec{r}\,'\rangle = -\frac{\hbar^2}{2\mu}\nabla^2\delta(\vec{r}-\vec{r}\,')$ and the definition of the interaction matrix

$$V_{ij}(\vec{r}) = \langle i|\,\hat{V}(\hat{\vec{r}})\,|j\rangle \ . \tag{2.70}$$

The requirement that $\hat{V}$ is hermitian yields $V_{ij} = V_{ji}^*$. We will assume that the interaction matrix is real though and that it has just a radial dependence $V_{ij}(r)$. That allows us to separate the functions $F_i(\vec{r})$ and do a partial wave expansion

$$F_i(\vec{r}) = \frac{1}{k_0 r}\sum_l (2l+1)G_{il}(r)P_l(\cos\theta)\ , \tag{2.71}$$

which leads to the following coupled differential equations:

$$\begin{aligned}\left[\frac{d^2}{dr^2}+k_0^2-\frac{l(l+1)}{r^2}-\frac{2\mu}{\hbar^2}V_{00}(r)\right]G_{0l}(r)&=\frac{2\mu}{\hbar^2}V_{01}(r)G_{1l}(r)\\ \left[\frac{d^2}{dr^2}+k_1^2-\frac{l(l+1)}{r^2}-\frac{2\mu}{\hbar^2}V_{11}(r)\right]G_{1l}(r)&=\frac{2\mu}{\hbar^2}V_{10}(r)G_{0l}(r)\ .\end{aligned} \tag{2.72}$$

The partial wave amplitudes G_{il} must satisfy the following conditions (similar to the discussion in section 2.1.1; contrary to the previous case, here the factor α_l is dimensionless, i.e. $\alpha_l = f_l \cdot k_0$):

$$\begin{aligned}G_{il}(0)&=0\\ G_{0l}&\simeq i^l\sin\left(k_0r-l\frac{\pi}{2}\right)+\alpha_l^{00}e^{ik_0r}\\ G_{1l}&\simeq\alpha_l^{01}e^{ik_1r}\ .\end{aligned} \tag{2.73}$$

Note that we assumed that we enter in the $|0\rangle$-channel and that $V_{ij}(r\to\infty)\to 0$. If we have potentials which don't vanish at infinity, but approach a constant value ϵ_i (e.g. hyperfine interaction), then the energy of the outgoing wave in the $|1\rangle$-channel will be $E_1 = E_0+\epsilon_0-\epsilon_1$ (see Figure 2.8) and that's why we define the outgoing wave number as

$$k_1=\sqrt{k_0^2+\frac{2\mu}{\hbar^2}\left(\epsilon_0-\epsilon_1\right)} \tag{2.74}$$

and the asymptotic behavior is still valid. Note that k_1 can now be imaginary, if the incoming channel lies below the outgoing channel. In this case the inelastic scattering is forbidden and the lower channel is closed. Note however that closed channels can still play an important role, e.g. in Feshbach resonances (see section 4.2.2).

The partial elastic and inelastic differential cross sections are now given by ($f_l =$

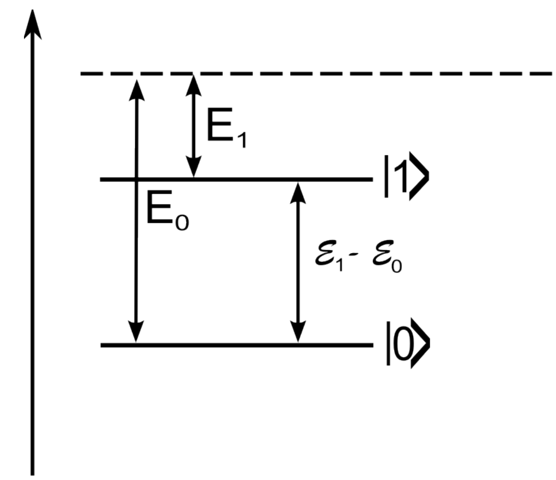

Figure 2.8: Energy conservation during inelastic scattering process with hyperfine interaction

$\frac{\alpha_l}{k_0})$

$$\begin{aligned}\frac{d\sigma_l^{00}}{d\Omega} &= \left|\frac{(2l+1)\alpha_l^{00}\cdot P_l(\cos\theta)}{k_0}\right|^2 \\ \frac{d\sigma_l^{01}}{d\Omega} &= \frac{k_1}{k_0}\left|\frac{(2l+1)\alpha_l^{01}\cdot P_l(\cos\theta)}{k_0}\right|^2 \quad .\end{aligned} \tag{2.75}$$

Integrating yields the according partial total cross sections

$$\sigma_l^{00} = \frac{4\pi}{k_0^2}(2l+1)\left|\alpha_l^{00}\right|^2 \qquad \text{and} \qquad \sigma_l^{01} = \frac{4\pi k_1}{k_0^3}(2l+1)\left|\alpha_l^{01}\right|^2 \ , \tag{2.76}$$

where we used

$$\int_{-1}^{1} dx \ P_l(x)P_m(x) = \frac{2\delta_{lm}}{2l+1} \ . \tag{2.77}$$

The factor k_1/k_2 arises for the following reason: The cross section is defined as the ratio of the flux of scattered particles to the flux of incident particles integrated over the solid angle. At a distance r from the origin the scattered flux is v_1 times the particle number (or probability to find a particle) per unit volume $\left|\frac{\alpha}{k_0 r}\right|^2$. The incident flux is given by v_0 per unit volume. As $v_i \sim k_i$ and therefore $\frac{v_1}{v_0} = \frac{k_1}{k_0}$, we get $d\sigma^{01} = \frac{k_1}{k_0}\left|\frac{\alpha^{01}}{k_0 r}\right|^2 \cdot r^2 d\Omega$, which yields the desired result.

There are several different ways of expressing the three independent parameters α^{00}, α^{01} and α^{11} which characterize the scattering process (for each partial wave independently). Mott and Massey [22] talk of two phase shifts $\delta^{(a)}$, $\delta^{(b)}$ and a mixing parameter χ. Many texts deal instead with the S-Matrix elemens S_{00}, S_{01} and S_{11} (see e.g. in [26]), where

$$S_{ij} = \delta_{ij} + 2i\sqrt{\frac{k_j}{k_i}}\alpha^{ij} \ . \tag{2.78}$$

The given discussion can be easily generalized when more than two states are coupled, which means that one just has to solve more coupled differential equations and therefore gets more independent parameters. Generally a cross section for each transition can be defined similarly to eq. (2.76).

CHAPTER 3

COLLISIONS BETWEEN ALKALI ATOMS

The goal of achieving BEC motivated the study of cold alkali collisions as we discussed in chapter 1. Experimental methods like photoassociation spectroscopy or clock-shift measurements (see section 4.2) led to accurate data for the alkali interaction potentials, which we would like to discuss in the beginning of this chapter. Afterwards we present a theoretical method, which allows us to compute the scattering length directly from the energy spectrum of the potential, in particular the highest bound state. This method is especially useful, because in practice the bound state energy can be determined spectroscopically. The rest of this chapter follows the structure of the last one, i.e. firstly we discuss elastic scattering before taking into account inelastic collisions. In section 3.3 we present a numerical solution of the elastic scattering problem for the Na-Rb potential and calculate not only the singlet and triplet s-wave scattering lengths, but also the bound state energies. At the end of this chapter we discuss some properties of inelastic alkali atom collisions and treat the two-channel scattering in the elastic limit.

3.1 Alkali interaction potentials

Alkali atoms in the ground level have zero angular momentum, $l = 0$, and can be treated as single electron atoms because all shells are closed except for the outermost one. The electron and nucleus have spins $\vec{s}$ and $\vec{i}$ and the corresponding spin states s, m_s (with $s = 1/2$) and i, m_i respectively. (Nuclear spins for common alkalis are given in Table 3.1.) Those spins couple to $\vec{f} = \vec{s} + \vec{i}$ with hyperfine quantum numbers f, m_f where $f = i \pm 1/2$ (as we limit our discussion on s-wave scattering).

Table 3.1: List of nuclear spins for alkali isotopes

Isotope	Nuclear spin i
^{7}Li	3/2
^{23}Na	3/2
^{39}K	3/2
^{41}K	3/2
^{85}Rb	5/2
^{87}Rb	3/2
^{133}Cs	7/2

The general problem of the calculation of interaction potentials for diatomic systems is very complicated. A helpful tool is the Born-Oppenheimer approximation [33], which employs an adiabatic assumption justified because the electrons move much faster than the heavier nuclei. Therefore one fixes the internuclear distance r, calculates the electronic eigenstates as a function of r and adds the nuclear energy in order to obtain the overall energy. The resulting potential is dominated by different terms in the long-range and short-range regions. According to [29] the important contributions to the interaction potential between two alkali atoms can be written as

$$V = V_c + V_{hf} + V_Z + V_d + V_{so} \ . \tag{3.1}$$

The different terms are the following:

- V_c is the central potential. It dominates the interaction at small interatomic distances.

  In the regime ($r \lesssim 20\ a_0$) the overlap between the electronic clouds of the two atoms is large and the system has to be treated by molecular concepts. The interaction is dominated by the electronic spins ($s_i = 1/2$) which couple to $\vec{S} = \vec{s_1} + \vec{s_2}$ and form either a singlet ($S = 0$) or triplet ($S = 1$) state.

The triplet potential must have a higher energy, because the electrons have a larger separation due to Pauli's exclusion principle [25] which yields an effective repulsion. As we concentrate on ground state collisions, i.e. $l_1 = l_2 = 0$, the corresponding molecular states are ${}^1\Sigma_g^+$ and ${}^3\Sigma_u^+$ (see Appendix C).
At slightly larger distances, when the overlap between the clouds decreases, the remaining spin-interaction can be written as the exchange term $\pm E_{\text{exch}} = A_{\text{ex}} r^{\gamma} e^{-\beta r}$ where the plus (minus) sign stands for the triplet (singlet) state. It reflects the effective repulsion between these two states due to the spin coupling. Furthermore the dispersion interaction becomes important in this regime, i.e. van der Waals- and higher order terms $\sim -C_6/r^6 - C_8/r^8 - ...$, which is due to the interaction between temporary induced dipole moments (and higher multipoles). The quantum numbers S, M_S are good at small distances and therefore the central potential can be written in terms of the singlet and triplet interaction potentials and their projection operators: $V_c(r) = \hat{P}^{(0)} V^{(0)}(r) + \hat{P}^{(1)} V^{(1)}(r)$.

- V_{hf} is the hyperfine interaction due to the coupling of the electronic and nuclear spin for each atom. It can be written as

$$V_{hf} = \sum_{n=1}^{2} A_n \vec{i_n} \cdot \vec{s_n} = \sum_{n=1}^{2} \frac{A_n}{2} \left(f_n(f_n+1) - i_n(i_n+1) - \frac{3}{4} \right) . \tag{3.2}$$

  A_n is the hyperfine constant for each atom.

- V_Z is the potential due to the Zeeman effect. This term is zero for a vanishing magnetic field, but can be generally written as

$$V_Z = \sum_{k=1}^{2} \left(\vec{\mu_k^e} \cdot \vec{B} + \vec{\mu_k^n} \cdot \vec{B} \right) , \tag{3.3}$$

  where $\vec{\mu_k^e}$ and $\vec{\mu_k^n}$ are the electron and nuclear magnetic moments. $\vec{\mu_k^e}$ is for example

$$\vec{\mu_k^e} = -g_S \mu_B \frac{\vec{s_k}}{\hbar} \tag{3.4}$$

with $g_S \approx 2$ and the Bohr Magneton μ_B. The nuclear magnetic moment is about a factor of m_n/m_e smaller and therefore the second term in V_Z can be usually neglected.

- V_d is the interaction between the dipole moments of the electrons and nuclei among each other. The nuclear contribution is generally much smaller and can be neglected. If we work in atomic units, we get the following dipole-dipole interaction (from [34])

$$V_d = -\alpha^2 \left(\frac{3(\hat{R}_{ee} \cdot \vec{s_1})(\hat{R}_{ee} \cdot \vec{s_2}) - \vec{s_1} \cdot \vec{s_2}}{R_{ee}^3} \right) \tag{3.5}$$

with the fine structure constant α. In our case the electron-electron separation $\vec{R}_{ee}$ can be approximated by the internuclear distance $\vec{r}$. This interaction is diagonal in the basis $(\vec{S}^2, S_n = \vec{S} \cdot \hat{r})$ and we get for the energy shift

$$V_d = -\frac{\alpha^2}{2r^3} \left(3m_S^2 - S(S+1) \right) \ , \tag{3.6}$$

where we used $\vec{s_1} \cdot \vec{s_2} = (\vec{S}^2 - \vec{s_1}^2 - \vec{s_2}^2)/2$ and $s_1 = s_2 = 1/2$.

- V_{so} is the spin-orbit interaction due to coupling between orbital angular momentum and spin.

The last two terms are much smaller than the others and can therefore be neglected in most cases. One exception occurs when one wants to calculate the inelastic collision rate in a doubly spin-polarized mixture, in which exchange collisions are forbidden (see section 3.4). In this case the dipole interaction is responsible for trap losses.

Figure 3.1 shows the interaction potential for Rb-Rb. One can see that at short-range the spin quantum numbers S, m_S (and I, m_I, if we take into account the nuclear spin as well) are good. At long-range, where the central potential goes to zero and the hyperfine interaction dominates, there are the good quantum numbers $f_1, m_{f_1}, f_2, m_{f_2}$. Between those two regimes there are just F and m_F as good quantum numbers, which correspond to the overall angular momentum of the colliding system

$$\vec{F} = \vec{f_1} + \vec{f_2} = \vec{S} + \vec{I} \, . \tag{3.7}$$

F and m_F are always good quantum numbers for zero magnetic field. In case of a non-vanishing $\vec{B}$, the rotational symmetry is broken and just m_F is conserved.

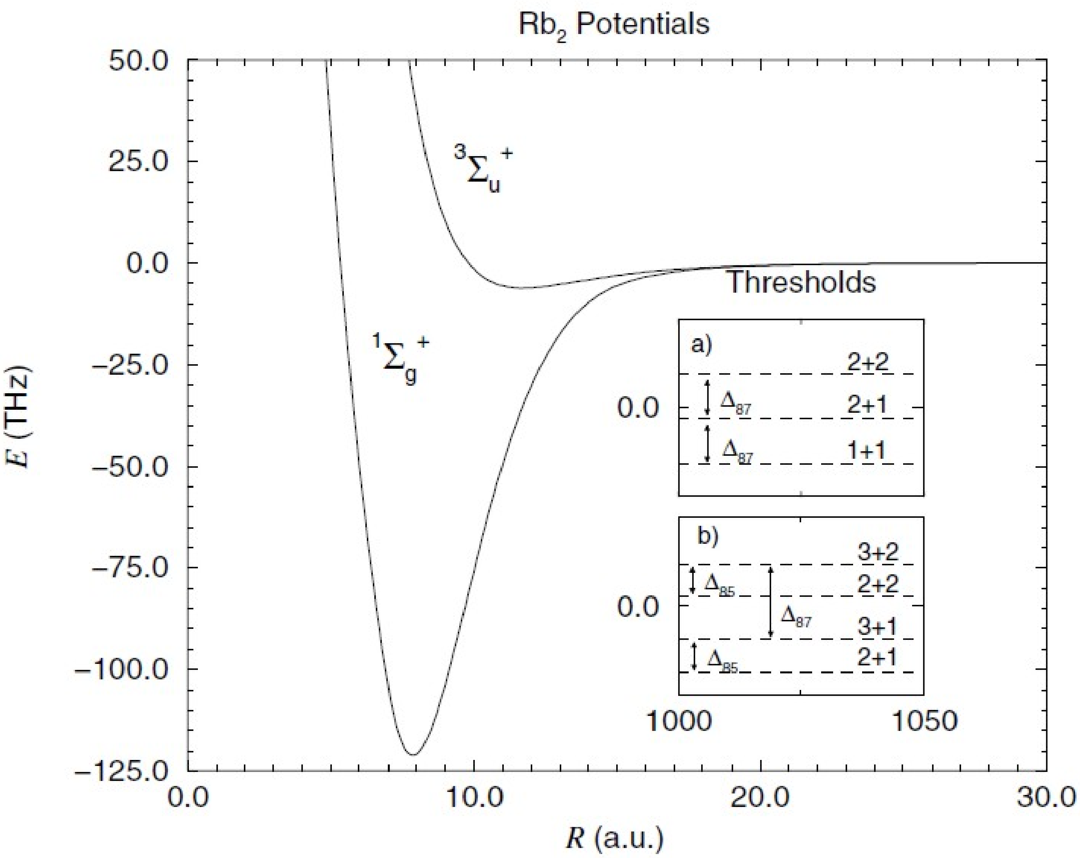

Figure 3.1: The singlet and triplet Rb_2 potentials. The inset shows the tresholds for the long-range part dominated by the hyperfine structure: a) ^{87}Rb + ^{87}Rb and b) ^{85}Rb + ^{87}Rb. The hyperfine levels are denoted by each atom's quantum numbers $f_1 + f_2$ and the hyperfine splittings are $\Delta_{85} = 3.036$ GHz and $\Delta_{87} = 6.835$ GHz, which is about 4 orders of magnitude less than the short-range interaction. (from [34])

3.2 Connection between the scattering length and the highest bound state

It is possible to determine the phase shift, i.e the scattering length, for s-wave scattering from the long-range part of the potential (by which we mean the van der Waals interaction $-C_6/r^6$, because the hyperfine interaction just gives an overall shift of the energies) and the knowledge of the energy of the highest bound state in the short-range part. One way of determining the scattering length is by analyzing the short-range potential spectroscopically to obtain the energy spectrum and the highest bound state directly. Further details concerning the experimental realization, especially for KRb potentials, have been described in [19].

Flambaum et al. [27] have given a derivation for a general long-range potential which is proportional to $-\alpha/r^n$. Applied to the case of the van der Waals interaction ($n = 6$, $\alpha = C_6$), the scattering length is given by

$$a = \bar{a}\left(1 - \tan\left(\Phi - \frac{\pi}{8}\right)\right) \tag{3.8}$$

with the mean scattering length

$$\bar{a} = \frac{\Gamma\left(\frac{3}{4}\right)}{2\sqrt{2}\cdot\Gamma\left(\frac{5}{4}\right)}\left(\frac{2\mu C_6}{\hbar^2}\right)^{\frac{1}{4}} \quad . \tag{3.9}$$

One can rewrite eq. (3.8) in terms of the "vibrational quantum number at dissociation" ν_D, which does not have to be an integer. The spacing between the bound states is in first order determined by the long-range potential. The vibrational quantum number is the number of an imaginary quasi-bound state at $E = 0$ (energy of dissociation). An integer value of ν_D means that there is actually a quasi-bound state at zero energy.

With this quantum number, the energy of the last bound state is given by [35]

$$E_\nu = -\left[(\nu_D - \nu)\, H_6\right]^3 \tag{3.10}$$

with $\nu = \mathrm{IntegerPart}(\nu_D)$ and the constant

$$H_6 = 2\hbar\sqrt{\frac{2\pi}{\mu}}\frac{\Gamma\left(\frac{7}{6}\right)}{\Gamma\left(\frac{1}{3}\right) C_6^{1/6}} \ . \tag{3.11}$$

When we look at eq. (3.8), we see that the scattering length goes to $\pm\infty$, if $\Phi - \frac{\pi}{8} = \frac{\pi}{2} + N\pi$ (N=1,2,3,...). That corresponds to the moment when one new bound state starts to appear (compare to the case of the rectangular well in section 2.1.3). With this knowledge, it is natural to rewrite

$$\Phi - \frac{\pi}{8} \equiv \pi\left(\nu_D + \frac{1}{2}\right) \tag{3.12}$$

and therefore get

$$a = \bar{a}\left[1 - \tan\left(\pi\left(\nu_D + \frac{1}{2}\right)\right)\right] \ . \tag{3.13}$$

With eq. (3.10) and the fact that $(\nu_D + n)$ and ν_D lead to the same scattering length (if n integer) we can write

$$\nu_D = \frac{\sqrt[3]{|E_{hbs}|}}{H_6} \ , \tag{3.14}$$

where E_{hbs} is the energy of the highest bound state.

In Figure 3.2 we show, how the scattering length changes with the vibrational quantum number (compare this also to the case of the rectangular well in Figure 2.5). With increasing ν_D it diverges whenever a new bound state starts to appear. This resonant behavior should be compared to the case of the rectangular well in section 2.1.3. Looking at eq. (3.13) also shows that a positive scattering length is three times more likely than a negative one. That means that the potential is on

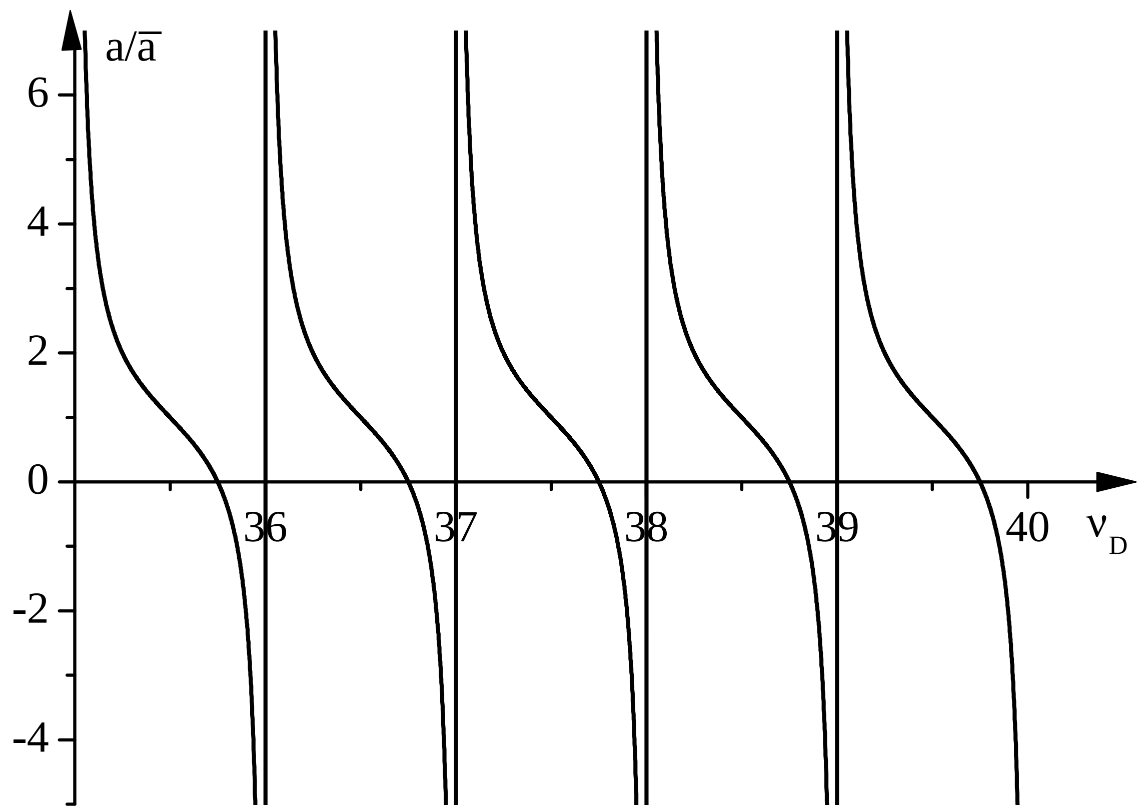

Figure 3.2: Scattering length for potentials with a long-range dependence $\propto -\frac{1}{r^6}$ in terms of the mean scattering length vs. vibrational quantum number (eq. (3.13))

average repulsive.

3.3 Elastic scattering of sodium and rubidium

The motivation of this work was to experimentally study mixtures of ultracold sodium-rubidium gases. We will compute the scattering lengths for Na-Rb collisions numerically by solving the Schrödinger equation for the interaction potential of sodium-rubidium. We take the potential data from ref. [18]. At the end of this section, we also determine some bound state energies for the singlet potential of $^{23}\mathrm{Na}^{85}\mathrm{Rb}$.

3.3.1 Singlet and triplet interaction potential for sodium-rubidium

Pashov et al. measured and calculated accurate potentials for Na-Rb [18]. We imported the data points and characteristic constants from their paper and interpolated the potentials with Mathematica (see Figure 3.3).

For intermediate internuclear distances ($r > R_0$), the potential goes like

$$V(r > R_0) = U_{inf} - \frac{C_6}{r^6} - \frac{C_8}{r^8} - \frac{C_{10}}{r^{10}} \pm E_{\mathrm{exch}} \tag{3.15}$$

with the exchange term

$$E_{\mathrm{exch}} = A_{\mathrm{ex}} r^{\gamma} e^{-\beta r} \ , \tag{3.16}$$

which is repulsive for the triplet state (plus sign) and attractive for the singlet potential (minus sign) (see section 3.1). We interpolated the data points from [18] between R_{min} and R_0 and extrapolated this function at short-range with

$$V(r < R_{min}) = A + \frac{B}{r^4} \ . \tag{3.17}$$

The overall result is shown in Figure 3.4.

```
(*Loading the data points for the singlet and triplet potentials*)
Directory[]
SetDirectory["labwork\spin-coupling\NaRb potentials"]
List1 = Sort[ReadList["NaRbsinglet.txt", {Number, Number}]];
List2 = Sort[ReadList["NaRbtriplet.txt", {Number, Number}]];
(*Define the constants for the potential*)
Uinf = 5030.52235;
R0 = 11.2967;
R02 = 11.3370;
C6 = 1.3237 * 10^7;
C8 = 2.9889 * 10^8;
C10 = 1.5821 * 10^10;
Aex = 2.8609 * 10^4;
γ = 5.0081;
β = 2.2085;
(*Interpolate the Singlet potential*)
f10 = Interpolation[List1];
f11[R_] := Uinf - C6 / R^6 - C8 / R^8 - C10 / R^10 - Aex * R^γ * Exp[-β * R];
B100 = -1 / 4 * f10'[2.1] * 2.1^5;
A100 = f10[2.1] - B100 / 2.1^4;
f12[R_] := N[A100 + B100 / R^4];
V1[R_] := If[R ≤ 2.1, f12[R], If[R ≤ R0, f10[R], f11[R]]];
(*Interpolate the Triplet potential*)
f20 = Interpolation[List2];
f21[R_] := Uinf - C6 / R^6 - C8 / R^8 - C10 / R^10 + Aex * R^γ * Exp[-β * R];
B200 = -1 / 4 * f20'[2.94444] * 2.94444^5;
A200 = f20[2.94444] - B200 / 2.94444^4;
f22[R_] := N[A200 + B200 / R^4];
V2[R_] := If[R ≤ 2.94444, f22[R], If[R ≤ R0, f20[R], f21[R]]];
```

Figure 3.3: Import of the potential data from ref. [18]

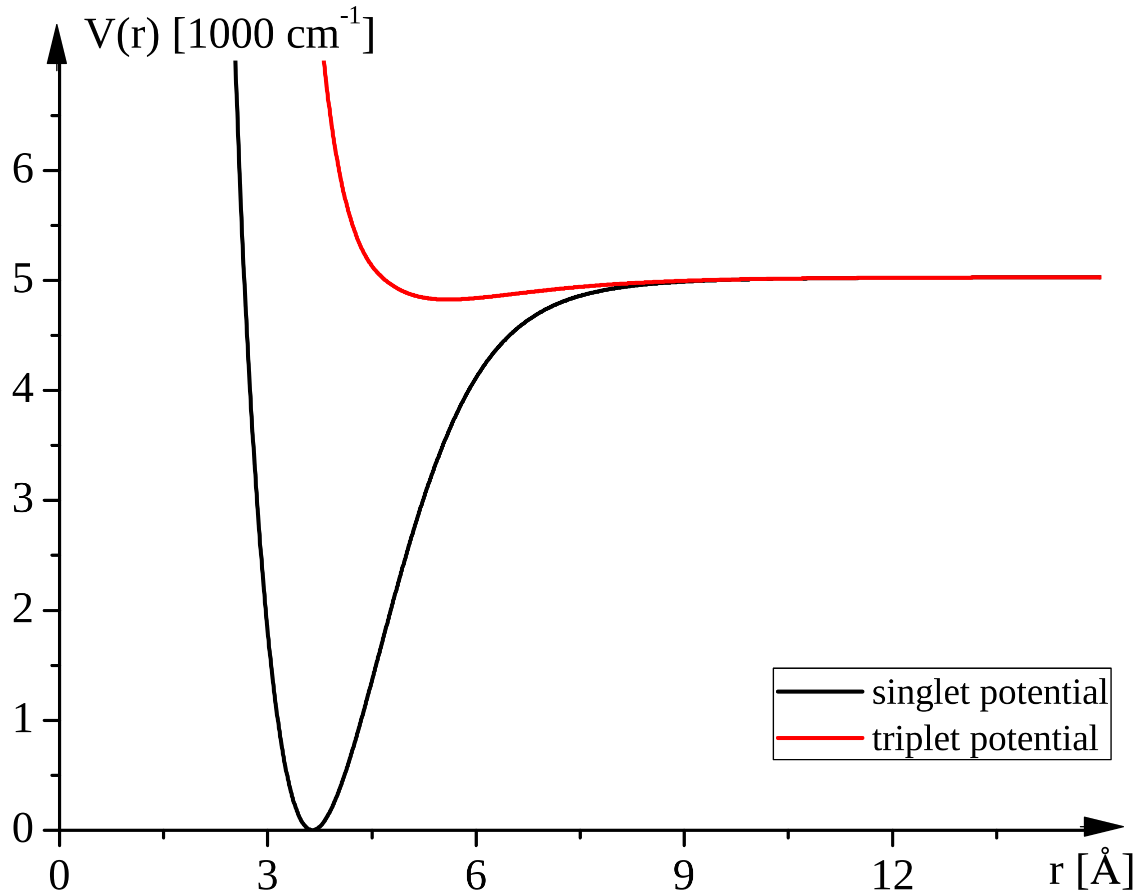

Figure 3.4: Interpolated singlet and triplet potentials for Na-Rb (data from [18])

In order to get a solution for the radial Schrödinger equation

$$\frac{d^2u(r)}{dr^2} + \frac{2\mu}{\hbar^2}(E - V(r))u(r) = 0 \tag{3.18}$$

we calculated the factor $\frac{2\mu}{\hbar^2}$ for ^{23}Na^{85}Rb and ^{23}Na^{87}Rb, respectively. Note that the dimensions of energy and length are cm^{-1} and Å, respectively. The dimension of reciprocal centimeter for energies corresponds to the inverse wavelength, i.e.

$$1 \text{ cm}^{-1} \equiv \frac{hc}{1 \text{ cm}} = 1.99 \cdot 10^{-23} \text{ J} = 1.24 \cdot 10^{-4} \text{ eV} . \tag{3.19}$$

Using a program from R.J. LeRoy which includes exact atomic masses [20] allowed us to get a high accuracy. The results are shown in Table 3.2. This program would also be able to solve the problem of determining the scattering length, bound state levels and even more characteristic properties of the potentials. But as it needs a special form for the input data, we decided instead to solve the Schrödinger equation numerically with Mathematica.

Table 3.2: Characteristic constants

	^{23}Na^{85}Rb	^{23}Na^{87}Rb
$2\mu/\hbar^2$ $\left[\text{cm}/\text{Å}^2\right]$	1.073194412	1.078475399

To provide a check of our numerical results we used two methods, a procedure which uses Numerov's method (Figure 3.5), explained in the Appendix D, and the built-in Mathematica function NDSolve for comparison (Figure 3.6). Although the Mathematica procedure is faster, it cannot be used for determining bound state energies as we will see in section 3.3.3. The source code is given in Figures 3.5, 3.6 and 3.7.

In order to verify that the Numerov code, which is not adaptive (i.e. the stepsize must be fixed as an input parameter), returns the correct results, we compared it with the Mathematica function NDSolve in several ways. In doing so we found out that

```
(*This Module integrates the Schrödinger equation with the
 Numerov method, starting with the initial condition that the
 wave function falls off very rapidly inside the potential*)
(*energy_ is the energy of the state,
Rmax_ is the radius until which the integration should be done,
S_=0 means singlet potential and S_=1 is the triplet case*)
(*With MRb_ you can choose between the Na23-Rb85 and Na23-Rb87 case*)
(*There is an additional normalization factor which should be
 first set to 1*)
(*The stepwidth dx has to be set*)
Wavefunction[energy_, Rmax_, S_, MRb_, norm1_, dx_] :=
 Module[{cons, V, y0, y1, y2, Liste, i, imax, norm, g1, g2, pos,
   iinit, elementnumber, drop},
  (*Distinguishing the two different cases for the mass of Rb*)
  If[MRb == 85, cons = 1.073194412,
   If[MRb == 87, cons = 1.078475399, Print["Check Rb mass"]]];
  (*Distinguishing the singlet and triplet case*)
  If[S == 0, V[R_] := V1[R], V[R_] := V2[R]];
  (*Setting the initial value for the radius -
   I choose the intersection between the energy and the potential
    minus 1 Angstrom, that is where the wave function should
   have definitely reached zero*)
  iinit =
   IntegerPart[(Evaluate[x /. FindRoot[energy == V[x], {x, 0.1}]] - 1) / dx];
  i = iinit;
  (*Setting the upper limit for the integration*)
  imax = Rmax / dx - i + 1 / dx;
  (*Setting the initial conditions*)
  y0 = 0;
  y1 = 10^-63;
  Liste = {{(i - 1) * dx, y0}, {i * dx, y1}};
```

(a)

Figure 3.5: Program to integrate the Schrödinger equation with Numerov's method

```
(*The variable drop defines the distance between the data points
 in the list*)
drop = IntegerPart[(Rmax / dx - iinit) / 1000];
If[drop == 0, drop = 1];
(*Numerov algorithm*)
While[i ≤ imax,
  y2 =
   N[((2 - 5 * dx^2 / 6 * cons * (energy - V[i * dx])) * y1 -
       (1 + dx^2 / 12 * cons * (energy - V[(i - 1) * dx])) * y0) /
     (1 + dx^2 / 12 * cons * (energy - V[(i + 1) * dx])), 10];
  Liste = Append[Liste, {Round[(i + 1) * dx, 0.0001], y2}];
  y0 = y1;
  y1 = y2;
  (*The next line makes sure that our list doesn't get too big*)
  If[i - iinit > drop && IntegerQ[i / drop],
   Liste = Drop[Liste, -(drop - 1)];];
  i++];
(*normalize the wavefunction by dividing through the last
 value (usually that is the largest one) and add offset*)
elementnumber = Length[Liste];
norm = Abs[Last[Last[Liste]]];
g1[x_] := norm1 * 1000 / norm * x + energy;
pos = {{1, 2}};
Do[pos = Append[pos, {j, 2}], {j, 2, elementnumber}];
Liste = MapAt[g1, Liste, pos];
(*Give the output back in a list*)
Return[Liste]
]
```

(b)

Figure 3.5: Continued

```
Wavefunction1[energy_, Rmax_, S_, MRb_] :=
 Module[{cons, V, xmin, sol, ymin},
  (*Distinguishing the two different cases for the mass of Rb*)
  If[MRb == 85, cons = 1.073194412,
   If[MRb == 87, cons = 1.078475399, Print["Check Rb mass"]]];
  (*Distinguishing the singlet and triplet case*)
  If[S == 0, V[R_] := V1[R], V[R_] := V2[R]];
  (*Setting the initial value for the radius -
   I choose the intersection between the energy and the potential
    minus 1 Angstrom, that is where the wave function should
   have definitely reached zero*)
  xmin = Evaluate[x /. FindRoot[energy == V[x], {x, 0.1}]] - 1;
  ymin = 0.1;
  (*Obtaining the solution with the built-in function NDSolve*)
  sol = NDSolve[{y''[x] + cons * (energy - V[x]) y[x] == 0, y[xmin] == 0,
     y[xmin + 0.01] == ymin}, y, {x, xmin, Rmax}, AccuracyGoal → 10,
    PrecisionGoal → 10, MaxStepSize → 0.01, MaxSteps → 1000000];
  Return[{sol, xmin, Rmax, energy}];
 ]
```

Figure 3.6: Procedure to integrate the Schrödinger equation with NDSolve

```
(*This Module helps to normalize and plot the Mathematica solution*)
(*sol is the solution obtained with the module Wavefunction1*)
(*Rmin and Rmax are the limits of the created plot*)
(*norm is a additional normalization factor*)
PlotSolution1[sol_, Rmin_, Rmax_, norm_] :=
 Module[{xmin, xmax, sol1, norm1, energy},
  sol1 = sol;
  xmin = Rmin;
  xmax = Rmax;
  energy = Extract[sol1, 4];
  If[xmin < Extract[sol1, 2], xmin = Extract[sol1, 2]];
  If[xmax > Extract[sol1, 3], xmax = Extract[sol1, 3]];
  norm1 = Abs[Extract[Evaluate[y[x] /. Extract[sol1, 1]] /. x → xmax, 1]];
  Plot[energy + norm / norm1 * Evaluate[y[x] /. Extract[sol1, 1]],
   {x, xmin, xmax}]
 ]

(*This Module creates a list of data points from the NDSolve
 solution and normalizes the data*)
(*Rmin (Rmax) gives the start (stop) value of the created list*)
(*norm is a additional normalization factor*)
MakeList[sol_, Rmin_, Rmax_, norm_] :=
 Module[{xmin, xmax, liste, norm1, energy, dx},
  liste = {};
  xmin = Rmin;
  xmax = Rmax;
  energy = Extract[sol, 4];
  dx = (xmax - xmin) / 1000;
  norm1 = Abs[Extract[Evaluate[y[x] /. Extract[sol, 1]] /. x → xmax, 1]];
  Do[
   liste = Append[liste,
     {N[i * dx + xmin],
      First[energy + norm / norm1 * Evaluate[y[x] /. Extract[sol, 1]] /.
        x → (i * dx + xmin)]}], {i, 0, 1000}];
  Return[liste]
 ]
```

Figure 3.7: Additional procedures *PlotSolution*1 and *MakeList*, which help to plot the numerical solution and to export it into another program by making a list of data points.

using a sufficiently small stepsize in the recursive method leads to the same solution. Lowering the stepsize is especially important when one is integrating the Schrödinger equation over a larger interval. That can be seen in Figure 3.8. A stepsize of 0.01 Å, which is usually sufficient when one integrates up to 30 Å, leads still to significant differences between the two methods. However, the results achieved with a stepsize of 0.0005 Å cannot be distinguished from the Mathematica NDSolve method.

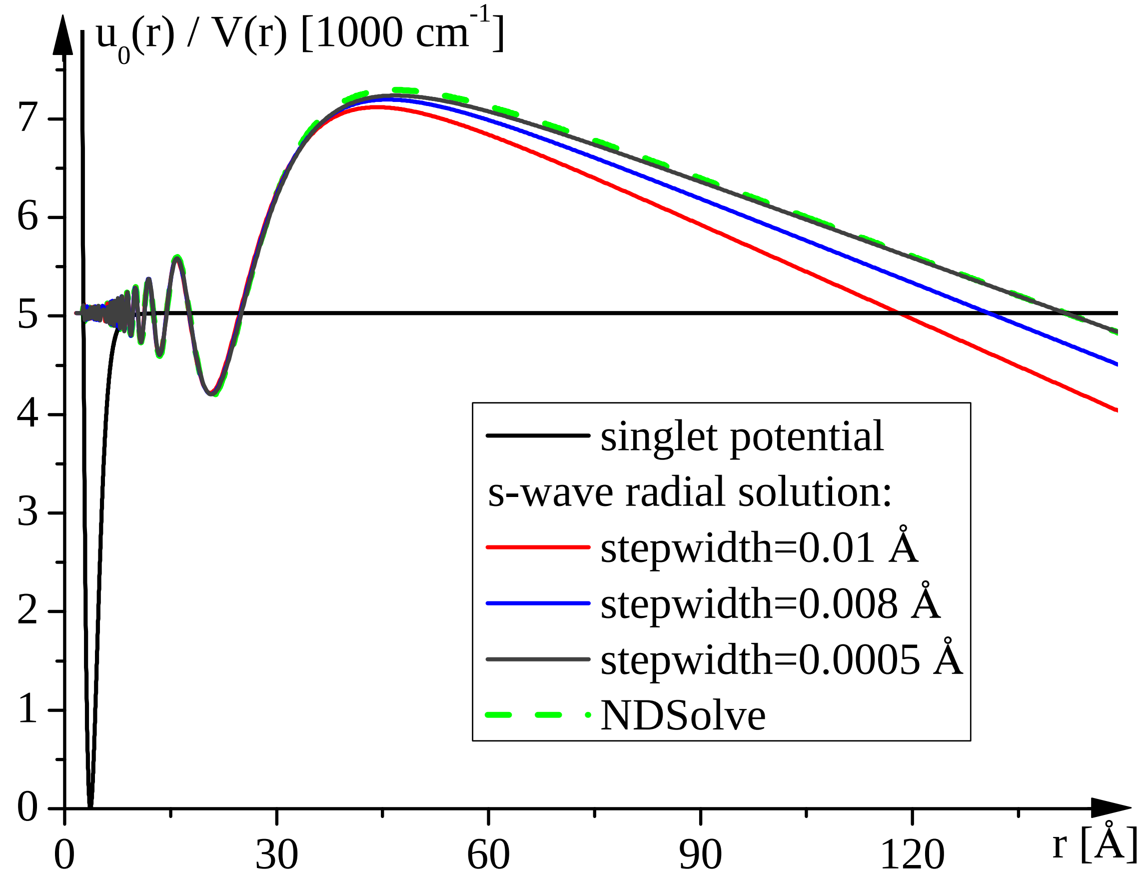

Figure 3.8: This figure shows that the wave function obtained with our procedure, which uses Numerov's method (see Figure 3.5), converges to the Mathematica solution (a smaller stepsize becomes especially important for a large integration interval).

3.3.2 Scattering lengths for sodium-rubidium

Now we would like to present the results for the scattering lengths for Na-Rb. The basic idea is to integrate the Schrödinger equation at the asymptotic potential energy, i.e. in the limit of $k = 0$, and then read off the scattering length as the last root of the asymptotic wave function (see section 2.1.2). For one initial condition we computed the inner turning point and from there we went 1 Å back "into" the potential and set the wave function to zero, which is valid as long as the potential falls off very steeply. The second condition is that the wave function one stepwidth further is unequal zero (its magnitude just determines a normalization factor which can be changed later). Both methods (Numerov and NDSolve) basically lead to the same solution with those initial conditions (see Figure 3.8).

While writing these procedures, it also became obvious how sensitive this method is to slight changes in the atomic masses (which determine the constants given in Table 3.2) and to different interpolations of the potential data points. Although we used the data from [18], we did not obtain exactly the same scattering lengths, which are shown in Table 3.3.

Table 3.3: Scattering lengths determined by Pashov et al. [18]

Isotope	Singlet $a^{(0)}$ $[a_0]$	Triplet $a^{(1)}$ $[a_0]$
^{23}Na^{85}Rb	396	81
^{23}Na^{87}Rb	109	70

The radial s-wave solutions for singlet and triplet potential for each case are given in Figure 3.9 and 3.10. We got the following results (using $a_0 \simeq 0.53$ Å) (see Table 3.4).

By comparing to Table 3.3 one finds a good overall agreement. There is only one noticeable difference in the singlet scattering length for ^{23}Na^{85}Rb. That can be explained by the fact that the scattering length gets generally more uncertain the larger it is, because slight changes in the short-range potential add up to significant

Table 3.4: Scattering lengths as multiples of a_0 determined with Numerov code (compare to Table 3.3)

Isotope	Singlet $a^{(0)}$ $[a_0]$	Triplet $a^{(1)}$ $[a_0]$
^{23}Na^{85}Rb	267	86
^{23}Na^{87}Rb	105	79

errors in the long-range wavefunction.

In conclusion we find that our simple numerical method leads to comparable results to the sophisticated programs which are used in most cases.

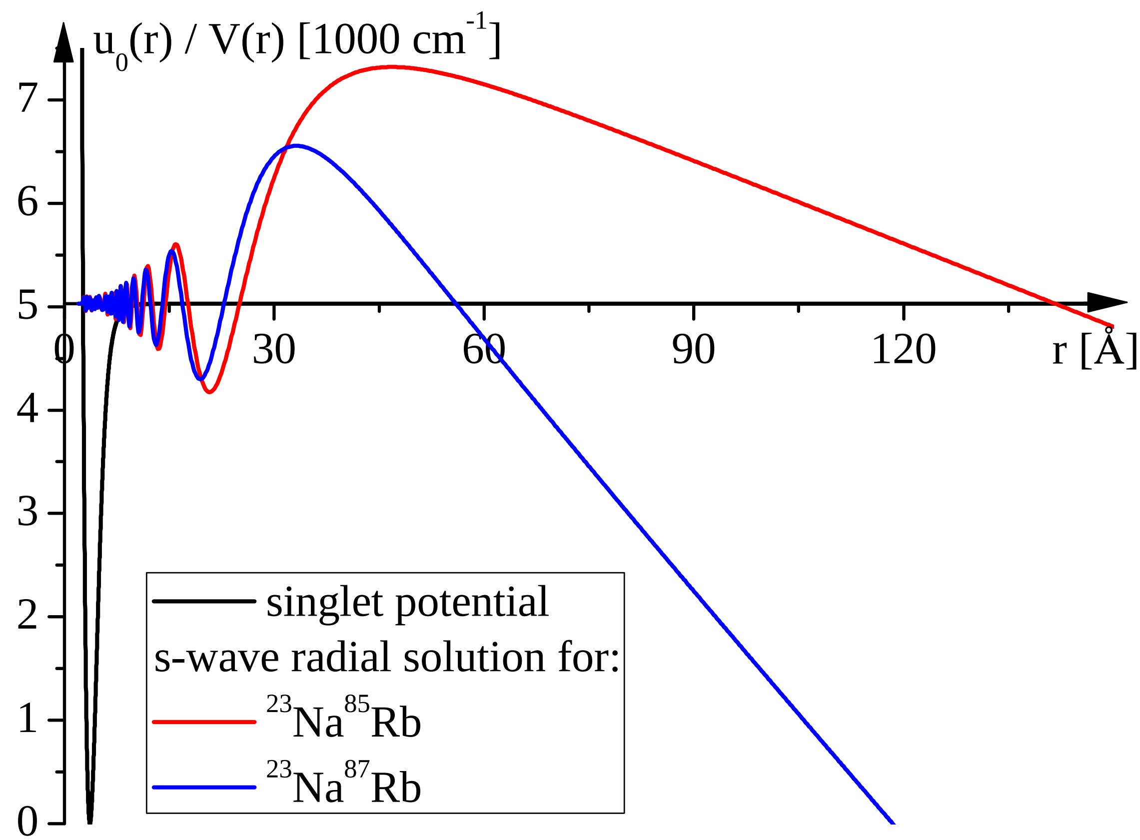

Figure 3.9: Determination of the singlet scattering length for Na-Rb; we read off $a^{(0)}(^{23}\mathrm{Na}^{85}\mathrm{Rb}) = 141.4$ Å and $a^{(0)}(^{23}\mathrm{Na}^{87}\mathrm{Rb}) = 55.9$ Å

3.3.3 Bound state energies and wave functions

Although it is relatively simple to integrate the Schrödinger equation for a given energy in the continuum, it turns out that finding bound states energies and wave

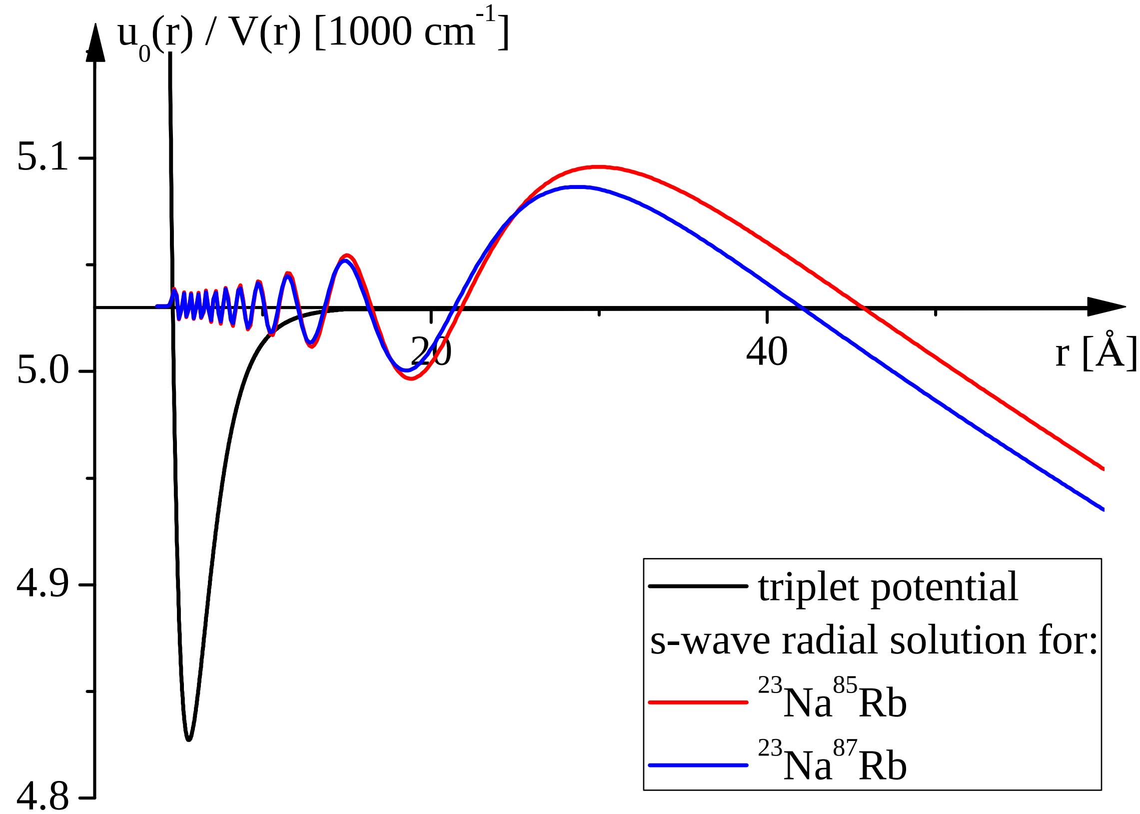

Figure 3.10: Determination of the triplet scattering length for Na-Rb; we read off $a^{(1)}(^{23}\mathrm{Na}^{85}\mathrm{Rb}) = 45.7$ Å and $a^{(1)}(^{23}\mathrm{Na}^{87}\mathrm{Rb}) = 41.9$ Å

functions is much more challenging, because one has to simultaneously determine the eigenvalues and eigenfunctions of the Hamiltonian. The basic idea is to integrate forwards and backwards and then trying to match the two solutions together (Figure 3.11). Wang et al. have presented a very efficient method in their paper [36]. The reason why we did not use their program is that it needs an analytic function for the potential, which is almost impossible to obtain for our case. Nevertheless we adapted the main idea and applied it to the Na-Rb interaction.

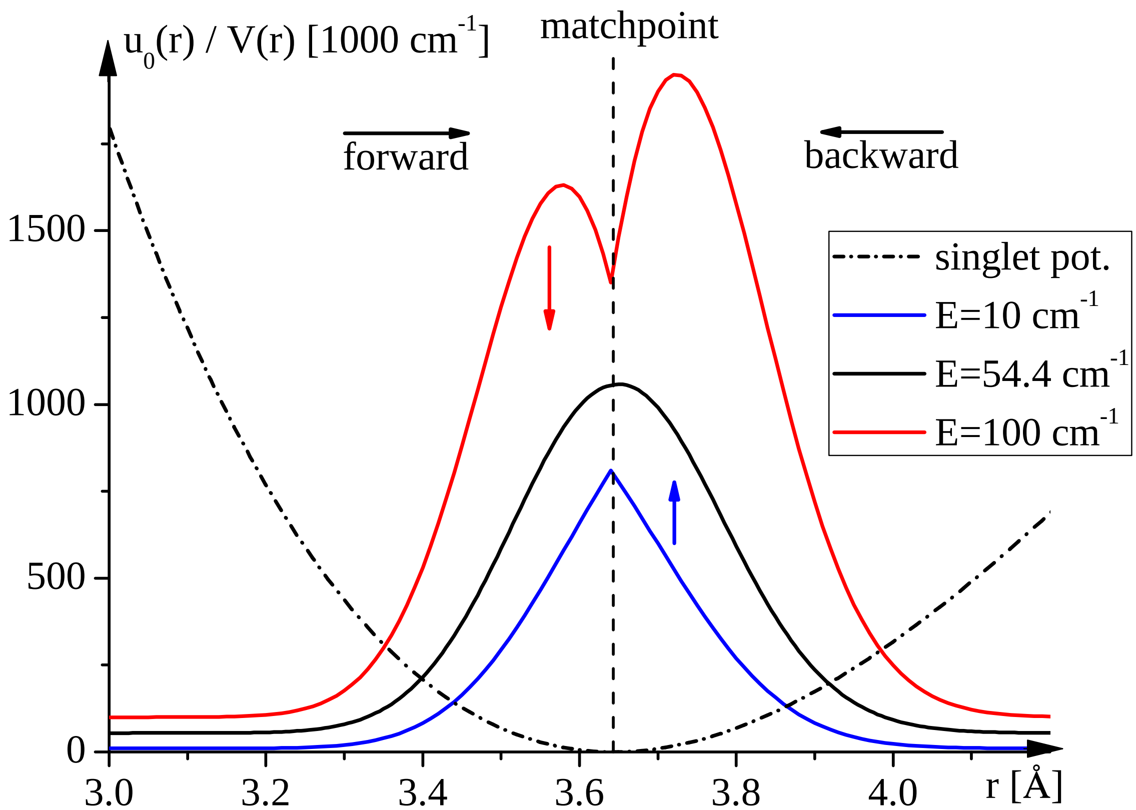

Figure 3.11: This figure sketches the basic idea of matching the two solutions together by varying the energy and therefore finding the bound state.

The great advantage of Numerov's method is, that it is easy to perform the recursion in the other direction. Therefore we developed the two main procedures *wavefunctionstart* (Figure 3.12) and *wavefunctionend* (Figure 3.13), which provide the short-range and long-range solution. The initial conditions are once again determined by the fact that the wave function falls off very rapidly inside the potential.

Because the slope on the right side is not so steep, we set the solution to zero at 20 Å, which is far outside the outer turning point for the usual binding energies. Note that it might be necessary to change this parameter if one is looking for binding energies near the continuum.

```
(*This Module works similarly to the module Wavefunction*)
(*It solves the Schrödinger equation from an initial value
 inside the potential up to the matching point,
which is the coordinate of the minimum of the potential,
for a given energy*)
Wavefunctionstart[energy_, S_, MRb_, dx_] :=
 Module[{cons, V, y0, y1, y2, Liste, i, imax, norm, g1, g2, pos,
   iinit, elementnumber, drop},
  (*Distinguishing the two different cases for the mass of Rb*)
  If[MRb == 85, cons = 1.073194412,
   If[MRb == 87, cons = 1.078475399, Print["Check Rb mass"]]];
  (*Distinguishing the singlet and triplet case*)
  If[S == 0, V[R_] := V1[R], V[R_] := V2[R]];
  (*Setting the initial value for the radius -
   I choose the intersection between the energy and the potential
    minus 1 Angstrom, that is where the wave function should
   have definitely reached zero*)
  iinit =
   IntegerPart[(Evaluate[x /. FindRoot[energy == V[x], {x, 0.1}]] - 1) / dx];
  i = iinit;
  (*Setting the upper limit for the integration*)
  imax = IntegerPart[(Evaluate[R /. Last[FindMinimum[V[R], {R, 1}]]]) /
     dx];
  (*Setting the initial conditions*)
  y0 = 0;
  y1 = 10^-63;
  Liste = {{(i - 1) * dx, y0}, {i * dx, y1}};
```

(a)

Figure 3.12: The procedure *wavefunctionstart*

As the matching point we chose the radial coordinate of the potential's minimum. Because we have already made sure that both solutions are normalized in the sense

```
(*Numerov algorithm*)
While[i ≤ imax - 1,
  y2 =
   N[((2 - 5 * dx ^ 2 / 6 * cons * (energy - V[i * dx])) * y1 -
       (1 + dx ^ 2 / 12 * cons * (energy - V[(i - 1) * dx])) * y0) /
     (1 + dx ^ 2 / 12 * cons * (energy - V[(i + 1) * dx])), 10];
  Liste = Append[Liste, {Round[(i + 1) * dx, 0.0001], y2}];
  y0 = y1;
  y1 = y2;
  i ++];
 (*normalize the wavefunction by dividing through value at the
  matching point and add offset*)
elementnumber = Length[Liste];
norm = Abs[Last[Last[Liste]]];
g1[x_] := 1000 / norm * x + energy;
pos = {{1, 2}};
Do[pos = Append[pos, {j, 2}], {j, 2, elementnumber}];
Liste = MapAt[g1, Liste, pos];
(*Give the output back in a list*)
Return[Liste]
]
```

(b)

Figure 3.12: Continued

```
Wavefunctionend[energy_, S_, MRb_, dx_] :=
 Module[{cons, V, yn, yn1, yn0, Liste, i, imin, norm, g1, g2, pos,
   iinit, elementnumber, drop},
  (*Distinguishing the two different cases for the mass of Rb*)
  If[MRb == 85, cons = 1.073194412,
   If[MRb == 87, cons = 1.078475399, Print["Check Rb mass"]]];
  (*Distinguishing the singlet and triplet case*)
  If[S == 0, V[R_] := V1[R], V[R_] := V2[R]];
  (*Setting the lower integration limit,
  which is the minimum of the potential*)
  imin = IntegerPart[(Evaluate[R /. Last[FindMinimum[V[R], {R, 1}]]]) / dx];
  (*Start integrating at a radius of 25 Angstrom
   (the wavefunction for usual bound states is zero at this distance)*)
  iinit = 25 / dx;
  i = iinit;
  (*Setting the initial conditions*)
  yn1 = 0;
  yn = 10^-63;
  Liste = {{i * dx, yn}, {(i + 1) * dx, yn1}};
  (*Numerov algorithm*)
  While[i ≥ imin + 1,
   yn0 =
    N[((2 - 5 * dx^2 / 6 * cons * (energy - V[i * dx])) * yn -
        (1 + dx^2 / 12 * cons * (energy - V[(i + 1) * dx])) * yn1) /
      (1 + dx^2 / 12 * cons * (energy - V[(i - 1) * dx])), 10];
   Liste = Prepend[Liste, {Round[(i - 1) * dx, 0.0001], yn0}];
   yn1 = yn;
   yn = yn0;
   i--];
  (*normalize the wavefunction by dividing through value at
   the matching point and add offset*)
  elementnumber = Length[Liste];
  norm = Abs[Last[First[Liste]]];
  g1[x_] := Round[1000 / norm * x + energy, 0.0001];
  pos = {{1, 2}};
  Do[pos = Append[pos, {j, 2}], {j, 2, elementnumber}];
  Liste = MapAt[g1, Liste, pos];
  (*Give the output back in a list*)
  Return[Liste]
 ]
```

Figure 3.13: *wavefunctionend*, which uses the reversed Numerov method

that at the matching point both functions take the same value, we just have to match the first derivative. Therefore we have written the procedure *Matchingcondition* (Figure 3.14), which just outputs the difference between the left and right solution in the first derivative at the matching point for a given energy. The program *FindEnergy* (Figure 3.15) then uses this module and looks for roots in the *Matchingcondition* in a given energy range. *PlotMatch* is used to plot the achieved solution.

```
(*This module determines the difference in the first derivative
 between the left and right solutions to the Schrödinger equation*)
(*The input are the energy limits (Emin and Emax) and the stepwidth dE,
as well as the stepwidth for the Numerov method
 (usually 0.01 is sufficient)*)
(*The output is a list with the differences in the first
 derivatives at the matching point and the according radial
 coordinates*)
Matchingcondition[S_, MRb_, dx_, Emin_, Emax_, dE_] :=
 Module[{energy, list1, list2, dy1, sol},
  sol = {};
  Do[
   list1 = Take[Wavefunctionstart[energy, S, MRb, dx], -2];
   list2 = Take[Wavefunctionend[energy, S, MRb, dx], 2];
   dy1 = (Last[Last[list2]] - Last[First[list2]]) / dx -
     (Last[Last[list1]] - Last[First[list1]]) / dx;
   sol = Append[sol, {energy, dy1}], {energy, Emin, Emax, dE}];
  Return[sol]
 ]
```

Figure 3.14: The procedure *Matchingcondition*

In order to demonstrate the functionality of our program, we determined the ground state energy and wave function as well as one intermediate binding energy for the ^{23}Na^{85}Rb singlet potential (See Figure 3.16).

A good way of verifying our method is to approximate the potential as a harmonic oscillator, determine its ground state energy and then comparing this to our result. It can be seen in Figure 3.16, that the ground state wave function has already the

```
(*This module uses the Matchingcondition module recursively in
 order to obtain a binding energy in the interval [Emin,Emax]*)
(*dx is again the stepwidth for the Numerov method*)
FindEnergy[S_, MRb_, dx_, Emin_, Emax_] := Module[{dE, E1, E2, list, i},
  E1 = Emin;
  E2 = Emax;
  Do[dE = N[(E2 - E1) / 10];
   list = Matchingcondition[S, MRb, dx, E1, E2, dE];
   Do[
    If[(Last[list[[i]]] > 0 && Last[list[[i + 1]]] < 0) ||
      (Last[list[[i]]] < 0 && Last[list[[i + 1]]] > 0),
     E2 = First[list[[i + 1]]];
     E1 = First[list[[i]]]],
    {i, 1, 10}],
   {5}];
  Return[E1 + (E2 - E1) / 2]
 ]

(*This module plots the solutions to the left and right of the
 matching point for a given energy between Rmin and Rmax*)
PlotMatch[energy_, S_, MRb_, dx_, Rmin_, Rmax_] := Module[{},
  ListPlot[Join[Wavefunctionstart[energy, S, MRb, dx],
    Wavefunctionend[energy, S, MRb, dx]], Joined -> True,
   PlotRange -> {{Rmin, Rmax}, {0, 8000}}]
 ]
```

Figure 3.15: The procedures *PlotMatch* and *FindEnergy*

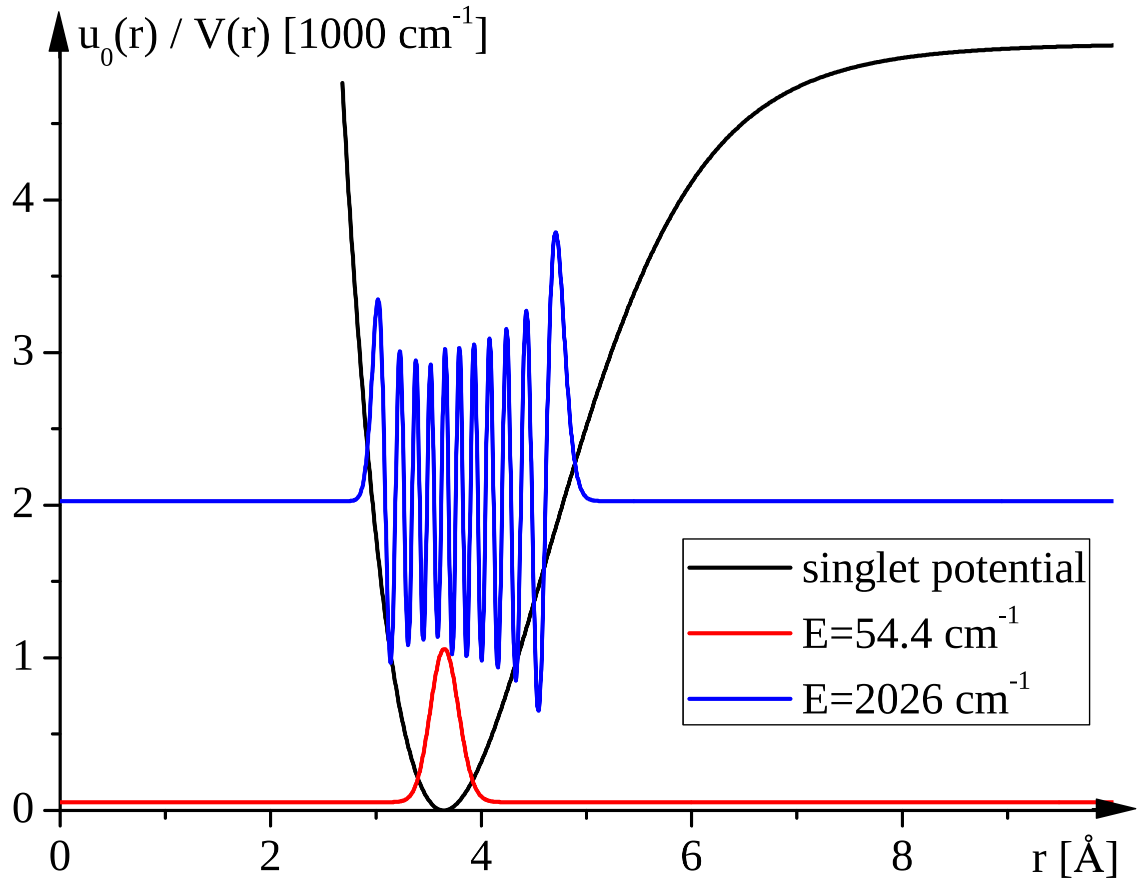

Figure 3.16: Bound states for $^{23}Na^{85}Rb$ singlet potential

right Gaussian shape. We can write the Hamiltonian as

$$\hat{H} = \frac{\hat{p}^2}{2\mu} + \frac{\mu\omega^2}{2}(R - R_0)^2 \; . \tag{3.20}$$

From the quadratic fit (Figure 3.17) we obtain $\mu\omega^2 = 6019\ \mathrm{cm}^{-1}/\mathrm{\AA}^2$. Therefore we get for the ground state energy of ^{23}Na^{85}Rb (with $2\mu/\hbar^2 = 1.073\ \mathrm{cm}/\mathrm{\AA}^2$ from Table 3.2)

$$E_0 = \frac{\hbar\omega}{2} = \frac{1}{2}\sqrt{\frac{\hbar^2 2\mu\omega^2}{2\mu}} = \sqrt{\frac{6019}{2\cdot 1.073}}\ \mathrm{cm}^{-1} \simeq 53\ \mathrm{cm}^{-1} \; . \tag{3.21}$$

That agrees perfectly with the result derived with the numerical method in Figure 3.16.

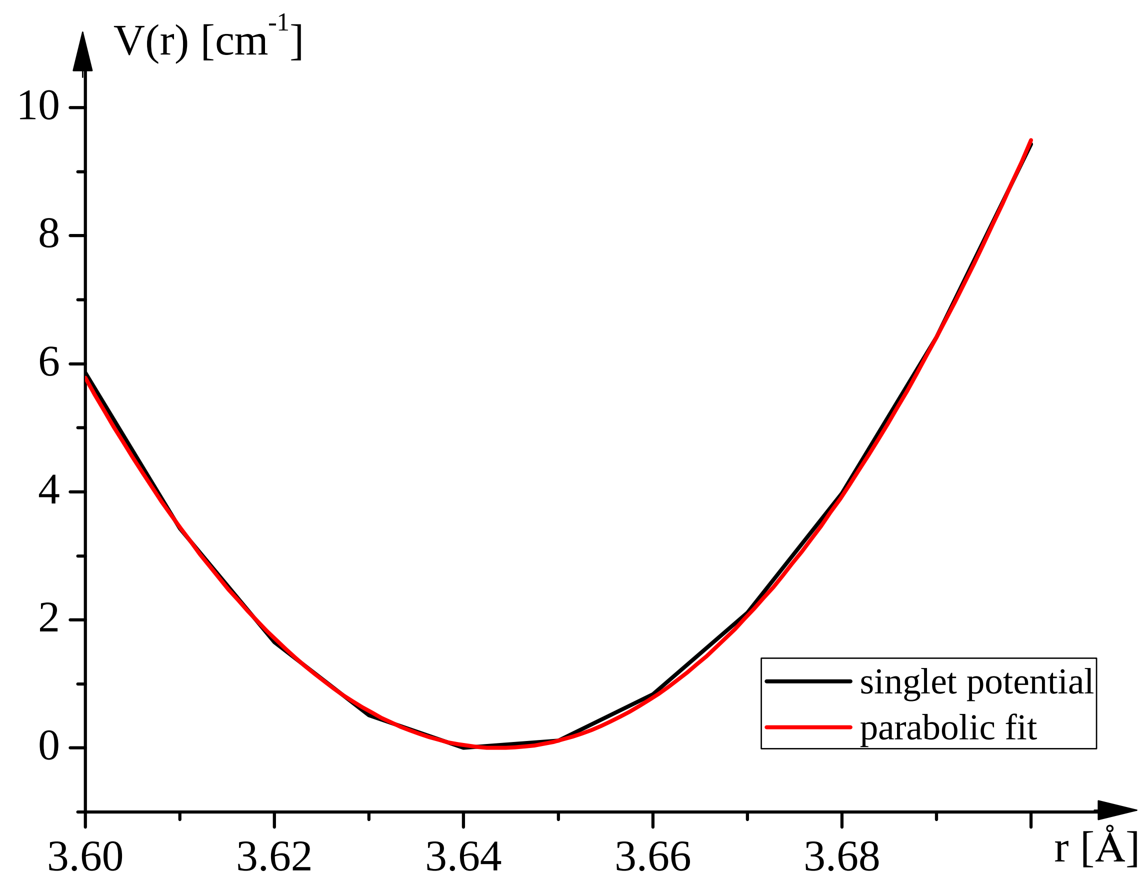

Figure 3.17: Parabolic fit of the minimum of the singlet potential for ^{23}Na^{85}Rb: $V(r) = \frac{1}{2}\cdot 6019\cdot(r - 3.644\ \mathrm{\AA})^2\ \mathrm{cm}^{-1}/\mathrm{\AA}^2$

3.4 Inelastic collisions for alkali atoms

Here we would like to give some information about inelastic collisions in ultracold alkali gases. It can be seen from the example in Appendix B that it is rather difficult to calculate inelastic cross sections even when the potentials are known as analytical functions. We discussed in section 3.1 that alkali potentials are complicated and generally not known analytically. Furthermore, many channels are coupled in general, which requires variational calculations in order to obtain the scattering matrix. The treatment of those numerical methods goes beyond the extent of this work. The interested reader is referred to e.g. J.P. Burke's PhD thesis, which deals with Rb-Rb collisions [34]. Nevertheless we can make some general statements about those inelastic processes.

As we discussed in 3.1, the quantum numbers F and m_F are good over the whole range of r as long as we have a negligible external magnetic field (due to the total rotational symmetry). Because there is no set of good quantum numbers at all distances which specifies all information about the angular momenta, the interaction potential matrix elements $\langle i| V |j\rangle$ cannot be diagonal over the whole range (see section 2.2.2). That implies that many channels are coupled together and means that if the entrance channel is $|f_1, m_{f_1}, f_2, m_{f_2}\rangle$, there are generally different possible exit channels. For example, for the collision of two ^{23}Na atoms entering in the channel $|2,0,2,0\rangle$ possible collisions are:

$$|2,0,2,2\rangle \rightarrow |2,0,2,2\rangle \text{ or } |2,0,2,2\rangle \rightarrow |1,1,1,1\rangle \text{ or } |2,0,2,2\rangle \rightarrow |1,0,2,2\rangle \ . \quad (3.22)$$

All those collisions are allowed because they have non-zero overlap with the state $|F, m_F\rangle = |2,2\rangle$. The latter two cases are called exchange collisions and are inelastic processes because the energy of the separated atoms after the scattering process $(t \rightarrow \infty)$ is not the same as it was before due to the hyperfine interaction. Note that inelastic collisions are just called exchange collisions, when the process happens due to spin-coupling. That is why dipolar transitions are not exchange collisions. For s-wave collisions these exchange collision rates lead to a constant as the energy (temperature) approaches zero. Typical values are around 10^{-11} cm^3/s (see [29]), i.e. at a particle density n (in cm^{-3}), there are $n \cdot 10^{-11}$ collisions per second.

A good schematic illustration can be seen in Figure 3.18. It shows the details, which are important for a discussion of the properties of those collisions. It shows the scattering process of two incoming atoms with $f_1 = 2$ and $f_2 = 3$. At large distances the hyperfine interaction determines the energy of the system. In the recoupling region of the potential, the spins get projected onto triplet and singlet states, which leads to different phase shifts in the region $r < R_0$ where the central potential is nonzero. As long as the atoms undergo the recoupling region fast (so that the intermediate range, where neither coupling scheme is valid, can be neglected), the projection can simply be calculated with Clebsch-Gordan coefficients and higher Racah coefficients [30]. After those phase shifts the system goes again through the recoupling region and gets projected on all possible hyperfine states. Two criteria determine if a transition is possible or not. Firstly the conservation of the good quantum numbers (angular momentum) and secondly the conservation of energy.

In BEC experiments exchange collisions lead to the creation of Zeeman states which are magnetically repelled from the trap. Therefore one attempts to put atoms in those trapped states where exchange collisions are suppressed. Generally there are two possibilities. Both atoms can be in the state $f = i + 1/2$ and $m_f = \pm f$ (doubly spin-polarized). In that case the overall spin $F = 2f$ and $M_F = \pm F$. Therefore the only allowed state at short-range is the triplet state, which would lead to a certain phase shift and, after collision is completed, the final state will be the same as the initial state with just a shifted wave function. Alternitavely, when both atoms have $f = i - 1/2$ and $m_f = \pm f$ exchange collisions are suppressed, because both spins

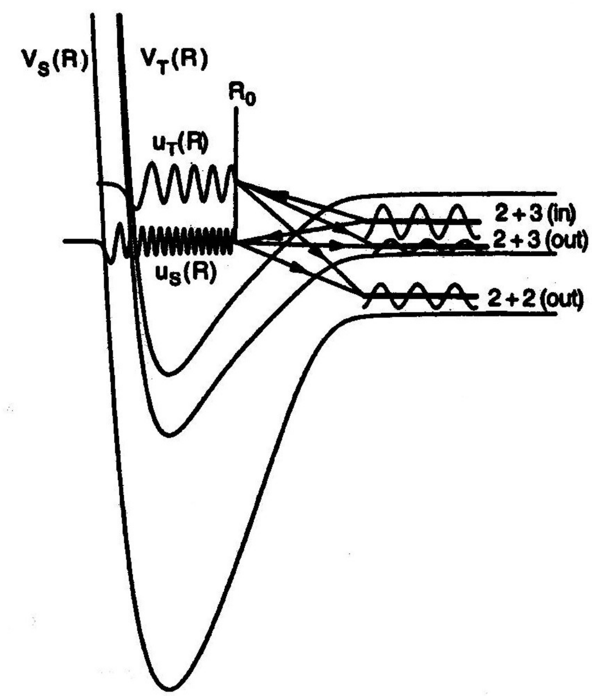

Figure 3.18: Sketch of an exchange collision for $^{23}Na_2$. The system is entering the scattering region in the channel $|f_1 = 2, f_2 = 3\rangle$ and exits in $|f_1 = 2, f_2 = 3\rangle$ and $|f_1 = 2, f_2 = 2\rangle$. The conservation of energy can be seen at the long-range part of the diagram. (from [29])

couple to $M_F = \pm 2f$ and the transition into higher hyperfine states with $f = i + 1/2$ is energetically forbidden for sufficiently low temperatures. Nevertheless inelastic collisions can also occur in spin-polarized mixtures due to the dipole interaction (see section 3.1), but the cross sections are much smaller than for directly (i.e. due to spin-coupling) overlapping states, where exchange collisions are allowed.

3.5 Examples for scattering lengths in the two-channel elastic approximation at low temperature

As we have just seen there are certain cases, e.g. doubly spin-polarized mixtures of alkali atoms, where exchange collisions are suppressed. If that is true, one can calculate the scattering length to a first approximation according to eq. (2.60). In order to illustrate the discussion given in section 2.2.1, we will also compute the "combined" scattering lengths for states for which exchange collisions are a priori not suppressed. Whether this approximation is useful or not depends on the case, but we will see that it often gives a rough estimate.

We consider both cases ^{23}Na^{85}Rb and ^{23}Na^{87}Rb. We calculated the singlet and triplet scattering lengths in section 3.3.2, but we will use the values presented by Pashov et al. (See Table 3.3). ^{23}Na and ^{87}Rb have a nuclear spin of $\frac{3}{2}$, ^{85}Rb has $\frac{5}{2}$ (see Table 3.1). With this information we can calculate the scattering lengths for different combinations of $f_1, m_{f_1}, f_2, m_{f_2}$. We have given some selected examples in Table 3.5 and 3.6. The computations in the examples involved finding the appropriate combinations of $P^{(0)}, P^{(1)}$ (with eq. (A.4)), i.e. all possibly different scattering lengths corresponding to eq. (2.60). The index 1 stands for the Na-atom and 2 for the corresponding Rb-atom. The collisions, where exchange collisions are suppressed (see above), are marked boldface.

We do the same calculation for sodium-sodium collisions. Those collisions have

Table 3.5: Selected examples for scattering lengths for $^{23}Na^{85}Rb$, this work. (For the rows in boldface exchange collisions are forbidden in the low energy limit.)

f_1	m_{f_1}	f_2	m_{f_2}	$P^{(0)}$	$P^{(1)}$	a $[a_0]$
1	**±1**	**2**	**±2**	1/6	5/6	133.5
1	0	2	-2	1/4	3/4	159.8
1	1	2	-2	1/3	2/3	186
1	-1	2	-1	5/24	19/24	146.6
1	1	2	-1	7/24	17/24	172.9
1	-1	3	-3	3/8	5/8	199.1
1	1	3	-3	1/8	7/8	120.4
2	**±2**	**3**	**±3**	**0**	**1**	**81**
2	2	3	-3	1/2	1/2	238.5
2	-2	3	-2	1/12	11/12	107.3
2	2	3	-2	5/12	7/12	212.3

Table 3.6: Selected examples for scattering lengths for $^{23}Na^{87}Rb$, this work. (For the rows in boldface exchange collisions are forbidden in the low energy limit.)

f_1	m_{f_1}	f_2	m_{f_2}	$P^{(0)}$	$P^{(1)}$	a $[a_0]$
1	**±1**	**1**	**±1**	**3/16**	**13/16**	**77.3**
1	-1	1	0	1/4	3/4	79.8
1	0	1	0	5/16	11/16	82.2
1	-1	2	-2	3/8	5/8	84.6
1	-1	2	2	1/8	7/8	74.9
2	**±2**	**2**	**±2**	**0**	**1**	**70**
2	-2	2	2	1/2	1/2	89.5

been studied among others by P.D. Lett [37]. Scattering lengths have been determined by F.A. van Abeelen and B.J. Verhaar [38] from analysis of bound-state photoassociation and Feshbach resonance field data (see section 4.2). We took their results for the singlet and triplet scattering length ($a_s = (19.1 \pm 2.1)a_0$ and $a_t = (65.3 \pm 0.9)a_0$) for our calculation and compared those results (see Table 3.7) to theirs for all combinations of hyperfine states in the $f_1 = f_2 = 1$ manifold (see in Figure 3.19). The results agree with each other within the error bars, not just for the boldface cases, where exchanges collisions are suppressed. Therefore our simple way of calculating the combined scattering length (eq. (2.60)) is a good approximation, even in cases where exchange collisions are not suppressed. That cannot be generalized though.

Table 3.7: Scattering length for $^{23}Na^{23}Na$ collisions with $f_1 = f_2 = 1$ computed with our simple approximation given by eq. (2.60) from the singlet and triplet scattering lengths determined by Verhaar [38].
(For the rows in boldface exchange collisions are forbidden in the low energy limit.)

f_1	m_{f_1}	f_2	m_{f_2}	a [a_0]
1	**1**	**1**	**1**	**56,6± 0,8**
1	1	1	0	53,8±0,9
1	1	1	-1	50,9±1,8
1	0	1	0	53,8±0,9
1	0	1	-1	53,8±0,9
1	**-1**	**1**	**-1**	**56,6±0,8**

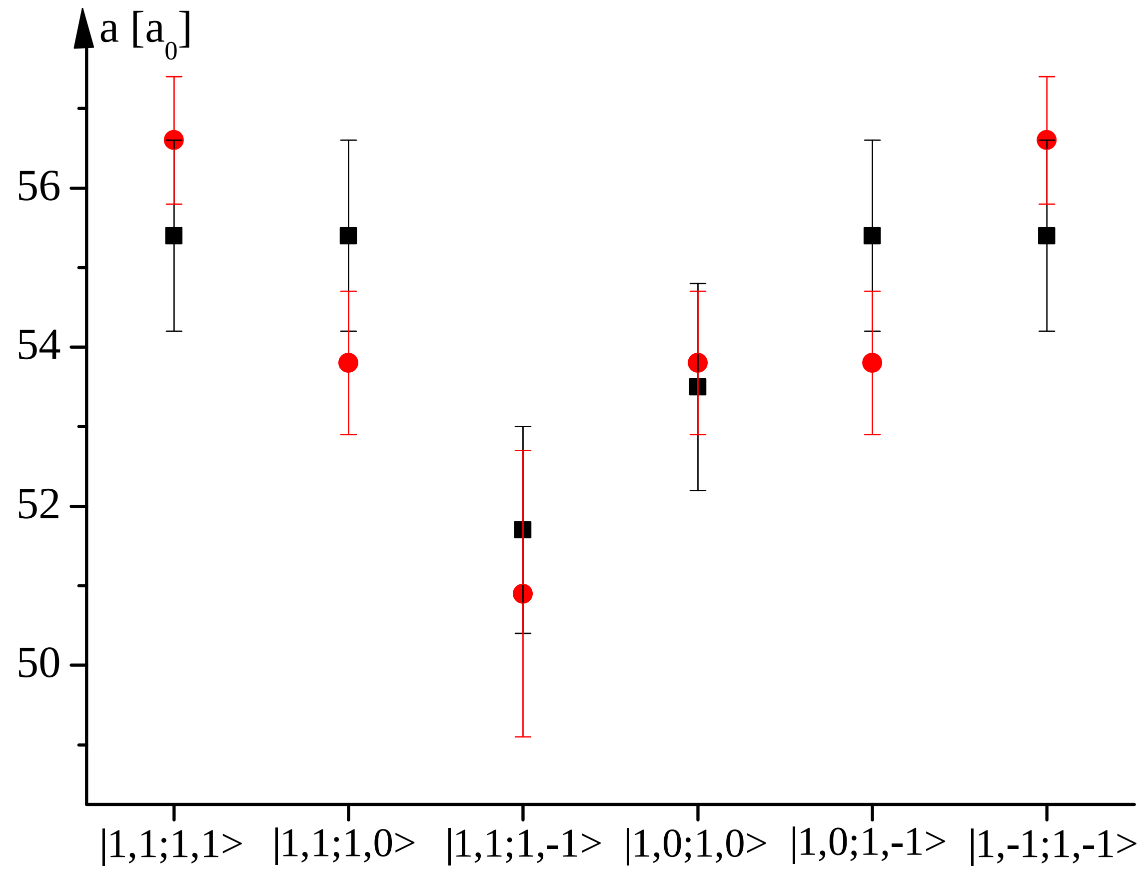

Figure 3.19: Comparison of results by Abeelen and Verhaar [38] (black squares) with corresponding errors and our calculation (red dots) (Table 3.7).
The entrance channels in the figure are given in the form of $|f_1, m_{f_1}; f_2, m_{f_2}\rangle$.

CHAPTER 4

APPLICATION AND EXPERIMENTAL METHODS

In this chapter we will discuss how the presented atomic collision data influence BEC experiments and ultracold atomic gas physics. Furthermore we will give an overview of how scattering lengths can be determined experimentally.

4.1 Influence of low energy collisions on BEC experiments

Bose-Einstein condensation in dilute gases can be described in mean-field theory by the Gross-Pitaevskii equation [39]. A helpful tool for approximately solving this equation is the Thomas-Fermi approximation, which is valid when collisional interaction dominates over kinetic energy. This approximation fails at the edge of the condensate, because the kinetic energy is proportional to the curvature of the wave function, which gets large at the surface of the cloud.

For translationally invariant (homogeneous) systems BEC in a trap requires repulsive interactions, i.e. a positive scattering length $a > 0$; for $a < 0$ attractive interactions cause instability. The limiting condition for a harmonic trap is given by [40]

$$2Na\sqrt{\frac{2m\omega_t}{\hbar}} > -1.62 \ , \tag{4.1}$$

where ω_t is the (isotropic) angular trap frequency of the confining trap potential $V_t = \frac{1}{2}m\omega_t^2 r^2$, N is the number of atoms in the condensate and a is the scattering length. Condensates with negative scattering lengths have been achieved, for example, with Lithium by Hulet et al. [41].

In the first part of this section we derive the Gross-Pitaevskii equations for two-species BEC (TBEC) and we will find a condition for the miscibility of two condensates following ref. [39], [42]. In the second part we discuss the relation between trap losses and inelastic collisions. At the end we will discuss the specific applications of the calculated scattering lengths in Na-Rb experiments.

4.1.1 Two-species Bose-Einstein condensates

Shortly after the realization of single-species BEC, efforts were made to create mixtures of different Bose-Einstein condensates. On the one hand condensates with atoms occupying different hyperfine states have been realized (for example with ^{87}Rb [43]). On the other hand experiments were carried out to achieve BEC mixtures of different atoms, e.g. Na-Rb [44]. The phase diagram of such multi-species condensates depends mainly on the scattering lengths, as we will show.

The following discussion is for example given in [39] or [42]. The interaction energy, which stands for interactions between atoms of the same species and amongst each other, is given by

$$\begin{aligned} E &= \frac{1}{2}U_1\frac{N_1(N_1-1)}{V} + \frac{1}{2}U_2\frac{N_2(N_2-1)}{V} + U_{12}\frac{N_1N_2}{V} \\ &\approx \frac{1}{2}U_1\frac{N_1^2}{V} + \frac{1}{2}U_2\frac{N_2^2}{V} + U_{12}\frac{N_1N_2}{V} \ . \end{aligned} \tag{4.2}$$

The constants U_1, U_2 and U_{12} are directly related to the corresponding scattering lengths in the following way:

$$U_{1,2} = \frac{4\pi\hbar^2 a_{1,2}}{m_{1,2}} \qquad \text{and} \qquad U_{12} = \frac{4\pi\hbar^2 a_{12}}{\mu} \ , \tag{4.3}$$

where a_1 and a_2 are the scattering lengths for scattering of pairs of atom 1 or pairs of atom 2, respectively. a_{12} is the scattering length, which corresponds to the scattering of atom 1 at atom 2 (e.g. the scattering length of Na-Rb calculated in chapter 3).

$\mu = m_1 m_2/(m_1 + m_2)$ is the reduced mass.

Given the single particle ground state wave functions $\phi_{1,2}$, we can define the condensate wave functions $\Psi_{1,2} = \sqrt{N_{1,2}}\ \phi_{1,2}$. Therefore we find that $n_{1,2} = |\Psi_{1,2}|^2$ and the total energy functional can be written as

$$E = \int d^3r \left\{ \frac{\hbar^2}{2m_1} |\nabla\Psi_1|^2 + V_1(r)n_1 + \frac{\hbar^2}{2m_2} |\nabla\Psi_2|^2 + V_2(r)n_2 \right. \\ \left. + \frac{1}{2}U_1 n_1^2 + \frac{1}{2}U_2 n_2^2 + U_{12} n_1 n_2 \right\} . \tag{4.4}$$

Minimizing this energy functional subject to the constraint that the particle numbers of each species remain constant, i.e. the wave functions remain normalized, leads directly to the coupled time-independent Gross-Pitaevskii equations (the Lagrange multipliers turn out to be the chemical potentials $\mu_{1,2}$)

$$\left[-\frac{\hbar^2}{2m_1}\nabla^2 + V_1(r) + U_1 |\Psi_1|^2 + U_{12} |\Psi_2|^2\right] \Psi_1 = \mu_1 \Psi_1 \tag{4.5}$$

$$\left[-\frac{\hbar^2}{2m_2}\nabla^2 + V_2(r) + U_2 |\Psi_2|^2 + U_{12} |\Psi_1|^2\right] \Psi_2 = \mu_2 \Psi_2 . \tag{4.6}$$

A condition for multi-species BEC can be easily derived by minimizing the interaction energy (eq. (4.2)) per unit volume

$$\frac{E}{V} = \frac{1}{2}U_1 n_1^2 + \frac{1}{2}U_2 n_2^2 + U_{12} n_1 n_2 \tag{4.7}$$

with respect to the particle densities $n_{1,2}$. The condition for the existence of a minimum is equivalent to the positive definiteness of the Hessian matrix, which leads to

$$U_1 > 0 \qquad \text{and} \qquad U_1 U_2 - U_{12}^2 > 0 , \tag{4.8}$$

or if we assume the single-species scattering lengths $a_{1,2}$ to be positive, the requirement for an overlapping mixture of BEC can be written as

$$-a_C \equiv -\frac{\sqrt{m_1 m_2}}{m_1+m_2}\sqrt{a_1 a_2} < a_{12} < \frac{\sqrt{m_1 m_2}}{m_1+m_2}\sqrt{a_1 a_2} \equiv a_C \ . \tag{4.9}$$

For $a_{12} < -a_C$, the attraction between atoms of type 1 and 2 is too big and the condensate collapses. For $a_{12} > a_C$ on the other hand, the repulsion between the two species is so large that the two condensates separate in space. A very good simulation of the phase diagram of Na-Rb dependent on the interspecies scattering length a_{12} is given in the paper of Ejnisman et al. [44] available at [45].

4.1.2 Inelastic collisions and trap losses

The big problem of realizing BEC was to cool an appropriate number of atoms down to sufficiently low temperatures (below μK) while keeping them in the gaseous phase. Therefore a variety of cooling mechanism have been developed (see section 1). Interactions between the atoms are especially important in evaporative cooling, which is usually the last step. The process is similar to the cooling of a cup of tea, where hot molecules take away kinetic energy by diffusing into the environment and therefore lowering the mean kinetic energy (i.e. temperature) of the remaining tea (which rethermalizes through elastic processes). In cold atomic experiments there are interactions between the trapped atoms and background atoms and among each other. Once the loading is turned off, inelastic collisions will lead to trap losses. The reason for the trap losses is the fact that one can usually just trap atoms in one particular hyperfine state and exchange collisions lead to untrapped states. However, energy may also be released in inelastic processes and hot atoms can exit from the trap. It follows that the atomic density will decay according to a rate equation of the form

$$\frac{dn}{dt} = -\Gamma n - K n^2 - L n^3 \ , \tag{4.10}$$

where the first term stands for the losses due to collisions with background atoms and the second and third term account for two-body and three-body inelastic collisions with rate coefficients K and L, respectively. n is the density of the trapped atoms. Elastic collisions lead to rethermalization of the cloud. More details about BEC theory and atomic trapping is for example given in [46] and [47].

From the derivation in section 2.2.2 one can theoretically obtain the S-Matrix (eq. (2.78)) and the related transition matrix $T_{\alpha\beta} = \delta_{\alpha\beta} - S_{\alpha\beta}$ for a scattering process with incoming channel α and outgoing channel β (see for example in [34]). The average rate for inelastic collisions from a state $\alpha = ij$ (where i and j stand for the state of each atom before the interaction) to $\beta = pq$ is then given by [29]

$$K_{ij\rightarrow pq} = \left\langle \frac{\pi\hbar}{\mu k} \sum_{l,m_l,l',m_l'} \left| T_{ij,pq}^{l,m_l,l',m_l'} \right| \right\rangle \ , \tag{4.11}$$

where we sum over all partial waves l, l' and thermal average $\langle ... \rangle$ over the collision energies. The two-body collision term for the trap loss in eq. (4.10) is then given by

$$\frac{dn_i}{dt} = -\sum_j \sum_{pq\neq ij} (1+\delta_{ij})\, K_{ij\rightarrow pq} n_i n_j \ , \tag{4.12}$$

where we assumed that all inelastic collisions contribute to the trap loss.

Cold atomic interactions are not only important for the evaporative cooling process. They are generally important for answering the question whether BEC is possible or not. The atoms have to remain in the metastable state of a dilute gas down to very low temperatures. In magnetic traps one uses spin-polarized mixtures, i.e. only the triplet potential plays a role. The aim is to prevent the formation of molecules, which would lead to condensation to the liquid or solid phase. For alkali atoms bound states in the triplet potential just occur in three-body collisions which are suppressed at sufficiently low densities. The only chance for the atoms to leave the trap are therefore dipolar collisions which flip the spin and hence lead to untrapped states (see section 1 and 3.1).

4.1.3 Two-species BEC for sodium-rubidium

In this section we would like to show how the results of this work can be used to determine the properties of Na-Rb mixtures. Previous calculations for Na-Rb have been done by Weiss et al. [17] and Pashov et al. [18]. Pashov's potential data provided the basis of this work. They did a close-coupling calculation in order to obtain very accurate potentials. As we have adapted those accurate functions for our calculation and obtained comparable scattering lengths (in section 3.3.2), we can similarly discuss the consequences for Na-Rb experiments.

As seen above, it is important for cooling purposes to achieve a sufficiently high ratio of elastic to inelastic collision rates. Therefore the discussion from chapter 2 can be applied. First of all we can estimate the elastic scattering length as the weighted average of the computed singlet and triplet scattering lengths (section 3.3) according to eq. (2.60). The elastic cross section is then given by (eq.(2.41)) $\sigma = 4\pi a^2$. The inelastic cross section due to spin-flip collisions has been derived in section 2.2.1 and is of the order of $\left(a^{(1)} - a^{(0)}\right)^2$. Therefore the difference of the singlet and triplet scattering lengths has to be smaller than the elastic scattering length. From this point of view ^{23}Na^{87}Rb seems to be the better choice to achieve two-species condensation (compare to Table 3.4).

But the condition for overlapping two-species BEC, which has been derived in 4.1.1, is not satisfied by ^{23}Na^{87}Rb, because $a > a_C$ for all possible combinations of hyperfine states and therefore the condensates separate. The most stable configuration is formed by a Rb-core with a Na-shell, because $a_{Rb}/m_{Rb} < a_{Na}/m_{Na}$ and therefore the repulsion between the sodium atoms pushes them apart [44]. For ^{23}Na^{85}Rb, two-species condensates do not seem to be feasible either because $a > a_C$.

However, there might be a chance to realize overlapping condensates with sodium and rubidium by applying an external magnetic field. Pashov et al. included the Zeeman shift in their calculation and therefore determined scattering lengths dependent on the external field [18]. They have found Feshbach resonance at experimentally achievable fields and hence the scattering lengths might be tuned into a regime where miscible condensates for Na-Rb are possible. The phase diagram for the Na-Rb condensate dependent on the scattering length was presented by Ejnisman et al. ([44],[45]). That motivates further studies of ultracold sodium-rubidium vapors.

4.2 Experimental methods to obtain the scattering parameters for alkali atoms

Theoretical considerations show that the knowledge of the singlet and triplet scattering lengths, and accurate data about the long-range part of the potentials are sufficient for computing all scattering parameters. That can be understood by the fact that the singlet and triplet scattering lengths contain all information about the phase shifts of the radial wave function at short-range ($r < R_0$). The outside behavior of the potentials is well-known and therefore the Schrödinger equation can be in principle integrated.

There are a lot of different methods to identify the scattering lengths. For hydrogen the potentials are well-known and therefore a can be determined through numerical integration. Potentials for alkali atoms heavier than Li on the other hand are not known accurate enough from theoretical considerations for determining the scattering lengths directly. Therefore molecular spectroscopy becomes important. For Li and Na conventional methods lead to results which are acceptable in their accuracy. For higher alkalis though, conventional molecular spectroscopy yields an uncertainty in the vibrational quantum number ν_D greater than 1, which leaves the scattering lengths undetermined (see section 3.2). That's why more accurate methods like photoassociation and direct cross section measurements have been developed, about which we would like to give an overview in the following.

4.2.1 Cold atom photoassociation

This method has been firstly experimentally realized by the Heinzen group at the University of Texas in 1993 [16]. The basic idea is to excite two colliding spin-polarized ground-state atoms into a molecular bound state by a laser field ω_L. A schematic illustration is given in Figure 4.1. As the atoms are spin-polarized, the potentials of interest will be the triplets. The ground-state potential behaves like r^{-6} at long-range due to the van-der-Waals interaction. The excited state, though, corresponds to a mixture of one atom in its s-state ($l = 0$) and the other one in its p-state ($l = 1$), which has a non-vanishing dipole moment that induces a dipole moment in the s-state atom. Therefore the long-range behavior is proportional to r^{-3}. That's why there are bound states at larger distances than for the ground-state mixture.

Because the two atoms collide at a very low temperature, the thermal width in the energy spectrum is very low ($\Delta f(T = 0.5$ mK$) \simeq 10$ MHz), which allows very accurate spectroscopy. The laser field ω_L can be tuned over a certain range. At those points where its energy corrsponds exactly to a ro-vibrational bound state of the excited potential an absorption line can be measured. The absorption rate will vary according to the Franck-Condon factor (overlap between the ground-state and excited bound-state wave function). As it can be seen in Figure 4.1, there are clearly points where the ground-state wave function vanishes. Because of the different long-range behavior of the potentials, it is possible to excite the molecule at ranges where the ground-state potential is basically zero. That's why one can study the long-range behavior of the ground-state wave function, which finally yields the scattering length. Because the upper potential is very deep, the wave function can be approximated to be

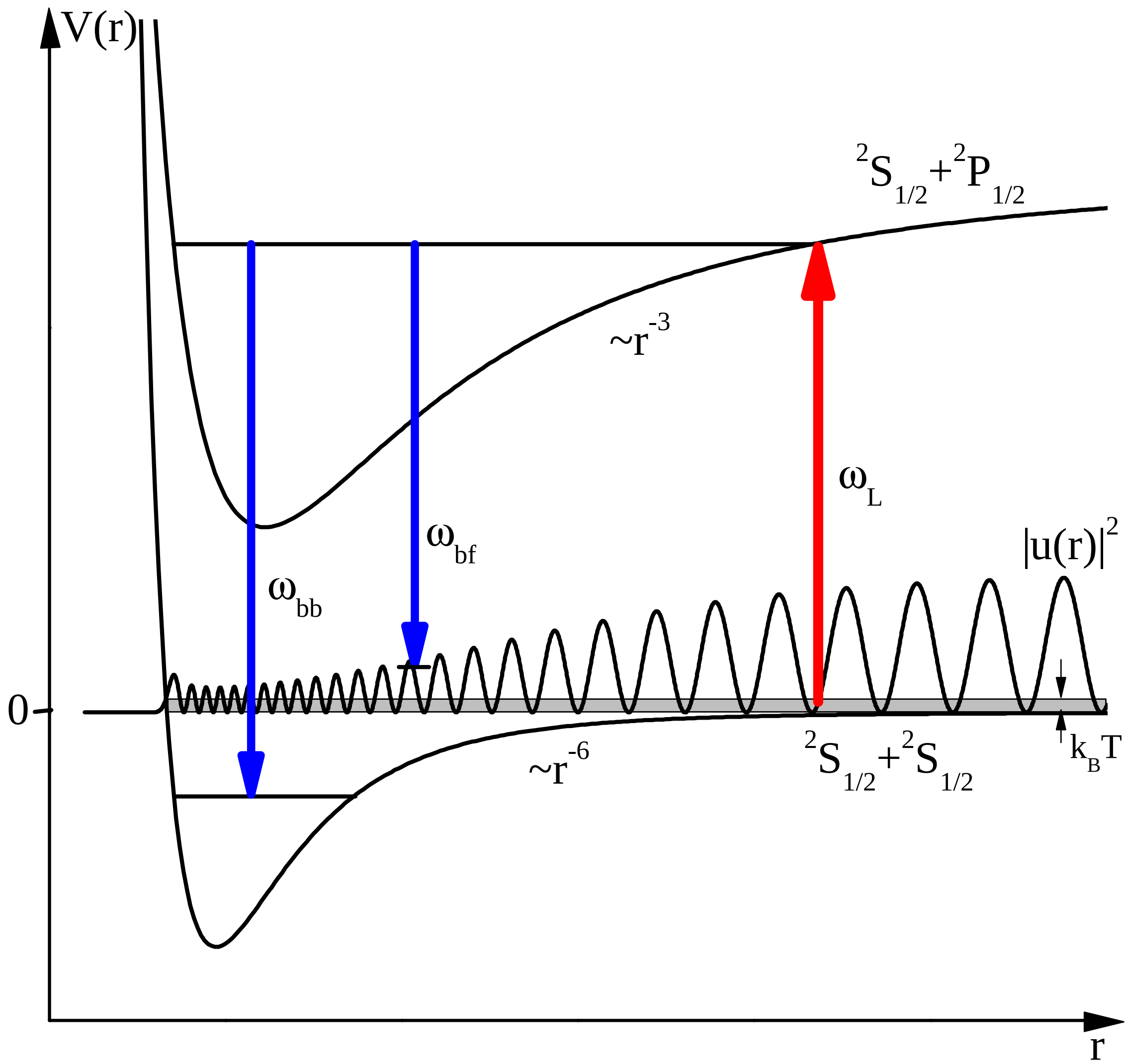

Figure 4.1: Schematic diagram of the cold atom photoassociation process. The potential of the excited molecular state goes as r^{-3} at large distances (dipole interaction), whereas the ground-state behaves like r^{-6} (van-der-Waals potential). ω_L is the frequency of the laser field, ω_{bb} and ω_{bf} are the frequencies of the emitted photons in bound-state → bound-state and bound-state → free-state transitions. $|u(r)|^2$ is the square of the radial wave function of the ground state.

located around the classical turning point, where transitions will therefore preferably occur.

The excited state might absorb another photon which could ionize the molecule. Other possibilities are the decay into a free state (ω_{bf}) (most likely hotter than the other atoms in the trap) or into a vibrational bound state of the ground-state potential (ω_{bb}). An advanced technique of photoassociation is the two-color method. Here, one fixes the frequency ω_L at an appropriate value where transitions occur. A second laser field with higher frequency is tuned and induces transitions from the excited bound state to a bound ground state per stimulated emission. Therefore one can analyze the spectrum of the ground-state potential.

On top of each vibrational level, there are rotational levels with much smaller spacing. Nevertheless those levels can be resolved due to the high resolution of the photoassociation method, which just depends on the temperature of the trapped atoms [29].

4.2.2 Cold collision experiments

The easiest way of determining the magnitude of the scattering length is simply measuring the elastic cross section, which is $8\pi a^2$ for identical bosons (see section 2.1.2). Such measurements can be done in rethermalization experiments, i.e. one perturbes the trapped atoms by suddenly switching on a magnetic field and measures the time until equilibrium is reached again.

In an atomic fountain clock, one measures the transition between two hyperfine states. Contrary to conventional atomic clocks which operate at room temperature, fountain clocks use ultracold atomic gases. Clairon et al. have first built a fountain clock (with ^{133}Cs) [48], which is much more accurate than conventional atomic clocks due to the low thermal width of the velocity distribution of the atoms. Despite the high accuracy, it turns out that elastic collsions between the atoms produce a shift in the measured frequency, which is related to the scattering length [49]. Those clock shifts can be measured and therefore lead to conclusions about elastic scattering properties.

Another very helpful tool are Feshbach resonances. Those occur when the quasi-bound state energy of a closed channel coincides with the incident energy of the atoms in the ground state. At those points the scattering length diverges. The potentials can be tuned around these resonances by a magnetic field due to the Zeeman interaction. Careful analysis of trap loss measurements around Feshbach resonances (or combining the tunable magnetic field with the photoassociation method) gives information on the scattering length [29].

CHAPTER 5

CONCLUSION

In this thesis, we have given an overview of the basic ideas of quantum mechanical scattering theory at low energy. We have tried to support the derivations with illustrative examples.

Afterwards we have dealt specifically with the case of alkali collisions, which is probably the most important application of those concepts. We started off by discussing the properties of the alkali interaction potentials. The numerical calculation of the scattering lengths for Na-Rb and its bound state energies can be seen as the main result of this thesis. It was shown how the one-dimensional Schrödinger equation can be solved for a potential which is not given as an analytical function.

At the end of our work, we have presented the connection between theory and experiment. We make no claim that this part is complete and refer the reader to contemporary papers about experiments in ultracold gases and BEC. We have specifically shown how our results for the scattering lengths can be applied to Na-Rb BEC mixtures. We conclude (similar to previous calculations [17]) that the sodium and rubidium condensates will separate in space and overlapping mixtures do not seem to be feasible. However, miscibility may possibly be achieved by tuning the collision parameters with an external magnetic field.

The treatment of inelastic collisions in Na-Rb gases could be the focus of further studies, which would require accurate knowledge of the interaction potentials. As presented in [34], very sophisticated numerical and variational methods are needed to describe these processes.

APPENDIX A

PROJECTION OF THE SINGLET AND TRIPLET STATE ON THE HYPERFINE STATE

We would like to derive the probability amplitudes A, which were used in section 2.2.1. Therefore we need to project the state $|f_1, m_{f_1}; f_2, m_{f_2}\rangle$ on the singlet (S=0) and triplet (S=1) states. While there are the good quantum numbers $f_1, m_{f_1}, f_2, m_{f_2}$ for a large distance between the atoms, the spins recouple when the atoms get closer and we have the good quantum numbers S, m_S, I, m_I. Therefore we start writing our state in terms of those states $|S, m_s; I, m_I\rangle$:

$$\begin{aligned}
|f_1, m_{f_1}; f_2, m_{f_2}\rangle &= \sum_{F,m_F} |(s_1,i_1)f_1,(s_2,i_2)f_2;F,m_F\rangle \langle f_1,f_2;F,m_F|f_1,m_{f_1};f_2,m_{f_2}\rangle \\
&= \sum_{F,m_F} \langle f_1,m_{f_1};f_2,m_{f_2}|f_1,f_2;F,m_F\rangle \sum_{S,I} |(s_1,s_1)S,(i_1,i_2)I;F,m_F\rangle \\
&\times \langle (s_1,s_2)S,(i_1,i_2)I;F,m_F|(s_1,i_1)f_1,(s_2,i_2)f_2;F,m_F\rangle \\
&= \sum_{F,m_F,S,I} \langle f_1,m_{f_1};f_2,m_{f_2}|f_1,f_2;F,m_F\rangle \\
&\times \langle (s_1,s_2)S,(i_1,i_2)I;F|(s_1,i_1)f_1,(s_2,i_2)f_2;F\rangle \\
&\times \sum_{m_S,m_I} |S,m_s;I,m_I\rangle \langle S,m_s;I,m_I|S,I;F,m_F\rangle \ .
\end{aligned} \tag{A.1}$$

In the second step above we used that the Clebsch-Gordan coefficients are real, so that $\langle f_1, f_2; F, m_F|f_1, m_{f_1}; f_2, m_{f_2}\rangle = \langle f_1, m_{f_1}; f_2, m_{f_2}|f_1, f_2; F, m_F\rangle$. Remember that

$m_F = m_{f_1} + m_{f_2} = m_S + m_I$ due to angular momentum conservation. We obtain the coefficients

$$
\begin{aligned}
A^{f_1,m_{f_1},f_2,m_{f_2}}_{S,m_s,I,m_I} &= \langle S, m_s; I, m_I | f_1, m_{f_1}; f_2, m_{f_2} \rangle \\
&= \sum_F \langle f_1, m_{f_1}; f_2, m_{f_2} | f_1, f_2; F, m_F \rangle \langle S, m_s; I, m_I | S, I; F, m_F \rangle \\
&\times \langle (s_1, s_2) S, (i_1, i_2) I; F | (s_1, i_1) f_1, (s_2, i_2) f_2; F \rangle \ .
\end{aligned}
\tag{A.2}
$$

In this equation we have two Clebsch-Gordan coefficients and we make use of the Wigner-9j-symbol [50] (which is independent of m_F):

$$
\begin{aligned}
&\langle (s_1, s_2) S, (i_1, i_2) I; F | (s_1, i_1) f_1, (s_2, i_2) f_2; F \rangle \\
&= \sqrt{(2S+1)(2I+1)(2f_1+1)(2f_2+1)} \begin{Bmatrix} s_1 & s_2 & S \\ i_1 & i_2 & I \\ f_1 & f_2 & F \end{Bmatrix} \ .
\end{aligned}
\tag{A.3}
$$

Now we can compute the projection probabilities for the singlet and triplet state, respectively. The only additionally required parameters are the nuclear spins i_1, i_2 (see Table 3.1). The final result is given by

$$
\begin{aligned}
P^{(S=0)}_{i_1,i_2}(f_1, m_{f_1}, f_2, m_{f_2}) &= \sum_{I,m_I} \left| A^{f_1,m_{f_1},f_2,m_{f_2}}_{S=0,m_s=0,I,m_I} \right|^2 \\
P^{(S=1)}_{i_1,i_2}(f_1, m_{f_1}, f_2, m_{f_2}) &= \sum_{I,m_I,m_s} \left| A^{f_1,m_{f_1},f_2,m_{f_2}}_{S=1,m_s,I,m_I} \right|^2 \ .
\end{aligned}
\tag{A.4}
$$

The presented calculation can be easily done with Mathematica (see Figure A.1 and A.2).

In order to calculate the elastic spin-flip cross section, we need to determine the

```
(*This procedure calculates the Wigner-9j-symbol*)
Clear[nineJSymbol, c, Ps, Pt];
nineJSymbol[{j1_, j2_, j3_}, {j4_, j5_, j6_}, {j7_, j8_, j9_}] :=
 Module[{kmin, kmax},
        kmin = Max[{Abs[j1 - j9], Abs[j4 - j8], Abs[j2 - j6]}];
            kmax = Min[{Abs[j1 + j9], Abs[j4 + j8], Abs[j2 + j6]}];
        Sum[(-1) ^ (2 k) (2 k + 1) SixJSymbol[{j1, j4, j7}, {j8, j9, k}]
    SixJSymbol[{j2, j5, j8}, {j4, k, j6}] SixJSymbol[{j3, j6, j9}, {k, j1, j2}],
   {k, kmin, kmax}]
        ]

(*Computing the coefficient C from the text*)
c[f1_, mf1_, f2_, mf2_, S_, ms_, i_, mI_, i1_, i2_] := Module[{F, mF, result},

  If[mf1 + mf2 == ms + mI && i ≤ Abs[i1 + i2] && i ≥ Abs[i1 - i2] && mI ≥ -i &&
    mI ≤ i && ms ≤ S && ms ≥ -S && f1 ≤ Abs[i1 + 1 / 2] && f1 ≥ Abs[i1 - 1 / 2] &&
    f2 ≤ Abs[i2 + 1 / 2] && f2 ≥ Abs[i2 - 1 / 2] && mf1 ≤ f1 && mf1 ≥ -f1 &&
    mf2 ≤ f2 && mf2 ≥ -f2,
   F = Min[Abs[S + i], Abs[f1 + f2]];
   mF = mf1 + mf2;
   result = 0;
   While[F ≥ Max[Abs[S - i], Abs[f1 - f2]],
    If[F ≥ mF && mF ≥ -F,
     result = result + ClebschGordan[{f1, mf1}, {f2, mf2}, {F, mF}] *
         ClebschGordan[{S, ms}, {i, mI}, {F, mF}] *
         Sqrt[(2 S + 1) (2 i + 1) (2 f1 + 1) (2 f2 + 1)] *
         nineJSymbol[{1 / 2, 1 / 2, S}, {i1, i2, i}, {f1, f2, F}];];
    F --];
   N[result],
   Text["Check quantum numbers! (Consider: mf1+mf2 != mS+mI)"]]]
```

Figure A.1: The Mathematica source code for calculating the singlet and triplet coefficients according to eq. (A.2); the coefficient A is labeled with c.

```
(*Singlet probability*)
Ps[f1_, mf1_, f2_, mf2_, i1_, i2_] := Module[{ms, i, mI, result},
  ms = 0;
  i = Abs[i1 + i2];
  result = 0;
  While[i ≥ Abs[i1 - i2],
   mI = i;
   While[mI ≥ -i,
    If[mI + ms == mf1 + mf2,
     result = result + (c[f1, mf1, f2, mf2, 0, ms, i, mI, i1, i2])^2;];
    mI--];
   i--];
  result]

(*Triplet probability*)
Pt[f1_, mf1_, f2_, mf2_, i1_, i2_] := Module[{ms, i, mI, result},
  i = Abs[i1 + i2];
  result = 0;
  While[i ≥ Abs[i1 - i2],
   mI = i;
   While[mI ≥ -i,
    ms = 1;
    While[ms ≥ -1,
     If[mI + ms == mf1 + mf2,
      result = result + (c[f1, mf1, f2, mf2, 1, ms, i, mI, i1, i2])^2;
      ];
     ms--];
    mI--];
   i--];
  result]
```

Figure A.2: Computing the singlet and triplet probabilities with Mathematica scattering amplitude (eq. (2.58))

$$f^{(f_1 \to f_1')} = \sum_S \left(\sum_{m_S, I, m_I} A_{S,m_s,I,m_I}^{f_1,m_{f_1},f_2,m_{f_2}} A_{S,m_s,I,m_I}^{f_1',m_{f_1},f_2,m_{f_2}} \right) f^{(S)} \equiv \sum_S B^{(S)} f^{(S)} \ . \tag{A.5}$$

Using identities about Racah coefficients (Wigner-9j-symbols) and Clebsch-Gordan coefficients, one can show that [31]

$$B^{(0)} = -B^{(1)} \equiv \frac{\sqrt{M_{SF}}}{2} \ . \tag{A.6}$$

In Table A.1 we just want to give 3 examples which illustrate this relation. For our calculation we used the Mathematica procedure which is shown in Figure A.3.

Eq. (2.61) follows directly when we use the relation between the scattering length and scattering amplitude (eq. (2.56)).

Table A.1: Examples for projection coefficients B in order to illustrate eq. (A.6)

f_1	m_{f_1}	f_1'	f_2	m_{f_2}	i_1	i_2	$B^{(0)}$	$B^{(1)}$
1	-1	2	1	-1	3/2	3/2	-0.11	0.11
2	1	1	3	1	3/2	5/2	-0.07	0.07
2	1	3	2	1	5/2	3/2	-0.12	0.12

```
Bs[f1_, mf1_, f12_, mf12_, f2_, mf2_, i1_, i2_] := Module[{ms, i, mI, result},
  ms = 0;
  i = Abs[i1 + i2];
  result = 0;
  While[i ≥ Abs[i1 - i2],
   mI = i;
   While[mI ≥ -i,
    If[mI + ms == mf1 + mf2 && mI + ms == mf12 + mf2,
     result = result + c[f1, mf1, f2, mf2, 0, ms, i, mI, i1, i2] *
         c[f12, mf12, f2, mf2, 0, ms, i, mI, i1, i2];];
    mI--];
   i--];
  result]

Bt[f1_, mf1_, f12_, mf12_, f2_, mf2_, i1_, i2_] := Module[{ms, i, mI, result},
  i = Abs[i1 + i2];
  result = 0;
  While[i ≥ Abs[i1 - i2],
   mI = i;
   While[mI ≥ -i,
    ms = 1;
    While[ms ≥ -1,
     If[mI + ms == mf1 + mf2 && mI + ms == mf12 + mf2,
      result = result + c[f1, mf1, f2, mf2, 1, ms, i, mI, i1, i2] *
          c[f12, mf12, f2, mf2, 1, ms, i, mI, i1, i2];
     ];
     ms--];
    mI--];
   i--];
  result]
```

Figure A.3: Module to compute the coefficients B defined in eq. (A.5)

APPENDIX B

EXAMPLE FOR THE SOLUTION OF THE TWO-STATE CLOSE-COUPLING EQUATION

In order to refer to the solution of the close-coupling equation (eq. (2.72)), we would like to present a very simple model for the 1s-2s excitation of hydrogen by electron impact. We will be able to determine the elastic and inelastic cross sections for this problem according to eq. (2.76). This calculation is for illustrative purposes only and is not related to alkali collisions by any means.

This example has been presented by B.H. Bransden and J.S.C. McKee ([51],[52]). We consider the hydrogen atom as a two-state system (1s-2s) and neglect all higher orbitals. Furthermore we are concentrating on s-wave scattering. Therefore we can write the overall wave function of the system as a product of the hydrogenic wave function (ϕ_i) and the s-wave function of the free electron (G_i) (which has no angular dependence, as $l = 0$)

$$\Psi(\vec{r},\vec{x}) = \phi_0(x)\frac{G_0(r)}{k_0 r} + \phi_1(x)\frac{G_1(r)}{k_0 r} \ , \tag{B.1}$$

where the indices 0 and 1 correspond to the 1s-state and the 2s-state in order to make the notation conform with the previous discussion. The according wave functions are

$$\phi_0(x) = \frac{1}{\sqrt{\pi}}\left(\frac{1}{a_0}\right)^{\frac{3}{2}} e^{-\frac{x}{a_0}} \tag{B.2}$$

$$\phi_1(x) = \frac{1}{4\sqrt{2\pi}}\left(\frac{1}{a_0}\right)^{\frac{3}{2}}\left(2 - \frac{x}{a_0}\right) e^{-\frac{x}{2a_0}} \tag{B.3}$$

with the energies

$$\epsilon_0 = -13.6 \text{ eV} \qquad\qquad \text{and} \qquad\qquad \epsilon_1 = -\frac{1}{2^2} \cdot 13.6 \text{ eV} \; . \tag{B.4}$$

The simplest approximation to the potential is given by

$$V(\vec{r}, \vec{x}) = Ke^2 \left(\frac{1}{|\vec{r} - \vec{x}|} - \frac{1}{r} \right) \tag{B.5}$$

with $K = \frac{1}{4\pi\epsilon_0}$. $\vec{r}$ and $\vec{x}$ represent the relative coordinate between the proton and the bound and free electron, respectively (see Figure B.1).

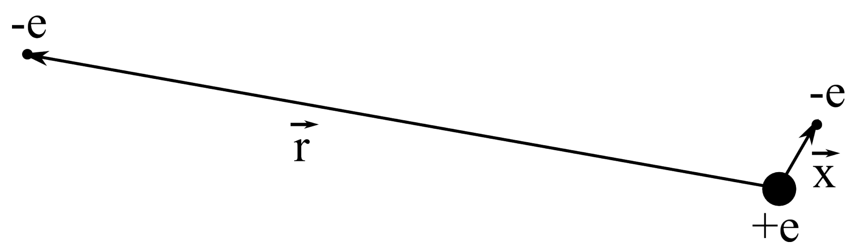

Figure B.1: Sketch of the scattering process of a free electron by a hydrogen atom. The distance between the proton and the free electron is denoted by $\vec{r}$. $\vec{x}$ indicates the the distance between the proton and the valence electron.

We are neglecting the possibility of electron exchange. That's why this model is not very realistic, but illustrates the previous discussion. A more careful treatment of this problem has been presented, for example, by Massey and Moiseiwitsch [53] or Marriott [54].

In the following we will work in atomic units. All lengths are given in units of a_0 and all energies as multiples of Bohr's ground state energy 13.6 eV or as wave numbers in units $1/a_0^2$, respectively. With $a_0 = \frac{\hbar^2}{m_e K e^2}$ and $\mu \approx m_e$, we get for the close-coupling equations (eq. (2.72))

$$\begin{aligned} \left(\frac{d^2}{dr^2} + k_0^2 - 2V_{00}(r) \right) G_0(r) &= 2V_{01}(r) G_1(r) \\ \left(\frac{d^2}{dr^2} + k_1^2 - 2V_{11}(r) \right) G_1(r) &= 2V_{10}(r) G_0(r) \end{aligned} \tag{B.6}$$

with $k_1^2 = k_0^2 - (\epsilon_1 - \epsilon_0) = k_0^2 - 3/4$ (in units $1/a_0^2$), as $\frac{2m_e}{\hbar^2} \cdot 13.6\ \text{eV} = \frac{2m_e}{\hbar^2} \cdot \frac{Ke^2}{2a_0} = \frac{1}{a_0^2}$. Furthermore, we get for the matrix elements $V_{ij}(r)$

$$\begin{aligned} V_{ij}(r) &= \int d^3x \phi_i(x)\phi_j(x)V(\vec{r},\vec{x}) \\ &= \int_0^{2\pi} d\phi \int_{-1}^{1} d\cos\theta \int_0^{\infty} dx\ x^2\phi_i(x)\phi_j(x) \left(\frac{1}{\sqrt{r^2+x^2-2rx\cos\theta}} - \frac{1}{r} \right) . \end{aligned} \tag{B.7}$$

That yields

$$V_{00}(r) = -\left(1+\frac{1}{r}\right)e^{-2r} \tag{B.8}$$

$$V_{11}(r) = -\left(\frac{1}{r}+\frac{3}{4}+\frac{1}{4}r+\frac{1}{8}r^2\right)e^{-r} \tag{B.9}$$

$$V_{01}(r) = V_{10}(r) = \frac{\sqrt{8}}{27}(2+3r)\,e^{-\frac{3}{2}r}\ . \tag{B.10}$$

As it can be seen in Figure B.2 the range of the potentials is about 10 a_0. For larger distances we expect sinusoidal solutions and therefore we require them to satisfy the conditions given in eq. (2.73). If we choose

$$\alpha^{00} = \frac{a}{1-ia} \tag{B.11}$$

and

$$\alpha^{01} = d\ , \tag{B.12}$$

we can rewrite the boundary conditions as

$$\begin{aligned} G_0(0) &= G_1(0) = 0 \\ G_0(r \gg 0) &\simeq \sin k_0 r + a\cos k_0 r \\ G_1(r \gg 0) &\simeq d e^{ik_1 r}\ . \end{aligned} \tag{B.13}$$

Note that there is actually a factor of $\frac{1}{1-ia}$, which does not change the solution as it is just a scaling factor for $G_i(r)$. Nevertheless it shows up in the total cross sections

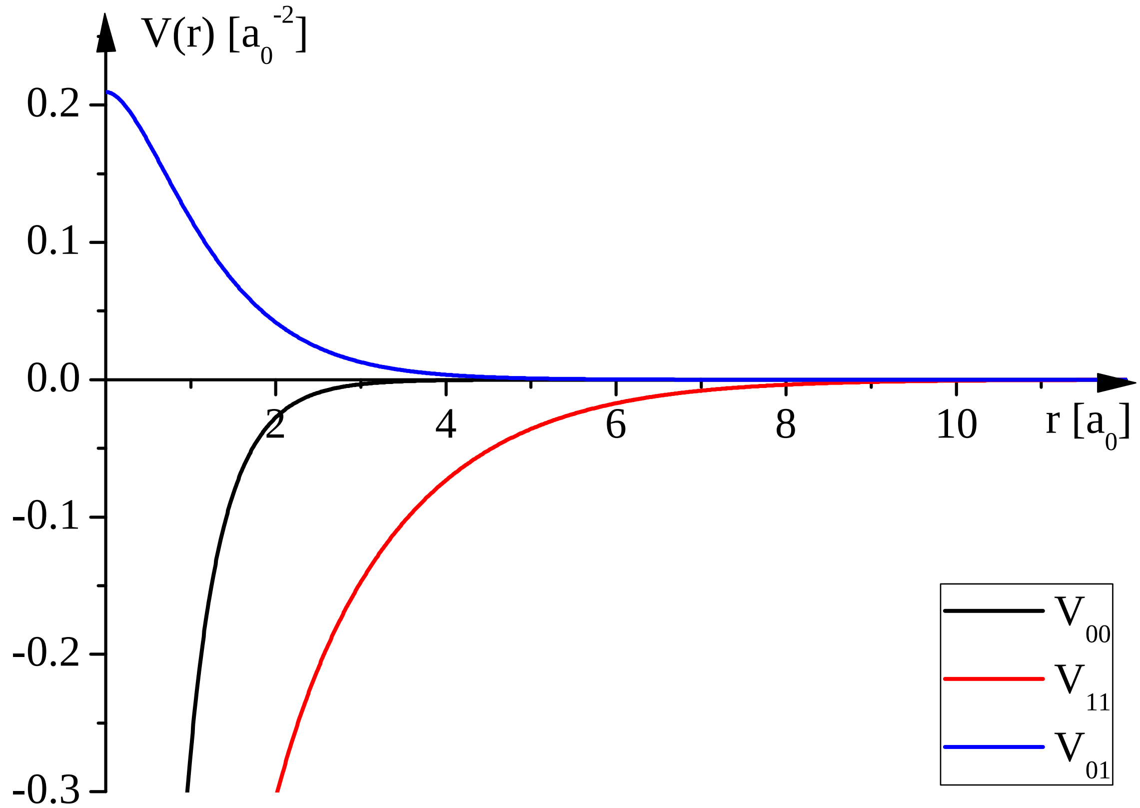

Figure B.2: Interaction potential for our simple model of the 1s-2s excitation; the range of the potentials is about 10 a_0.

(compare to eq. (2.76)), which are

$$\sigma^{00} = \frac{4\pi}{k_0^2}\left|\frac{a}{1-ia}\right|^2 \qquad \text{and} \qquad \sigma^{01} = \frac{4\pi k_1}{k_0^3}\left|\frac{d}{1-ia}\right|^2 . \tag{B.14}$$

The non-trivial part of solving this problem is to find two *independent* pairs of solutions $F_0^j(r), F_1^j(r)$ $(j = 1, 2)$ for eq. (B.6), which satisfy the boundary conditions

$$\begin{aligned} F_0^j(0) = F_1^j(0) &= 0 \\ F_0^j(r \gg 1) &\simeq A^j \sin k_0 r + B^j \cos k_0 r \\ F_1^j(r \gg 1) &\simeq C^j \sin k_0 r + D^j \cos k_0 r \end{aligned} \tag{B.15}$$

with real coefficients A^j, B^j, C^j, D^j. Once we have found those solutions, we can write $G_i(r)$ as a linear combination

$$\begin{aligned} G_0(r) &= \lambda F_0^1(r) + \mu F_0^2(r) \\ G_1(r) &= \lambda F_1^1(r) + \mu F_1^2(r) \end{aligned} \tag{B.16}$$

with complex coefficients λ and μ. By comparing eq. (B.15) to eq. (B.13) we find the following set of 8 linear equations (4 for real and imaginary part), which determine the scattering parameters a and d:

$$\lambda \begin{pmatrix} A^1 \\ B^1 \\ C^1 \\ D^1 \end{pmatrix} + \mu \begin{pmatrix} A^2 \\ B^2 \\ C^2 \\ D^2 \end{pmatrix} = \begin{pmatrix} 1 \\ a \\ id \\ d \end{pmatrix} \tag{B.17}$$

Similarly we can find a solution for the cross sections σ^{10} and σ^{11}, if we start in the

2s-state. In this case we would have to choose different boundary conditions

$$\begin{aligned} G_0(0) &= G_1(0) = 0 \\ G_0(r \gg 0) &\simeq g e^{ik_0 r} \\ G_1(r \gg 0) &\simeq \sin k_1 r + h \cos k_1 r \ . \end{aligned} \tag{B.18}$$

We can again write this solution as a superposition of our independent solutions (eq. (B.15)) and therefore get a similar set of linear equations

$$\eta \begin{pmatrix} A^1 \\ B^1 \\ C^1 \\ D^1 \end{pmatrix} + \nu \begin{pmatrix} A^2 \\ B^2 \\ C^2 \\ D^2 \end{pmatrix} = \begin{pmatrix} ig \\ g \\ 1 \\ h \end{pmatrix} \tag{B.19}$$

The cross sections are then given by

$$\sigma^{11} = \frac{4\pi}{k_1^2} \left| \frac{h}{1 - ih} \right|^2 \qquad \text{and} \qquad \sigma^{10} = \frac{4\pi k_0}{k_1^3} \left| \frac{g}{1 - ih} \right|^2 \ . \tag{B.20}$$

In order to obtain the two independent solutions for $F_0^j(r), F_1^j(r)$ $(j = 1, 2)$, we integrated eq. (B.6) numerically with Mathematica. We used the built-in procedure NDSolve. As initial conditions for the numerical solution, we chose

$$\begin{aligned} &F_0^j(0) = F_1^j(0) = 0 \qquad j = 1, 2 \\ &F_1^{1\prime}(0) = F_0^{2\prime}(0) = 1 \\ &F_0^{1\prime}(0) = x \\ &F_1^{2\prime}(0) = y \ , \end{aligned} \tag{B.21}$$

where x and y can be varied. $x = y = 0.0001$ turned out to be a good choice in order to make the two solutions independent. One solution for $E = 20$ eV is shown in

Figure B.3. We analyzed the long-range part of those solution and fitted a sinosoidal

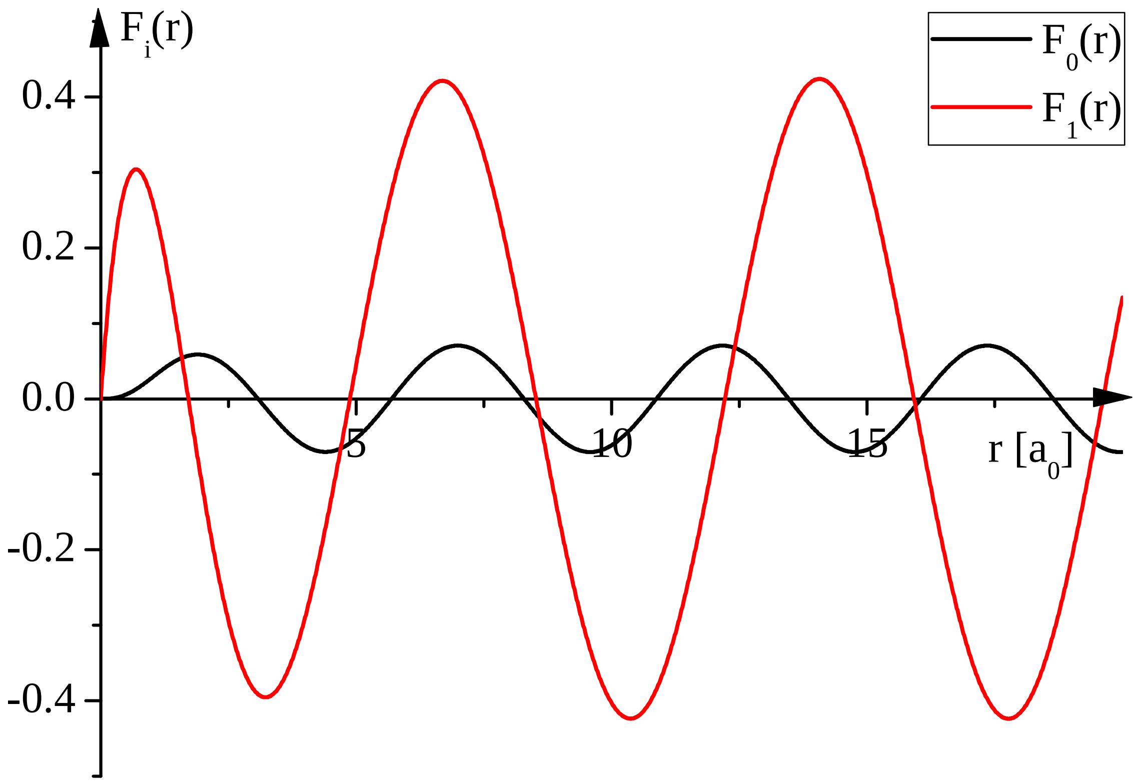

Figure B.3: Numerical solution for $E = 20$ eV ($k_0^2 = 1.47\ a_0^{-2}$), for $r > 10\ a_0$ it has a sinusoidal shape.

function of the form

$$F_i(r) \simeq \tilde{A}_i \sin\left(k_i r + \delta_i\right) \ . \tag{B.22}$$

From the coefficients $\tilde{A}_i, \delta_i$ we can compute the coefficients A, B, C, D using the following identity

$$C_1 \sin \omega t + C_2 \cos \omega t = C \sin(\omega t + \varphi) \tag{B.23}$$

with $C = \sqrt{C_1^2 + C_2^2}$ and $\tan\varphi = \frac{C_2}{C_1}$. The source code for the procedure to obtain the independent solutions is given in Figure B.4. The according cross sections are calculated with the program crosssection (Figure B.5).

The final results for the cross sections are shown in Figure B.6, B.7 and B.8. In Table B.1 and B.2 we compare our results to those calculated by Bransden and McKee in [51] and find a very good agreement.

```
(*This procedure finds two independent solutions for the coupled
  differential equation for a given energy and returns the long-
 range coefficients Ai,Bi,Ci,Di (i=1,2)
  x and y are the initial conditions for the slopes of the two solutions at r=
 0*)
solution[energy_, x_, y_] :=
 Module[{sol1, sol2, max11, max12, max21, max22, root11, root12, root21,
   root22, δ11, δ12, , δ21, δ22, k0, k11, A1, B1, C1, D1, A2, B2, C2, D2,
   r11, r12, r21, r22},
  (*Defining the wave numbers k0,k1*)
  k0 = Sqrt[energy / 13.6];
  k11 = Sqrt[k0 ^ 2 - 0.75];
  (*Obtaining a numerical solution for the coupled differential equation*)
  sol1 =
   NDSolve[
    {{f1''[r] + (k1^2 + 2 Exp[-2 r] * (1 + 1 / r)) * f1[r] ==
        2 * Sqrt[8] / 27 * (2 + 3 r) Exp[-3 r / 2] * f2[r],
      f2''[r] + (k1^2 - 3 / 4 + 2 Exp[-r] (1 / r + 3 / 4 + 1 / 4 * r + 1 / 8 * r ^ 2)) * f2[r] ==
        2 * Sqrt[8] / 27 * (2 + 3 r) Exp[-3 r / 2] * f1[r]},
     {f1[10 ^ (-10)] == 10 ^ (-10), f1'[10 ^ (-10)] == x, f2[10 ^ (-10)] == 10 ^ (-10),
      f2'[10 ^ (-10)] == 1}} /. k1 → k0, {f1[r], f2[r]}, {r, 10 ^ (-14), 100}];
  sol2 =
   NDSolve[
    {{f1''[r] + (k1^2 + 2 Exp[-2 r] * (1 + 1 / r)) * f1[r] ==
        2 * Sqrt[8] / 27 * (2 + 3 r) Exp[-3 r / 2] * f2[r],
      f2''[r] + (k1^2 - 3 / 4 + 2 Exp[-r] (1 / r + 3 / 4 + 1 / 4 * r + 1 / 8 * r ^ 2)) * f2[r] ==
        2 * Sqrt[8] / 27 * (2 + 3 r) Exp[-3 r / 2] * f1[r]},
     {f1[10 ^ (-10)] == 10 ^ (-10), f1'[10 ^ (-10)] == 1, f2[10 ^ (-10)] == 10 ^ (-10),
      f2'[10 ^ (-10)] == y}} /. k1 → k0, {f1[r], f2[r]}, {r, 10 ^ (-14), 100}];

  (*Analyzing the long-range behavior of the first solution*)
  (*First we are searching for a root of the numerical solution at long-
   range and obtain the phase shift δ*)
  root11 = Evaluate[r /. FindRoot[Evaluate[f1[r] /. sol1], {r, 40}]];
  root12 = Evaluate[r /. FindRoot[Evaluate[f2[r] /. sol1], {r, 40}]];
  δ11 = Mod[-k0 * root11, 2 Pi];
  δ12 = Mod[-k11 * root12, 2 Pi];
```

(a)

Figure B.4: Procedure to obtain two independent solutions for eq. (B.6) and the coefficients A^j, B^j, C^j, D^j

```
(*Obtaining one maximum of the solution at long-range*)
max11 = First[FindMaximum[Evaluate[f1[r] /. sol1], {r, 40, 50},
    WorkingPrecision → 10]];
max12 = First[FindMaximum[Evaluate[f2[r] /. sol1], {r, 40, 50},
    WorkingPrecision → 10]];
r11 =
  Evaluate[
   r /. Last[FindMaximum[Evaluate[f1[r] /. sol1], {r, 40, 45},
      WorkingPrecision → 10]]];
r12 =
  Evaluate[
   r /. Last[FindMaximum[Evaluate[f2[r] /. sol1], {r, 40, 45},
      WorkingPrecision → 10]]];

(*Analyzing the long-range behavior of the second solution in the same way*)
root21 = Evaluate[r /. FindRoot[Evaluate[f1[r] /. sol2], {r, 40}]];
root22 = Evaluate[r /. FindRoot[Evaluate[f2[r] /. sol2], {r, 40}]];
δ21 = Mod[-k0 * root21, 2 Pi];
δ22 = Mod[-k11 * root22, 2 Pi];

max21 = First[FindMaximum[Evaluate[f1[r] /. sol2], {r, 40, 50},
    WorkingPrecision → 10]];
max22 = First[FindMaximum[Evaluate[f2[r] /. sol2], {r, 40, 50},
    WorkingPrecision → 10]];
r21 =
  Evaluate[
   r /. Last[FindMaximum[Evaluate[f1[r] /. sol2], {r, 40, 45},
      WorkingPrecision → 10]]];
r22 =
  Evaluate[
   r /. Last[FindMaximum[Evaluate[f2[r] /. sol2], {r, 40, 45},
      WorkingPrecision → 10]]];
```

(b)

Figure B.4: Continued

```
(*Calculating the long-range coefficients defined in the text*)
 A1 = max11 / Sqrt[1 + Tan[δ11] ^ 2];
 B1 = max11 * Tan[δ11] / Sqrt[1 + Tan[δ11] ^ 2];
 C1 = max12 / Sqrt[1 + Tan[δ12] ^ 2];
 D1 = max12 * Tan[δ12] / Sqrt[1 + Tan[δ12] ^ 2];
 A2 = max21 / Sqrt[1 + Tan[δ21] ^ 2];
 B2 = max21 * Tan[δ21] / Sqrt[1 + Tan[δ21] ^ 2];
 C2 = max22 / Sqrt[1 + Tan[δ22] ^ 2];
 D2 = max22 * Tan[δ22] / Sqrt[1 + Tan[δ22] ^ 2];

 (*There can still be a phase difference of π between the numerical
   solution and the sinosoidal function at long-range,
 so we compare the both solutions and in case of a difference,
 we get rid of the phase shift*)
 If[(First[Evaluate[f1[r] /. sol1] /. r → r11] > 0 &&
     (A1 * Sin[k0 * r11] + B1 * Cos[k0 * r11]) < 0), A1 = -A1; B1 = -B1];
 If[(First[Evaluate[f2[r] /. sol1] /. r → r12] > 0 &&
     (C1 * Sin[k11 * r12] + D1 * Cos[k11 * r12]) < 0), C1 = -C1; D1 = -D1];
 If[(First[Evaluate[f1[r] /. sol2] /. r → r21] > 0 &&
     (A2 * Sin[k0 * r21] + B2 * Cos[k0 * r21]) < 0), A2 = -A2; B2 = -B2];
 If[(First[Evaluate[f2[r] /. sol2] /. r → r22] > 0 &&
     (C2 * Sin[k11 * r22] + D2 * Cos[k11 * r22]) < 0), C2 = -C2; D2 = -D2];

 (*Returning the coefficients*)
 Return[{A1, B1, C1, D1, A2, B2, C2, D2,
    {Mod[δ11 - δ21 - Pi / 2, Pi], Mod[δ12 - δ22 - Pi / 2, Pi]}, sol1, sol2}];
 ];
```

(c)

Figure B.4: Continued

```
(*This program calculates the different cross sections for a given
 energy and given initial conditions x and y (defined as before)*)
crosssection[energy_, x_, y_] :=
 Module[{k0, k1, A1, A2, B1, B2, C1, C2, D1, D2, sol, sol1, sol2, a1, a2,
   a, d1, d2, d, g1, g2, ge, h1, h2, h, σ11, σ12, σ21, σ22},
  (*Defining the wave numbers k0,k1*)
  k0 = Sqrt[energy / 13.6];
  k1 = Sqrt[k0^2 - 0.75];
  (*Get the long-range coefficient from the procedure solution*)
  sol = solution[energy, x, y];
  A1 = Extract[sol, {1}];
  B1 = Extract[sol, {2}];
  C1 = Extract[sol, {3}];
  D1 = Extract[sol, {4}];
  A2 = Extract[sol, {5}];
  B2 = Extract[sol, {6}];
  C2 = Extract[sol, {7}];
  D2 = Extract[sol, {8}];

  (*Solve the system of linear equations for the case when the system
    is initially in the 1s-state*)
  sol1 = Solve[{A1 * l1 + A2 * m1 == 1, A1 * l2 + A2 * m2 == 0, B1 * l1 + B2 * m1 == α1,
     B1 * l2 + B2 * m2 == α2, C1 * l1 + C2 * m1 == -δ2, C1 * l2 + C2 * m2 == δ1,
     D1 * l1 + D2 * m1 == δ1, D1 * l2 + D2 * m2 == δ2}, {α1, α2, δ1, δ2, l1, l2, m1, m2}];
  a1 = Evaluate[α1 /. sol1];
  a2 = Evaluate[α2 /. sol1];
  a = a1 + I * a2;
  d1 = Evaluate[δ1 /. sol1];
  d2 = Evaluate[δ2 /. sol1];
  d = d1 + I * d2;
```
(a)

Figure B.5: Procedure to compute the total cross sections given in eq. (B.14) and (B.20)

```
(*Calculate the cross sections*)
  σ11 = 4 / k0^2 * Abs[a / (1 - I * a)]^2;
  σ12 = 4 k1 / k0^3 * Abs[d / (1 - I * a)]^2;

  (*Solve the system of linear equations for the case when the system
    is initially in the 2s-state*)
  sol2 = Solve[{A1 * l1 + A2 * m1 == -γ2, A1 * l2 + A2 * m2 == γ1, B1 * l1 + B2 * m1 == γ1,
      B1 * l2 + B2 * m2 == γ2, C1 * l1 + C2 * m1 == 1, C1 * l2 + C2 * m2 == 0,
      D1 * l1 + D2 * m1 == η1, D1 * l2 + D2 * m2 == η2}, {γ1, γ2, η1, η2, l1, l2, m1, m2}];
  g1 = Evaluate[γ1 /. sol2];
  g2 = Evaluate[γ2 /. sol2];
  ge = g1 + I * g2;
  h1 = Evaluate[η1 /. sol2];
  h2 = Evaluate[η2 /. sol2];
  h = h1 + I * h2;

  (*Calculate the cross sections*)
  σ22 = 4 / k1^2 * Abs[h / (1 - I * h)]^2;
  σ21 = 4 k0 / k1^3 * Abs[ge / (1 - I * h)]^2;

  (*Return the solution*)
  Return[{First[σ11], First[σ12], First[σ21], First[σ22]}];
  ];
```

(b)

Figure B.5: Continued

Because we did a close-coupling calculation, our results have to obey the particle conservation theorem which implies the following connection between σ^{01} and σ^{10} [22]:

$$k_0^2 \sigma^{01} = k_1^2 \sigma^{10} \ . \tag{B.24}$$

That this relation is indeed satisfied can be seen in Figure B.6.

It can be seen in Figure B.8 and Table B.2 that the description in the low energy regime is not very accurate. Firstly we observe that the numerical calculation is not very stable when $k_1 \simeq 0$. Another even more crucial point is that electron exchange becomes more likely in this regime as the incident electron has a very low energy and therefore the effective time of interaction is longer. Our derivation neglects this possibility completely and can therefore not be used for an accurate description in this energy range.

Table B.1: Comparison of our results with those given in [51] when starting in the groundstate.

Energy E_0 [eV]	σ^{00} $[\pi a_0^2]$		σ^{01} $[\pi a_0^2]$	
	this work	[51]	this work	[51]
11.5	2.539	2.52	0.290	0.286
13.5	2.147	2.12	0.203	0.204
19.4	1.433	1.42	0.104	0.102
30.4	0.835	0.828	0.0456	0.0450
54.0	0.398	0.394	0.0157	0.0155

In summary we have seen how to numerically solve a coupled differential equation of the type of eq. (2.72). Next to the presented numerical solution, there are also several variational methods, which can be used as an approximation. For the given problem such methods are for example presented in [52].

Table B.2: Comparison of our results for σ^{11} with [51], the energy is given relative to the 2s-level. The overall agreement is very good except for the lowest energy. It can be also seen in Figure B.8 that there occur numerical errors in this regime. The reason for that is mainly that $k1 \simeq 0$. A more careful analysis of the low-energy regime is given in the text.

Energy E_1 [eV]	σ^{11} [πa_0^2]	
	this work	[51]
1.35	0.216	2.05
3.38	1.953	1.97
9.32	3.394	3.40
20.30	2.400	2.39
43.90	1.178	1.17

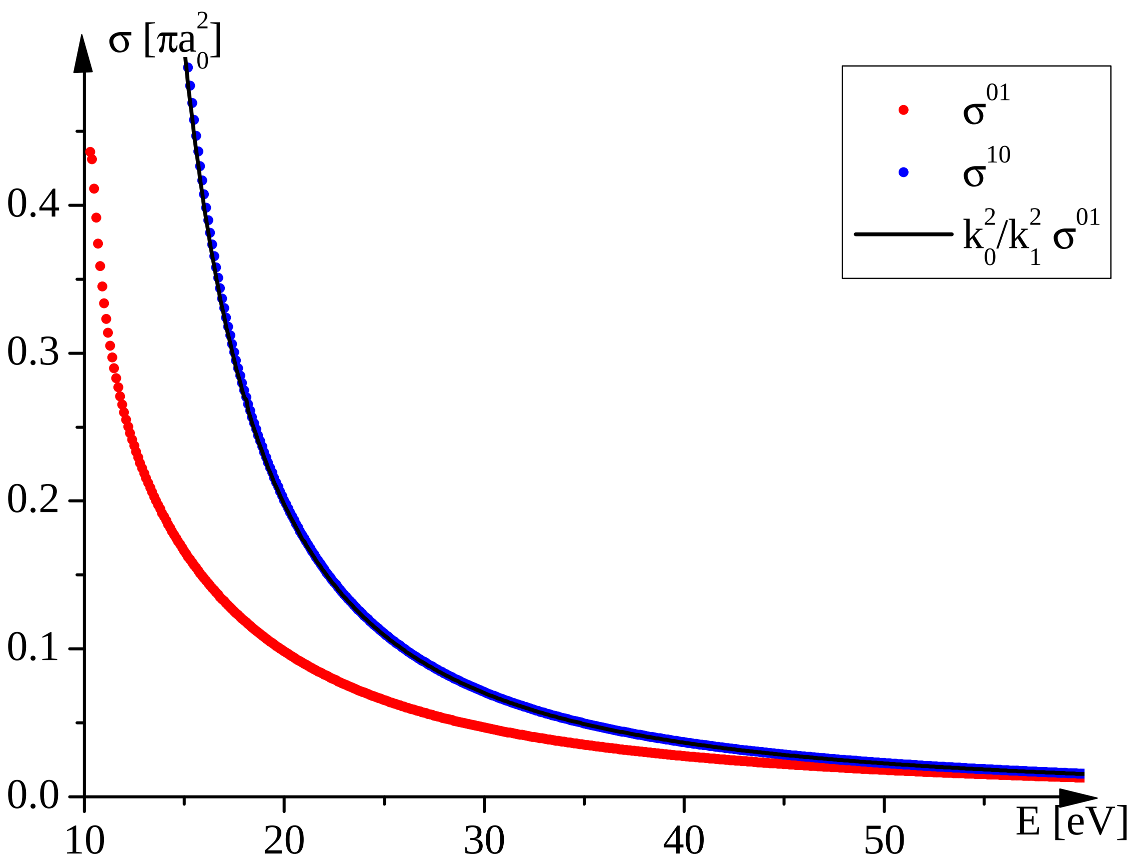

Figure B.6: Cross sections for transitions $1s \leftrightarrow 2s$. It is shown that the solutions satisfy eq. (B.24)

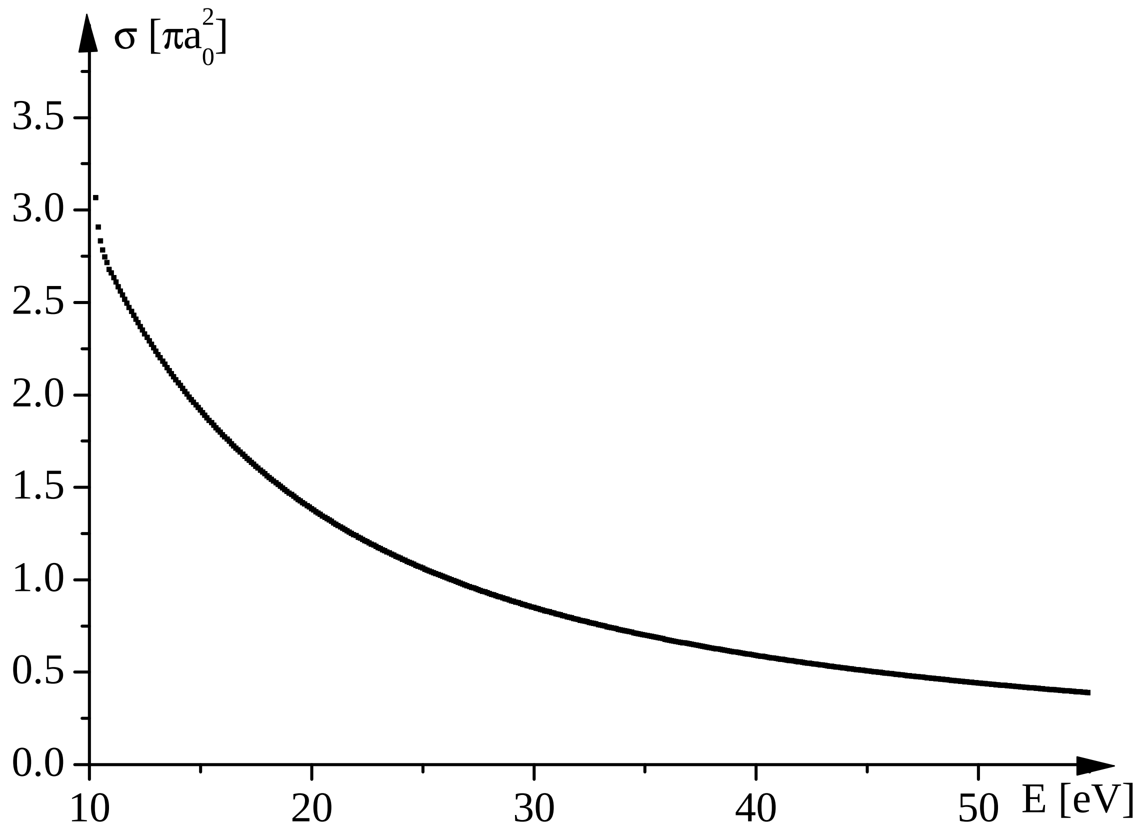

Figure B.7: Cross section for elastic scattering by the ground state σ^{00}

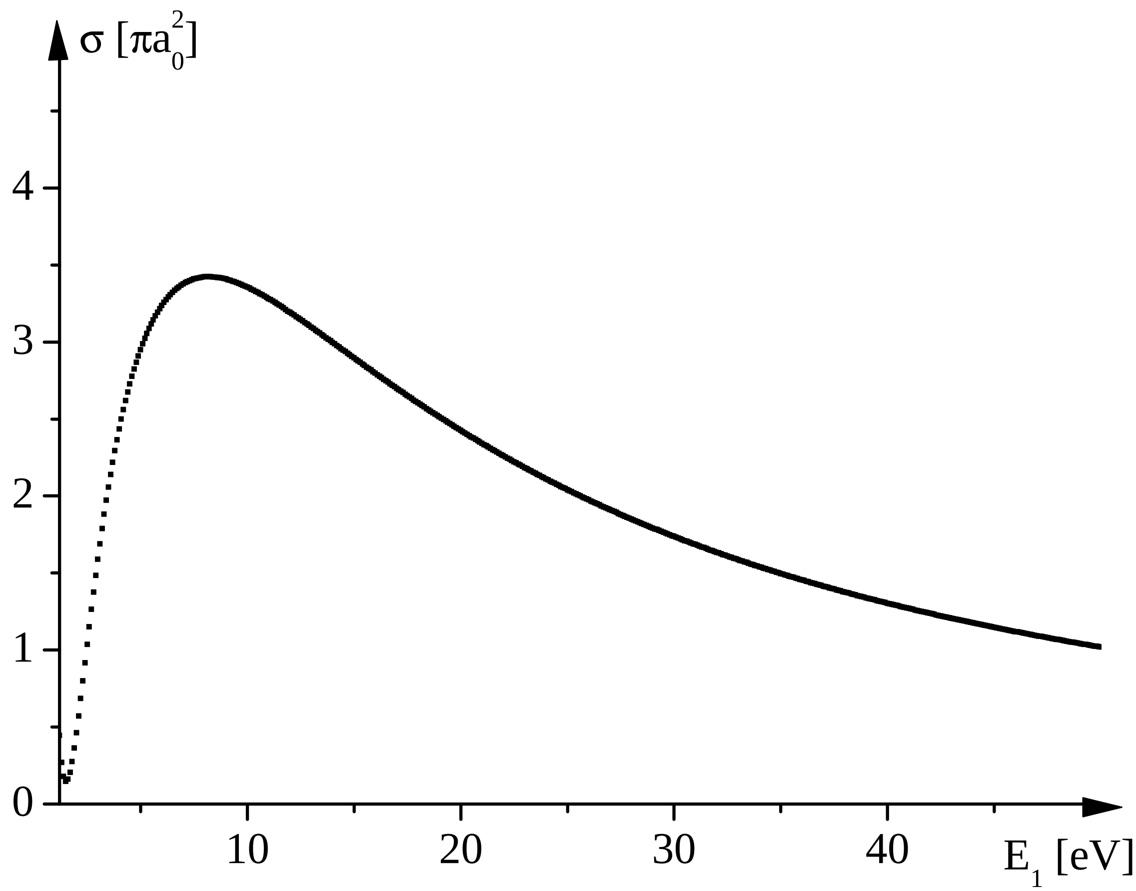

Figure B.8: Cross section for elastic scattering by the excited state $\sigma^{11}(E_1)$ ($E_1 = E - 10.2$ eV is the energy relative to the 2s-level). Because $k1 \simeq 0$, there occur numerical errors in the low energy regime, where our model does not describe the process very accurately anyway. A more careful discussion is given in the text.

APPENDIX C

MOLECULAR TERM SYMBOLS

We would like to explain the meaning of molecular term symbols of the general form

$$^{2S+1}\Lambda^{\pm}_{\Omega,\mathrm{g/u}} \ . \tag{C.1}$$

First of all we assume linear diatomic molecules. Similarly to the LS-coupling scheme known from single atoms, we can define the total electronic orbital angular momentum and spin

$$\vec{L} = \sum_i \vec{l}_i \qquad \text{and} \qquad \vec{S} = \sum_i \vec{s}_i \ . \tag{C.2}$$

There is no overall rotational symmetry in a diatomic molecule, which implies that L is not a good quantum number. But there is a rotational symmetry about the interatomic axis (which we choose to be our quantization axis) and therefore M_L is a good quantum number. The motion of the electrons in an electrostatic field is invariant under motion (time-) reversal. (That is not true for magnetic fields!) Due to this symmetry states with $+M_L$ and $-M_L$ are degenerate (as those two quantum numbers refer to counterwise rotations around the internuclear axis about the same angle). That allows us to define the good quantum number

$$\Lambda = |M_L| \quad (\Lambda = 0, 1, 2, 3, ..., L \ \Rightarrow \ \Sigma, \Pi, \Delta, \Phi, ...) \ , \tag{C.3}$$

where the Σ-state is non-degenerate and all states with $\Lambda \geq 1$ are doubly degenerate ($\pm M_L$).

The total spin is always conserved as long as there are no external fields. Hence S is a good quantum number. The spin is unaffected by the electrostatic field between the nulei and the electrons, but for $\Lambda > 0$ the motion of the electrons causes an internal magnetic field, which forces the total spin to precess around the internuclear axis. That's why we have M_S as another good quantum number, which is not defined for Σ-states ($\Lambda = 0$). Note: In the literature M_S is sometimes also labeled with Σ, which could lead to confusion with the $\Lambda = 0$-state.

Similarly to atoms where $\vec{L}$ and $\vec{S}$ couple to $\vec{J}$, we can define an overall electronic angular momentum along the internuclear axis which is denoted by Ω. Again, positive and negative values of Ω are degenerated due to time-reversal symmetry. Therefore one defines

$$\Omega = |\Lambda + M_S| \ . \tag{C.4}$$

As for Σ-states M_S is not defined, the index Ω can be omitted. The remaining two indices in the term symbol (eq. (C.1)) denote symmetry properties.

The reflection through a plane, which contains the internuclear axis, is a symmetry operation for any diatomic molecule. For Σ-states the reflection through such a plane either keeps the electronic eigenfunction unchanged (+) or changes its sign (-). As Σ-states are non-degenerate, this specification is important in that case. For $\Lambda \geq 1$-states, which are doubly degenerate, eigenfunctions to this symmetry operation can always be constructed, but because of the degeneracy this specification is irrelevant.

Another symmetry operation is the inversion of the electron position at the midpoint of the internuclear axis for diatomic molecules with nuclei of the same charge (e.g. $^{85}Rb_2$ or $^{85}Rb^{87}Rb$, but not NaRb or CO). This inversion is equivalent to the nuclear interchange with the electron positions held fixed. If the electron eigenfunctions remain unchanged under such an operation, the state is labeled with g (which stands for *gerade* - German for even). Otherwise the wave function changes sign, which is denoted by u (*ungerade* - German for odd).

The preceding discussion is for example given in [55].

APPENDIX D

NUMEROV'S METHOD

Numerov's method was devoloped by the Russian astronomer and geophysicist Boris V. Numerov in the 1920s ([56],[57] and [58]). It is a numerical method to solve differential equations of the following form:

$$y''(x) + f(x)y(x) = 0 \ . \tag{D.1}$$

Hence it can be used to solve the one-dimensional Schrödinger equation.

Starting with two consecutive initial values for $y(x)$ ($y(x_0) = y_0$ and $y(x_1) = y_1$), Numerov's method provides a solution according to the following recursion:

$$y_{n+1} = \frac{\left(2 - \frac{5h^2}{6} f_n\right) y_n - \left(1 + \frac{h^2}{12} f_{n-1}\right) y_{n-1}}{1 + \frac{h^2}{12} f_{n+1}} \ , \tag{D.2}$$

where $f_n = f(x_n)$ and $y_n = y(x_n)$ and the stepwidth $h = x_{n+1} - x_n$.

Proof:

Firstly we Taylor expand $y_{n\pm1}$:

$$y_{n+1} = y(x_n + h) = y_n + hy'_n + \frac{h^2}{2!}y''_n + \frac{h^3}{3!}y'''_n + \frac{h^4}{4!}y^{(4)}_n + \frac{h^5}{5!}y^{(5)}_n + \mathfrak{O}(h^6) \tag{D.3}$$

$$y_{n-1} = y(x_n - h) = y_n - hy'_n + \frac{h^2}{2!}y''_n - \frac{h^3}{3!}y'''_n + \frac{h^4}{4!}y^{(4)}_n - \frac{h^5}{5!}y^{(5)}_n + \mathfrak{O}(h^6) \ . \tag{D.4}$$

Adding those two equations together yields

$$y_{n+1} + y_{n-1} = 2y_n + h^2 y''_n + \frac{h^4}{12}y^{(4)}_n + \mathfrak{O}(h^6) \ . \tag{D.5}$$

Now we substitute y''_n from eq. (D.1) and get

$$y_{n+1} + y_{n-1} = 2y_n - h^2 f_n y_n + \frac{h^4}{12} y_n^{(4)} + \mathfrak{O}(h^6) \ . \tag{D.6}$$

We can also express the fourth derivative by the differential equation

$$y^{(4)}(x) = -\frac{d^2}{dx^2} \left[f(x) y(x) \right] \ . \tag{D.7}$$

Using the difference quotient yields

$$y_n^{(4)} = -\frac{\frac{f_{n+1}y_{n+1} - f_n y_n}{h} - \frac{f_n y_n - f_{n-1} y_{n-1}}{h}}{h} = -\frac{f_{n+1}y_{n+1} - 2f_n y_n + f_{n-1}y_{n-1}}{h^2} \ . \tag{D.8}$$

Hence

$$f_n y_n = \frac{1}{h^2} \left(2y_n - y_{n+1} - y_{n-1} - \frac{h^4}{12} \frac{f_{n+1}y_{n+1} - 2f_n y_n + f_{n-1}y_{n-1}}{h^2} \right) + \mathfrak{O}(h^4) \ . \tag{D.9}$$

Rearranging and neglecting of terms of $\mathfrak{O}(h^4)$ yields eq. (D.2).

$\blacksquare$

In section 3.3.3 we reverse this recursion by simply solving for y_{n-1}.

BIBLIOGRAPHY

[1] E.A. Cornell, J.R. Ensher, and C.E. Wieman. Experiments in dilute atomic Bose-Einstein condensation. *Bose-Einstein Condensation in Atomic Gases, Proceedings of the International School of Physics "Enrico Fermi" Course CXL*, 1999.

[2] S.N. Bose. Plancks Gesetz und Lichtquantenhypothese. *Zeitschrift für Physik*, 26, 1924.

[3] C.E. Hecht. The possible superfluid behaviour of hydrogen atom gases and liquids. *Physica*, 25(7-12), 1959.

[4] W.C. Stwalley and L.H. Nosanow. Possible "New" Quantum Systems. *Physical Review Letters*, 36(15), 1976.

[5] T.W. Hänsch and A. Schawlow. Cooling of gases by laser radiation. *Optical Communications*, 13(68), 1975.

[6] D.J. Wineland and H. Dehmelt. Proposed 10^{14} $D\nu < \nu$ Laser Fluorescence Spectroscopy on Tl+ Mono-Ion Oscillator III (side band cooling). *Bulletin of the American Physical Society*, 20(637), 1975.

[7] E. Raab, M. Prentiss, A. Cable, S. Chu, and D. Pritchard. Trapping of Neutral Sodium Atoms with Radiation Pressure. *Physical Review Letters*, 59(2631), 1987.

[8] J. Dalibard and C. Cohen-Tannoudji. Dressed-atom approach to atomic motion in laser light: the dipole force revisited. *Journal of the Optical Society of America B*, 2:1707–1720, 1985.

[9] J. Dalibard, C. Salomon, A. Aspect, E. Arimondo, R. Kaiser, N. Vansteenkiste, and C. Cohen-Tannoudji. *Atomic Physics 11.* World Scientific, Singapore, 1989.

[10] S. Chu, D.S. Weiss, P.J. Ungar, and Y. Shevy. *Atomic Physics 11.* World Scientific, Singapore, 1989.

[11] J. Dalibard and C. Cohen-Tannoudji. Laser cooling below the doppler limit by polarization gradients: simple theoretical models. *Journal of the Optical Society of America B*, 6:2023–2045, 1989.

[12] P.J. Ungar, D.S. Weiss, E. Riis, and S. Chu. Optical molasses and multilevel atoms: theory. *Journal of the Optical Society of America B*, 6:2058–2071, 1989.

[13] N.R. Newbury, C.J. Myatt, E.A. Cornell, and C.E. Wieman. Gravitational Sisyphus Cooling of ^{87}Rb in a Magnetic Trap. *Physical Review Letters*, 74(12):2196–2199, 1995.

[14] H.F. Hess. Evaporative cooling of magnetically trapped and compressed spin-polarized hydrogen. *Physical Review Letters B*, 34(5), 1986.

[15] M.H. Anderson, J.R. Ensher, M.R. Matthews, C.E. Wieman, and E.A. Cornell. Observation of Bose-Einstein Condensation in a Dilute Atomic Vapor. *Science*, 269(5221), 1995.

[16] J.D. Miller, R.A. Cline, and D.J. Heinzen. Photoassociation Spectrum of Ultracold Rb Atoms. *Physical Review Letters*, 71(14), 1993.

[17] S.B. Weiss, M. Bhattacharya, and N.P. Bigelow. Calculation of the interspecies s-wave scattering length in an ultracold Na-Rb vapor. *Physical Review A*, 68(4), 2003.

[18] A. Pashov et al. Potentials for modeling cold collisions between Na (3S) and Rb (5S) atoms. *Phys. Rev. A*, 72, 2005.

[19] A. Pashov, O. Docenko, M. Tamanis, R. Ferber, H. Knöckel, and E. Tiemann. Coupling of the $X^1\Sigma^+$ and $a^3\Sigma^+$ states of KRb. *Phys. Rev. A*, 76, 2007.

[20] R.J. LeRoy. LEVEL 7.5 - A Computer Program for Solving the Radial Schrödinger Equation for Bound and Quasibound Levels. *University of Waterloo, Chemical Physics Research Report*, 2002.

[21] E. Rutherford. The scattering of α and β Particles by Matter and the Structure of the Atom. *Philosophical Magazine*, 6(21), 1911.

[22] N.F. Mott and H.S.W. Massey. *The Theory of Atomic Collisions*. Clarendon Press, Oxford, 3rd edition, 1965.

[23] J.J. Sakurai. *Modern Quantum Mechanics*. Addison-Wesley, New York, 1994.

[24] E.W. Weisstein. Spherical Bessel Differential Equation. From MathWorld-A Wolfram Web Resource http://mathworld.wolfram.com/SphericalBesselDifferential-Equation.html (date accessed 06/2009).

[25] W. Pauli. The Connection Between Spin and Statistics. *Physical Review Letters*, 58(8), 1940.

[26] K.M. O'Hara. *Optical Trapping and Evaporative Cooling of Fermionic Atoms*. PhD thesis, Duke University, 2000.

[27] G.F. Gribakin and V.V. Flambaum. Calculation of scattering length in atomic collisions using the semiclassical approximation. *Phys. Rev. A*, 48(1), 1993.

[28] C. Ramsauer. Über den Wirkungsquerschnitt der Gasmoleküle gegenüber langsamen Elektronen. *Annalen der Physik*, 369(6):513–540, 1921.

[29] D.J. Heinzen. Ultracold atomic interactions. *Bose-Einstein Condensation in Atomic Gases, Proceedings of the International School of Physics "Enrico Fermi" Course CXL*, 1999.

[30] J.M. Vogels, B.J. Verhaar, and R.H. Blok. Diabatic models for weakly bound states and cold collisions of ground-state alkali-metal atoms. *Physical Review A*, 57(5):4049–4052, 1998.

[31] A. Dalgarno and M.R.H. Rudge. Spin-change cross sections for collisions between alkali atoms. *Proceedings of the Royal Society of London. Series A, Mathematical and Physical Sciences*, 286(1407):519–524, 1965.

[32] R. Côté, A. Dalgarno, H. Wang, and W.C. Stwalley. Potassium scattering lengths and prospects for Bose-Einstein condensation and sympathetic cooling. *Physical Review A*, 57(6), 1998.

[33] M. Born and R. Oppenheimer. Zur Quantentheorie der Moleküle. *Annalen der Physik*, 84, 1927.

[34] J.P. Burke Jr. *Theoretical Investigation of Cold Alkali Atom Collisions*. PhD thesis, University of Colorado, 1999.

[35] R.J. LeRoy and R.B. Bernstein. Dissociation energy and long-range potential of diatomic molecules from vibrational spacings of higher levels. *The Journal of Chemical Physics*, 1970.

[36] Z. Wang et al. A Mathematica program for the two-step twelfth-order method with multi-derivative for the numerical solution of a one-dimensional Schrödinger equation. *Computer Physics Communications*, 2004.

[37] E. Tiesinga, C.J. Williams, P.S. Julienne, K.M. Jones, P.D. Lett, and W.D. Phillips. A spectroscopic determination of scattering lengths for sodium atom collisions. *J. Res. Natl. Inst. Stand. Technol.*, 101:505–520, 1996.

[38] F.A. van Abeelen and B.J. Verhaar. Determination of collisional properties of cold Na atoms from analysis of bound-state photoassociation and Feshbach resonance field data. *Phys. Rev. A*, 59(1), 1999.

[39] C.J. Pethick and H. Smith. *Bose-Einstein Condensation in Dilute Gases*. Cambridge University Press, 2002.

[40] P.A. Ruprecht, M.J. Holland, K. Burnett, and M. Edwards. Time-dependent solution of the nonlinear Schrödinger equation for Bose-condensed trapped neutral atoms. *Physical Review A*, 51(6), 1995.

[41] C.A. Sackett, C.C. Bradley, M. Welling, and R.G. Hulet. Bose-Einstein Condensation of Lithium. *Applied Physics B*, 65:433–440, 1997.

[42] L.P. Pitaevskii and S. Stringari. *Bose-Einstein Condensation*. Clarendon Press, 2004.

[43] C.J. Myatt, E.A. Burt, R.W. Ghrist, E.A. Cornell, and C.E. Wieman. Production of Two Overlapping Bose-Einstein Condensates by Sympathetic Cooling. *Physical Review Letters*, 78(4), 1997.

[44] R. Ejnisman, H. Pu, Y.E. Young, N. P. Bigelow, and C.K. Law. Studies of two-species Bose-Einstein condesation. *Optics Express*, 2(8), 1998.

[45] R. Ejnisman et al. Density distribution of a Na-Rb TBEC for different values of a_{12}. Video from [44] available under http://www.opticsinfobase.org/oe/-viewmedia.cfm?uri=oe-2-8-330&seq=2 (date accessed 06/2009), 1998.

[46] J. Weiner, V. Bagnato, S. Zilio, and P.S. Julienne. Experiments and theory in cold and ultracold collisions. *Rev. Mod. Phys.*, 71:1–85, 1999.

[47] F. Dalfovo, S. Giorgini, L.P. Pitaevskii, and S. Stringari. Theory of bose-einstein condensation in trapped gases. *Reviews of Modern Physics*, 71(3), 1999.

[48] A. Clairon et al. Ramsey Resonance in a Zacharias Fountain. *Europhysics Letters*, 1991.

[49] S.J.J.M.F. Kokkelmans, B.J. Verhaar, K. Gibble, and D.J. Heinzen. Predictions for laser-cooled Rb clocks. *Physical Review A*, 56(6), 1997.

[50] D.M. Brink and G.R. Satchler. *Angular Momentum*. Clarendon Press, Oxford, 2nd edition, 1968.

[51] B.H. Bransden and J.S.C. McKee. The 1s-2s excitation of hydrogen by electron impact. *Proceedings of the Physical Society*, 1956.

[52] B.H. Bransden. *Atomic Collision Theory*. W.A. Benjamin, Inc., 1970.

[53] H.S.W. Massey and B.L. Moiseiwitsch. Calculation of the 1s-2s electron excitation cross section of hydrogen by a variational method. *Proceedings of the Physical Society*, 1953.

[54] R. Marriott. Calculation of the 1s-2s electron excitation cross section of hydrogen. *Proceedings of the Physical Society*, 1958.

[55] G. Herzberg. *Molecular Spectra and Molecular Structure I. Spectra of Diatomic Molecules*. D. Van Nostrand Company, Inc., 1963.

[56] E. Hairer, S.P. Norsett, and G. Wanner. *Solving Ordinary Differential Equations I: Nonstiff Problems*. Springer, 1993.

[57] B.V. Numerov. A method of extrapolation of perturbations. *Monthly Notices of the Royal Astronomical Society*, 1924.

[58] B.V. Numerov. Note on the numerical integration of $d^2x/dt^2 = f(x, t)$. *Astronomische Nachrichten*, 1927.